

PARTICLE CHARACTERIZATION IN ROCKET EXHAUST PLUMES

E. Eugene Callens, Jr.
J. Scott Fisher

Department of Mechanical and Industrial Engineering
Louisiana Tech University
P.O. Box 10348
Ruston, LA 71272-0046

July 1997

Technical Report

Contract No. 31-4136-59060
and NASA (1995)-Stennis-06
and NAS13-580

Prepared for:
National Aeronautics and Space Administration
John C. Stennis Space Center
Stennis Space Center, MS 39529-6000

ABSTRACT

A method to characterize particles in rocket exhaust plumes is developed. The particle velocity, size, and material composition are determined from crater characteristics resulting from impacts into aluminum and copper targets passed through the plume. The targets are mounted on a steel arm approximately 21 inches (53 cm) long which is rotated through the plume at sufficient velocity to prevent material failure resulting from thermal effects. A Scanning Electron Microscope (SEM) with secondary x-ray detectors is used to determine the particle material, and a standard optical measurement microscope is used to determine the crater diameter and depth. The crater diameter and depth are used, in turn, as inputs to a ballistics computer code to estimate the velocity and size of the particle. The target has a safe residence time in the plume of approximately 50 ms before reaching an unacceptably high temperature. The arm must reach a velocity of 104 ft/s (32 m/s) before entering the plume to produce the design residence time of 20 ms. The arm is actuated by a torsion spring with a 5-inch (13 cm) outer diameter, 0.625-inch (16 mm) wire diameter, and 11 coils. A prototype of the entire rocket exhaust particle impact characterization system (PICS) was constructed and statically tested.

TABLE OF CONTENTS

	Page
Abstract.....	ii
List of Tables.....	v
List of Figures	viii
 Chapter	
1. INTRODUCTION.....	1
Statement of Problem.....	1
Background	3
Proposed Approach.....	6
2. OVERVIEW OF PARTICLE IMPACT CHARACTERIZATION SYSTEM.....	9
Probe and Probe Actuation Mechanism	9
Target Configuration.....	13
3. THERMAL RESPONSE OF THE TARGET MATERIAL.....	15
Statement of the Thermal Problem	15
Properties at the Nozzle Exhaust Plane.....	19
Properties Downstream of the Bow Shock	20
Properties Behind the Shock Wave Along the Side of the Target.....	21
Semi-Infinite Approximation of Target Material	22
Finite-Difference Formulation of Thermal Response Problem	24
Results of the Finite-Difference Analysis.....	37
4. KINETIC RESPONSE OF PARTICLES IN THE EXHAUST.....	44
Development of Particle Velocity Governing Equations.....	44
Solution Method for the Particle Velocity Equation.....	46

Results of the Analysis	51
Estimation of Crater Depth and Diameter	57
5. DESIGN OF PROTOTYPE.....	63
Energy Analysis of the Probe.....	63
Design of the Spring.....	68
Parts List and Shop Drawings	73
Prototype Assembly	99
Prototype Testing.....	103
Operation of the PICS.....	105
Fabrication Instructions for the Targets	106
Appendix	
A. THERMAL RESPONSE PROGRAM IN THE C PROGRAMMING LANGUAGE	112
B. TABULATED DATA FROM THE THERMAL RESPONSE PROGRAM.....	124
C. PARTICLE VELOCITY PROGRAM IN THE C PROGRAMMING LANGUAGE	127
D. TABULATED DATA FROM THE PARTICLE VELOCITY PROGRAM.....	135
LIST OF WORKS CITED.....	141

LIST OF TABLES

	Page
1. Approximate Melting Temperatures of Some Potential Exhaust Particles.....	3
2. Properties of Materials Used in Thermal Calculations	23
3. Thermal Resistances and Capacitances for Specified Nodes	28
a. Centerline Convection Node	28
b. Centerline Target Node.....	28
c. Centerline Target-Support Node.....	29
d. Centerline Support Node	29
e. Centerline Insulated Node.....	30
f. Full Node on the Exposed Flat Face.....	30
g. Full Node in the Target Material	31
h. Front Corner Node Along the Longitudinal Material Interface.....	31
i. Node Along the Longitudinal Material Interface.....	32
j. Rear Corner Node Along the Longitudinal Material Interface.....	32
k. Full Node in the Support Material	33
l. Node Along the Insulated Boundary	33
m. Convection Corner Node	34
n. Target Node on the Curved Exterior Surface	34

o.	Nodes on the Material Boundary on the Curved Exterior Surface.....	35
p.	Support Node on the Curved Exterior Surface.....	35
q.	Insulated Node on the Curved Exterior Surface	36
r.	Node Along a Radial Material Boundary.....	36
4.	Safe Residence Times.....	37
5.	Properties of Materials for Penetration Code	57
6.	Velocities and Energies the Probe Encounters During Operation	69
7.	Inputs and Outputs for Spring Calculation Program.....	70
8.	Specifications for Required Torsion Spring.....	71
9.	Parts List.....	73
10.	Experimental Velocity Data.....	104
B1.	Temperature Profiles (°R) Along Exposed Flat Surface of Aluminum Target (Figure 13).....	125
B2.	Temperature Profiles (°R) Along the Exposed Flat Surface of Copper Target (Target 14)	125
B3.	Temperature Profiles (°R) Along Centerline of Aluminum Target and Steel Holder (Figure 15)	125
B4.	Temperature Profiles (°R) Along Centerline of Copper Target and Steel Holder (Figure 16).....	126
B5.	Temperature Profiles (°R) Along the Exposed Curved Surface of Aluminum Target and Steel Holder (Figure 17)	126
B6.	Temperatures °R Along the Exposed Curved Surface of Copper Target and Steel Holder (Figure 18).....	126
D1.	Nozzle Flow Properties as a Function of X/X _c	136

D2.	Velocity (ft/sec) of a 10 μm Particle in the Exhaust Flow of Various Size Rockets as a Function of X/X_e	136
D3.	Velocity (ft/sec) of a 50 μm Particle in the Exhaust Flow of Various Size Rockets as a Function of X/X_e	137
D4.	Velocity (ft/sec) of a 100 μm Particle in the Exhaust Flow of Various Size Rockets as a Function of X/X_e	137
D5.	Velocity (ft/sec) of a 300 μm Particle in the Exhaust Flow of Various Size Rockets as a Function of X/X_e	138
D6.	Velocity (ft/sec) of a 500 μm Particle in the Exhaust Flow of Various Size Rockets as a Function of X/X_e	138
D7.	Velocity (ft/sec) of a 1000 μm Particle in the Exhaust Flow of Various Size Rockets as a Function of X/X_e	139
D8.	Velocity (ft/sec) of a 3000 μm Particle in the Exhaust Flow of Various Size Rockets as a Function of X/X_e	139
D9.	Velocity (ft/sec) of a 5000 μm Particle in the Exhaust Flow of Various Size Rockets as a Function of X/X_e	140
D10.	Particle Velocity at the exit plane, V_{pe} (ft/sec), and Particle Impact Velocity, V_p (ft/sec)	140

LIST OF FIGURES

		Page
1.	Rocket and PICS During Rocket Testing.....	8
2.	PICS - Side View.....	10
3.	PICS - Initial and Terminal Positions.....	11
	a. Front View with Slider Locked in Place (Initial Position).....	11
	b. Front View with Slider Released (Terminal Position).....	11
4.	Cross Section View of the Pneumatic Clip with the Slider Locked in Place.....	12
5.	Target Configuration.....	14
	a. Side View.....	14
	b. Front View.....	14
6.	Target Geometry.....	16
7.	Flow Field Around the Target.....	17
8.	Thermodynamic Conditions in the Flow Field.....	22
9.	Node Geometry for Finite-Difference Formulation.....	24
10.	Electrical Analogy for Thermal Conduction Through a Node.....	25
11.	Nodal Volume for Finite-Difference Approximation.....	26
12.	Nomenclature for Finite-Difference Formulation Parameters.....	27
13.	Temperature Profiles Along Exposed Flat Surface of Aluminum Target.....	39
14.	Temperature Profiles Along Exposed Flat Surface of Copper Target.....	39

15.	Temperature Profiles Along Centerline of Aluminum Target and Steel Holder.....	40
16.	Temperature Profiles Along Centerline of Copper Target and Steel Holder.....	40
17.	Temperature Profiles Along Exposed Curved Surface of Aluminum Target and Steel Holder.....	41
18.	Temperature Profiles Along Exposed Curved Surface of Copper Target and Steel Holder.....	41
19.	Axial Temperatures for Aluminum Target and Steel Holder at Thermal Failure ($t=51$ ms).....	42
20.	Axial Temperatures for Copper Target and Steel Holder at Thermal Failure ($t=384$ ms).....	42
21.	Temperatures of Exposed Flat Surface at Thermal Failure.....	43
22.	Bow Shock in Front of Target.....	44
23.	Assumed Nozzle Shape.....	48
24.	Drag Coefficient of a Smooth Sphere.....	50
25.	Mach Number in the Nozzle.....	52
26.	Gas Velocity in the Nozzle.....	53
27.	Gas Density in the Nozzle.....	53
28.	Particle Velocity in the Nozzle for $X_e = 1$ inch.....	54
29.	Particle Velocity in the Nozzle for $X_e = 6$ inch.....	54
30.	Particle Velocity in the Nozzle for $X_e = 12$ inch.....	55
31.	Particle Velocity in the Nozzle for $X_e = 24$ inch.....	55
32.	Particle Velocity in the Nozzle for $X_e = 48$ inch.....	56
33.	Particle Velocity Versus Particle Diameter for Various Size Nozzles.....	56

34.	Crater Diameter in 6061-T651 Aluminum as a Function of HTPB Particle Size.....	59
	a. Particle Size Range 10 to 3,000 μm	59
	b. Particle Size Range 1 to 100 μm	59
35.	Crater Depth into 6064-T651 Aluminum as a Function of HTPB Particle Size.....	60
	a. Particle Size Range 10 to 3,000 μm	60
	b. Particle Size Range 1 to 100 μm	60
36.	Crater Diameter in Copper as a Function of HTPB Particle Size.....	61
	a. Particle Size Range 10 to 3,000 μm	61
	b. Particle Size Range 1 to 100 μm	61
37.	Crater Depth in Copper as a Function of HTPB Particle Size.....	62
	a. Particle Size Range 10 to 3,000 μm	62
	b. Particle Size Range 1 to 100 μm	62
38.	Probe Entering the Plume.....	64
39.	Sections of Arm Used in Moment of Inertia Calculation.....	67
40.	Spring Torque Versus Spring Arm Deflection.....	71
41.	Target Translation Velocity and Rotational Versus Spring Arm Deflection.....	72
42.	Stress in Spring Versus Spring Deflection.....	72
43.	Section Required to Manufacture Probe Arm.....	77
44.	Bends Required in Section to Manufacture Probe Arm.....	78
45.	Call-Out of Hole in Tip of Probe Arm.....	79

46.	Probe Collar.....	80
47.	Shaft.....	81
48.	Vertical Support.....	82
49.	Baseplate.....	83
50.	Pipe Section Required to Manufacture Mandrel.....	84
51.	End Plugs Required to Manufacture Mandrel.....	85
52.	Spring Arm Holder.....	86
53.	Horizontal Support.....	87
54.	Slider Holder.....	88
55.	Pin Holder.....	89
56.	Pin.....	90
57.	Bottom Plate.....	91
58.	Top Plate.....	92
59.	Pressure Vessel.....	93
60.	Plunger.....	94
61.	Slider.....	95
62.	Welds on Bottom Plate, Slider Holder, and Pin Holder.....	96
63.	Welds Required to Attach Vertical Supports, Horizontal Supports, and Spring Arm Holder to Baseplate (Top View).....	97
64.	Welds Required to Attach Vertical Supports and Spring Arm Holder to Baseplate (Front View).....	98
65.	Spring with Mandrel Partially Inserted.....	99
66.	Shaft Inserted Through the Probe Arm Collar.....	100

67.	Spring Arm Inserted into the Spring Arm Holder	101
68.	Gaskets in the Top and Bottom Plates	101
69.	Gasket Between Plunger and Bottom Plate.....	102
70.	Top and Bottom Plates Connected by Bolts.....	102
71.	Pneumatic Clip Attached to Baseplate	103
72.	Test Apparatus.....	104
73.	Experimental and Theoretical Probe Velocity	105
74.	Insert Required to Manufacture Targets	108
75.	Jig Part #1	109
76.	Jig Part #2.....	110
77.	Jig Part #3	111

CHAPTER 1

INTRODUCTION

Statement of Problem

Presently, particles from rocket exhausts are typically collected by placing sticky tape far downstream of the nozzle exit to capture low velocity particles that have survived the severe aerothermal environment of the plume. This procedure suffers from the problem that particles from the ambient surroundings are entrained in the far plume and captured on the tape. It is difficult to determine which particles come from the surroundings and which ones come from the rocket engine. This method also provides no information on particles that may have been consumed in the extremely high temperatures of the exhaust near the exit.

Another method, used in some vertical test facilities, involves shooting a dart with sticky tape through the exhaust (Sambamurthi, 1996). The particles impact the tape while the tape is in the plume and become attached to it. Unfortunately, this method also collects particles from the ambient surroundings and possibly also from the ground when the dart lands.

Typical rocket test facilities have the capability to determine the elemental composition of the exhaust gas by spectroscopy (Olive, 1988). The major deficiency of this method, as applied to the current problem, is its inability to determine the molecular

composition of particles in the exhaust. Spectroscopy can determine which basic elements are present but cannot determine how they are combined. It is very important to know which molecules are exiting the rocket since numerous molecules can contain any given element.

The current problem is to determine the size, number density, and material composition of particles from the nozzle exhaust flow. Several significant measurement problems associated with the high gas temperatures and supersonic velocity of the nozzle flow are identified as follows:

1. Temperatures can be in excess of $3,000^{\circ}\text{R}$ ($1,667\text{ K}$) in the nozzle exhaust flow.

Table 1 lists melting temperatures of potential particulates. Since several of these materials have melting temperatures well below $3,000^{\circ}\text{R}$ ($1,667\text{ K}$), it is necessary to capture the particles as soon as possible, or they may melt or ablate away. It is not possible to place the probe in the current design into the nozzle upstream of the nozzle exit plane because of geometry constraints and high temperatures. Therefore, for best results, the particles should be characterized at the exhaust plane of the nozzle.

2. The gas and particle velocity ranges also present a problem. Typical exhaust velocities for hybrid rocket engines are approximately $8,000\text{ ft/sec}$ ($2,438\text{ m/sec}$). A particle number density of approximately $100\text{ particles/ft}^3$ ($3.5 \times 10^{-5}\text{ particles/cm}^3$) is the initial design condition. It is desired to have distinct craters on the target; therefore, the desired number of craters is of the order of twenty. This design crater number density results in target residence times in the plume on the order of 20 ms . Since the

probe moves only through approximately 180°, this residence time presents a significant problem in accelerating and decelerating the probe without breaking it. Particle velocities in the range of 1,000 to 8,000 ft/sec (305 to 2,438 m/sec) are expected. Impacting particles must have enough velocity to create deep craters. It is possible that particles may coalesce and form large particles without sufficient velocity to form craters in the target.

Table 1. Approximate Melting Temperatures of Some Potential Exhaust Particles

Potential Particle	Approximate Melting Temperature °R
Hydroxyl-Terminated Polybutadiene (HTPB)	800
Al ₂ O ₃	4,180
Steel	3,226
Aluminum	1,680
Copper	2,442
Titanium	3,500

- The high temperatures may also cause chemical reactions between particles in the flow and the exhaust gases. If the particles do not impact the target before these reactions are complete, the sample collected will not be typical of the particles in the exhaust flow.
- The system should be inexpensive, easy to operate, and reliable.

Background

Bowman (1976) presents a good overview of the uses for probes in combustion research. He indicates that probes have been used in many research applications other

than sampling particles exiting a rocket engine. They are commonly used for temperature measurement as well as gas, two-phase, and velocity sampling. Pneumatic probes, hot-wire anemometers, and microphone probes may be used for measuring velocities in various types of flows. Probes used in combustion research are usually water-cooled. Cernansky (1976) has used probes to sample NO and NO₂ levels in gas turbine combustors with limited success. His research indicates some of the problems, such as quenching effects, which are inherent in gas sampling probes. Since the current work is primarily concerned with particle characterization techniques, these problems will not be discussed here. Bilger (1975) and Bennet (1976) provide good overviews of that topic.

Since this study is concerned with the characterization of particles from rocket exhausts, the literature review will focus on this subject. All published work located during the literature review involves capture of Al₂O₃ particles, since these particles are a primary constituent of solid rocket fuel. As early as 1980, the Jet Propulsion Laboratory at the California Institute of Technology was interested in collecting particles from the Space Shuttle's solid rocket motor exhaust (Strand et al., 1980). They used quartz-crystal mass monitors, Nucleopore filters, sticky-tape impactors, photoelectric cloud detectors, and electrical mobility analyzers to measure particulate concentrations and mass distributions. Strand found that the sticky-tape impactors and the electrical mobility analyzers provided the most useful data. Cofer et al. (1985) also investigated particles in the exhaust of the Space Shuttle. Their experiment involved flying an airplane, equipped with a Teflon filter, downward in a tight spiral through the exhaust of mission STS-61A immediately after launch. Any particles they collected were then examined with an SEM

to determine their size. Particles captured were between 0.1 μm and 10 μm in diameter. Particles smaller than 0.1 μm were not visible to the electron microscope, and it is believed that particles larger than 10 μm fell to Earth before they could be collected.

Laredo et al. (1991) investigated plume particle size measurements in solid propellant micromotors. Their research involved collecting particles in the chamber, nozzle, and plume of a subscale rocket. Particles from the chamber and nozzle were collected using special scattering techniques. Supersonic particles were collected by placing an impact probe consisting of a stainless steel wedge coated with copper into the flow for 0.5 seconds. Particles as large as 50 μm were common; however, some as large as 85 μm were found. It was found that particle breakup was dominant in the throat and the chamber and that collision coalescence dominated downstream of the throat.

Kreutle (1978) determined that particles collected after solid rocket firings were roughly spherical. This research involved collecting particles from the surfaces of the rocket after a test firing. Infrared optical properties have also been employed to analyze particle properties (Konopka et al., 1983). Konopka gives an excellent overview of research to this end. However, his work resulted primarily in determining certain properties of Al_2O_3 particles.

A more recent report relating to the use of impact probes to capture particles in rocket exhausts was published by Sambamurthi (1995). His method was to launch darts covered with sticky tape into the far downstream region (~150 ft or 45.7 m from the nozzle exit plane) of a large-scale solid rocket motor. The darts were 30 to 48 inches

(76.2 to 121.9 cm) long and were launched from the ground with a launch pressure of 800 psig (5.5 MPa) and at an angle of 80° with the horizontal. Many of the darts did not land nose forward and were unusable. The other darts were "mostly uncontaminated." Sambamurthi's research indicates that Al_2O_3 particles in the far plume region of a full-scale solid rocket exhaust are approximately 8 to 11 μm in diameter. This report details an attempt to take Sambamurthi's idea of passing a probe quickly through a rocket exhaust plume to capture particles. Implementation of this idea and operating parameters of the detailed procedure differ significantly from Sambamurthi's method.

Proposed Approach

This study addresses the problems of particle characterization by passing a probe through the rocket exhaust plume to encounter the particles. The high-velocity particles impact the relatively soft target surface of the probe and leave craters on its surface. The craters are then examined under an SEM equipped with secondary x-ray detectors to determine particle composition, and a standard optical measurement microscope is then used to measure crater depth and diameter. The crater depth and diameter data are used as inputs for a ballistics impact code to predict the velocity and size of the particles. Since this method collects only high-velocity particles, which normally do not exist in the ambient environment, the possibility of collecting particles from the ambient environment is eliminated.

The probe consists of an steel arm that supports a target of aluminum and copper at the end of the arm. The arm and target move transverse to the flow as shown in

Figure 1, where the probe arm is rotating perpendicular to the plane of the paper. The probe is actuated with a torsion spring and released by a pneumatic clip controlled by a delay generator receiving its input from the rocket firing circuit. The entire apparatus is called the Particle Impact Characterization System (PICS). This study outlines the design procedure for the PICS. The procedure includes a model of the thermodynamic properties of the plume, a model of the kinetic response of the particles in the plume, and a study of the thermal response of both the arm and target to the severe aerothermal environment. Also included are the kinetics calculations for the arm and the torsion spring design, as well as instructions on how to manufacture the PICS and the targets.

The proposed method obtains information on particles in the high velocity, high temperature plume environment. The experimenter can obtain information on particle characteristics as a function of axial location in the plume by operating several probes at various axial locations.

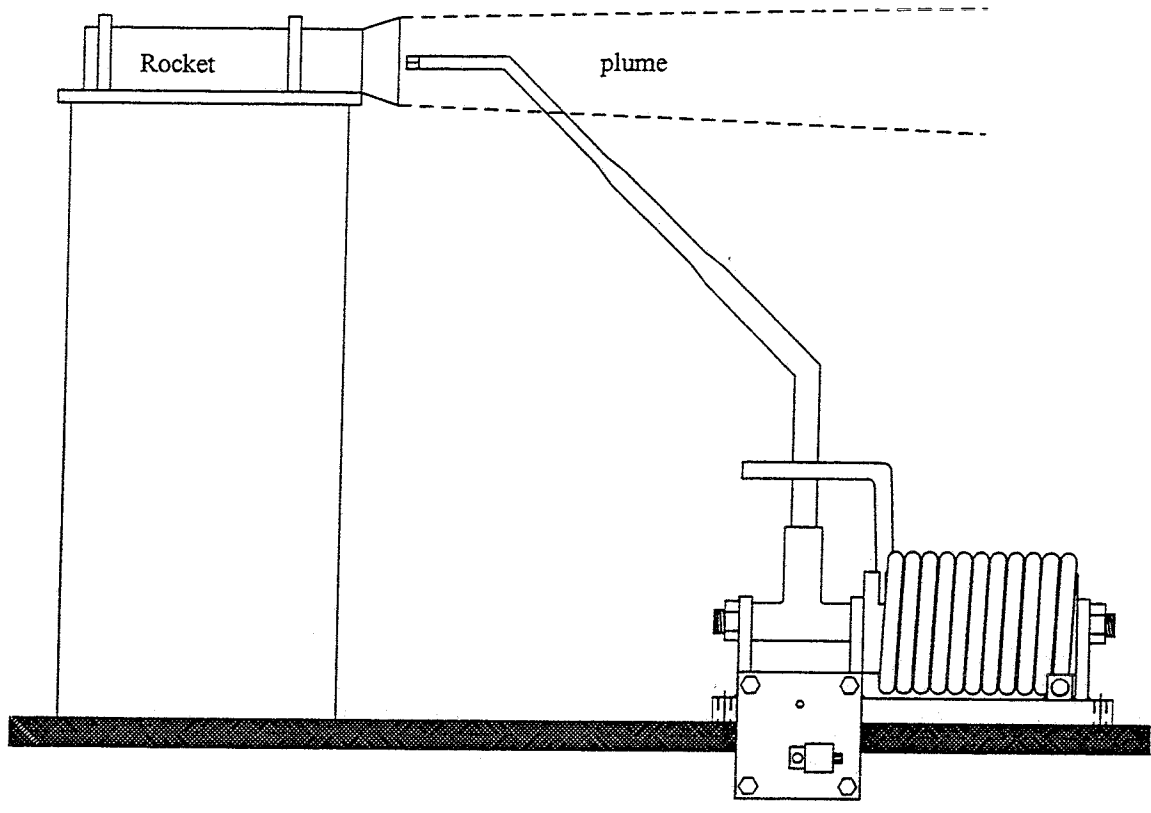


Figure 1. Rocket and PICS During Rocket Testing

CHAPTER 2

OVERVIEW OF PARTICLE IMPACT CHARACTERIZATION SYSTEM

Probe and Probe Actuation Mechanism

Figure 1 presents the basic configuration of the PICS. The arm is actuated by a torsion spring and stopped by an automobile tire, as seen in Figures 2 and 3. The PICS consists of the following:

1. the probe arm which holds the target while it moves through the plume
2. a torsion spring which accelerates the arm
3. a mandrel which provides support to the torsion spring when it is deflected
4. a probe arm collar which connects the arm to a shaft and allows the arm to rotate around the shaft
5. a shaft which keeps the probe arm collar and spring mandrel in proper alignment
6. a baseplate which can be bolted to a surface for support
7. three vertical supports which hold the shaft in place and are welded to the baseplate
8. a slider which holds the arm in the cocked position (Figures 3b and 4)
9. a pneumatic clip which releases the slider when a current is applied to an electric valve on the clip (Figure 4)
10. a delay generator which activates the electric valve
11. a chain which connects the slider to the arm.

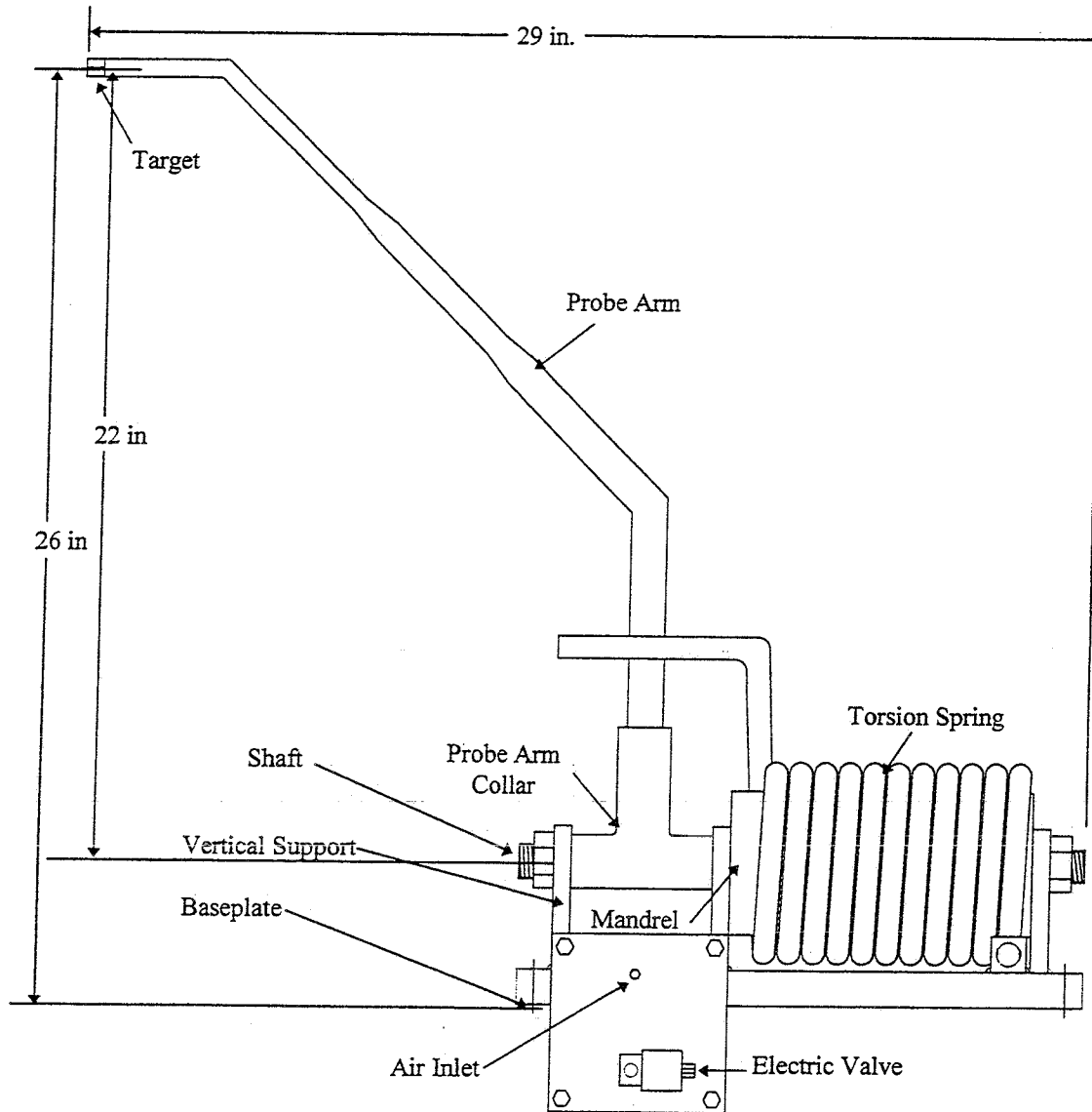
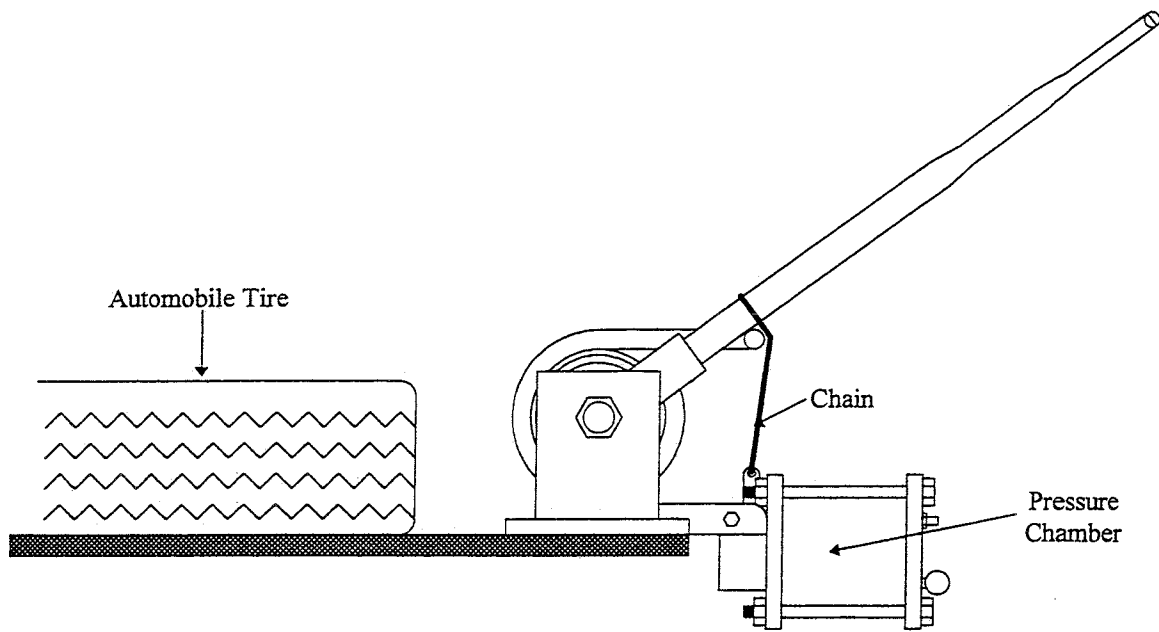
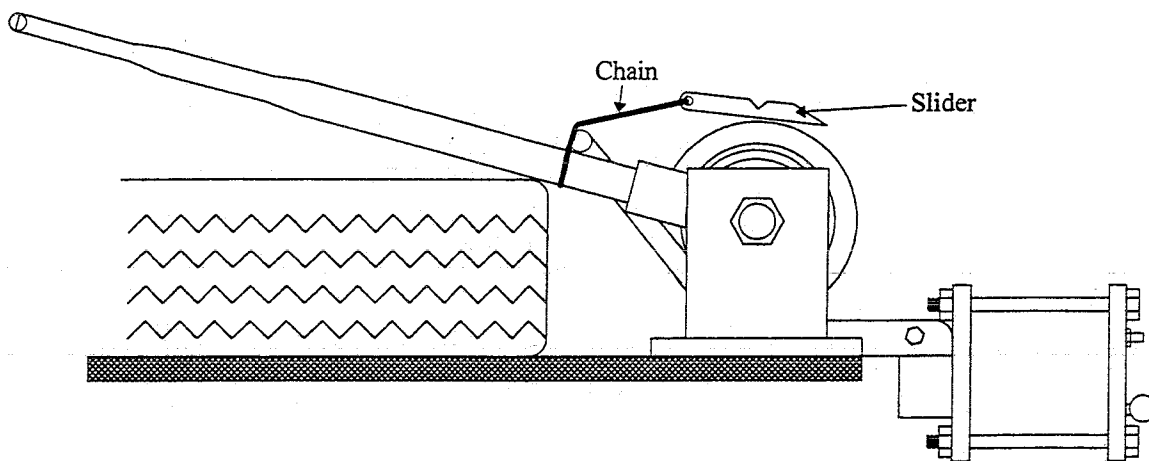


Figure 2. PICS - Side View



a. Front View with Slider Locked in Place (Initial Position)



b. Front View with Slider Released (Terminal Position)

Figure 3. PICS - Initial and Terminal Positions

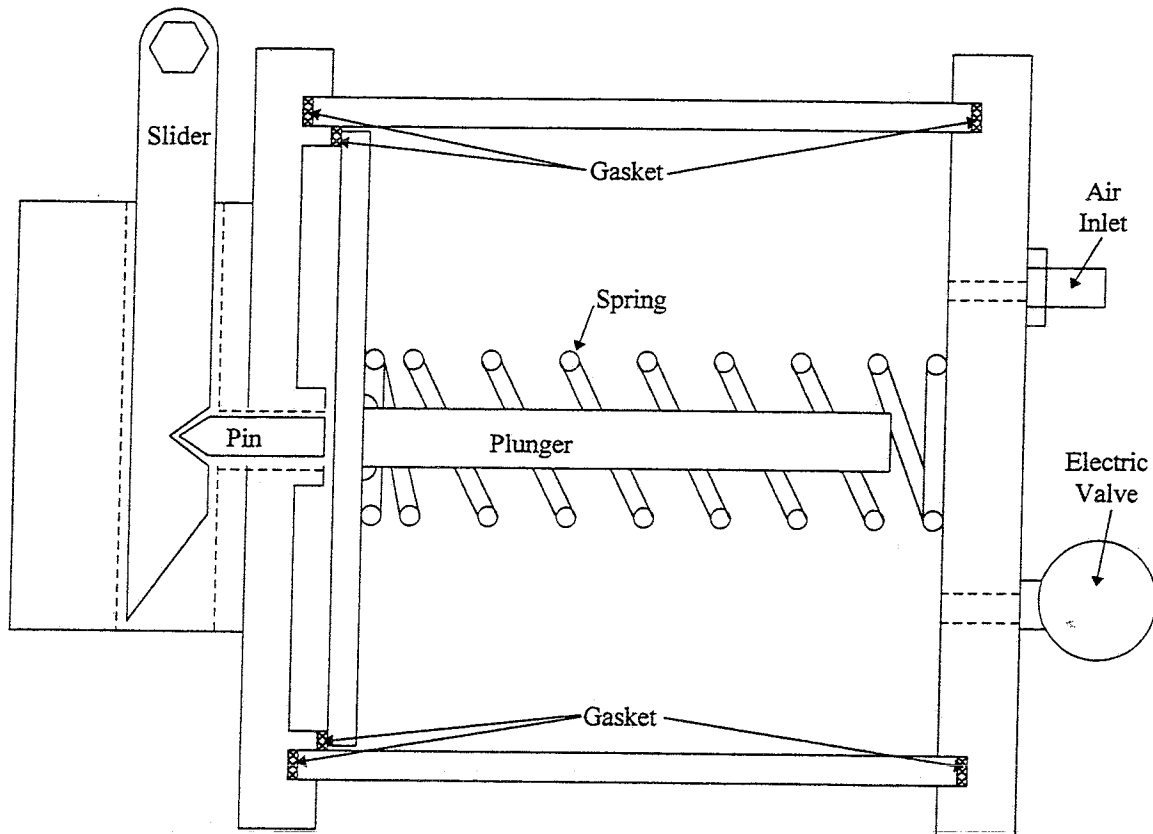


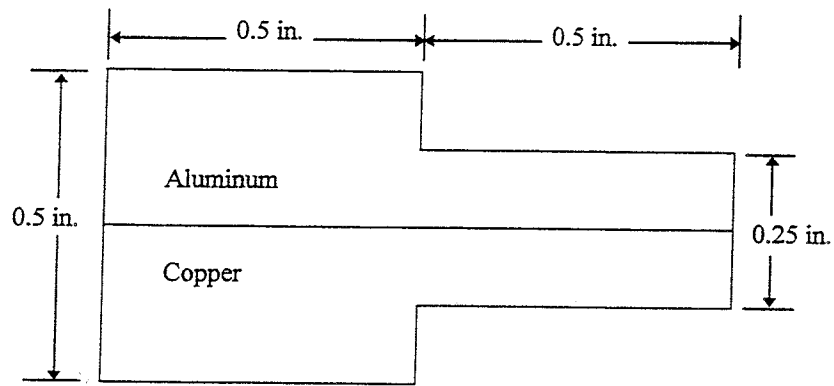
Figure 4. Cross Section View of the Pneumatic Clip with the Locked in Place

The pneumatic clip is pressurized to 70 psig (482.6 kPa) with the slider in place inside the clip. A chain is wrapped around the probe and spring arm. A standard trailer winch (designed for recreational boat trailers) may be used to cock the spring if desired. Once the spring has been deflected enough to produce the desired launch velocity, the chain is connected to the slider by means of an industrial-strength spring clip. At this point, the arm is ready to fire. When the electric valve is opened by the delay generator, pressure drops inside the chamber and the pin is allowed to move perpendicular to the slider. Force from the torsion spring pulls the slider towards the spring, pushing the pin up in the

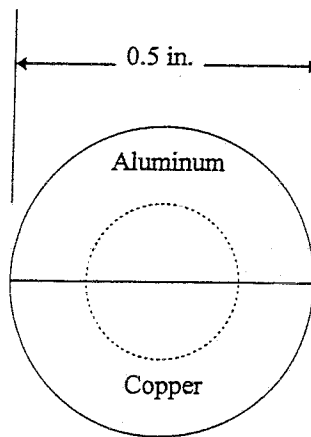
process and releasing the arm. At full deflection, the spring moves through a 135° included angle with the horizontal and the arm moves because of its inertia during the last 45° of travel. It is during this period that the bottom of the arm impacts the tire. The tire absorbs the energy of the arm and simultaneously keeps the arm from impacting anything rigid which could damage either the arm or the target. Inherent to this design is the fact that the unloaded spring can act as a stop which prevents the arm from rebounding into the plume as it recoils from the tire. The automobile tire was empirically determined to be capable of bringing the probe to rest safely.

Target Configuration

The basic design of the target is illustrated in Figure 5. It consists of two half-cylinders which form a stepped cylindrical shaft 1 inch (2.54 cm) in length. The front 0.5 inch (1.27 cm) of the shaft is 0.5 inch (1.27 cm) in diameter, and the rear half is 0.25 inch (0.635 cm) in diameter. The 0.25-inch (0.635 cm) section is inserted into a hole in the tip of the arm to attach the target to the arm. Two materials are required to create the target because, if only one material is used and a particle of that material impacts the target, the SEM would not be able to determine the particle material from the target. The selection of target materials to use is based on the determination of those materials that can withstand the plume temperature during the exposure time and that are also soft enough to allow sizable impact craters. Aluminum and copper were chosen as potential target materials because of their softness, coupled with relatively high thermal diffusivity.



a. Side View



b. Front View

Figure 5. Target Configuration

Calculations in Chapter 3 verify that aluminum and copper can safely withstand the specified residence times.

CHAPTER 3

THERMAL RESPONSE OF THE TARGET MATERIAL

Since the thermal conditions in a rocket exhaust plume are unfavorable for most common engineering materials, it is desirable to know how long the probe can reside in the plume before the probe experiences thermal failure. This residence time represents an operational limit for the PICS.

Since the probe is composed of two materials with different thermal properties, it is necessary to determine the time required for each material to reach the service temperature (critical temperature), taken to be 75% of its melting temperature for this application. The smaller of these two critical times will be the design residence time in the plume for the probe. The calculation of the critical times will assume that the entire target is of a single material. It is a conservative assumption in that the calculated minimum critical time will be less than the value when the second material is present.

Statement of the Thermal Problem

The thermal response of the target as a function of time is obtained from the unsteady heat conduction equation which, in cylindrical coordinates, is (Myers, 1987)

$$\frac{1}{\alpha} \frac{\partial T}{\partial t} = \frac{\partial^2 T}{\partial r^2} + \frac{1}{r} \frac{\partial T}{\partial r} + \frac{1}{r^2} \frac{\partial^2 T}{\partial \theta^2} + \frac{\partial^2 T}{\partial z^2} \quad (1)$$

where T = temperature

t = time

α = thermal conductivity

r = distance in the radial direction

z = distance in the axial direction

θ = distance in the angular direction.

Equation 1 requires two boundary conditions in each direction (z , r , and θ) and an initial condition. Figure 6 presents the target geometry. The boundary conditions for the target thermal problem follow:

1. On the exposed flat face, there is a shock layer downstream of the near-normal portion of the bow shock. The temperature in this region is conservatively taken to be the static temperature downstream of the normal shock with an assumed heat transfer coefficient of $h_2 = 1,800 \text{ BTU/hr}\cdot\text{ft}^2\cdot\text{R}$ ($10,220 \text{ Watt/m}^2\cdot\text{K}$), as shown in Figure 7. The assumed flow properties in the nozzle exhaust plume are taken from Callens (1994).

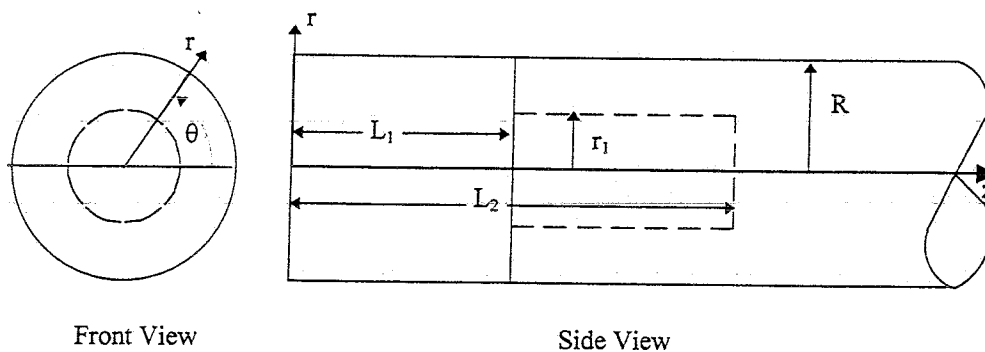


Figure 6. Target Geometry

The boundary condition is

$$h_2 A (T_2 - T_s) = -k_t A \left. \frac{\partial T}{\partial z} \right|_s ; \quad z = 0, 0 \leq r \leq R \quad (2)$$

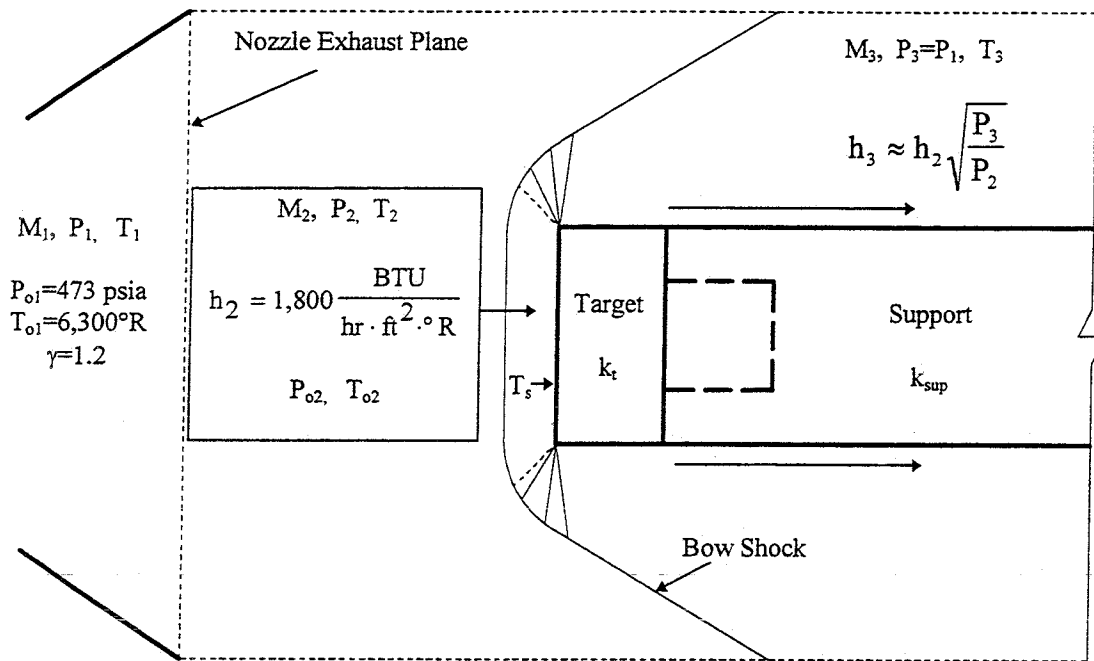


Figure 7. Flow Field Around the Target

- On the curved exposed surfaces, the temperature is taken to be the value corresponding to the conditions after the flow expands around the corner until the static pressure is equal to the static pressure at the exhaust plane of the rocket. The ratio of heat transfer coefficients, h_3/h_2 , varies approximately with $(P_3/P_2)^{1/2}$ (Bailey, 1965). The two boundary conditions are

$$h_3 A (T_3 - T_s) = -k_t A \left. \frac{\partial T}{\partial z} \right|_R ; \quad 0 \leq z \leq L_1, r = R \quad (3)$$

$$h_3 A (T_3 - T_s) = -k_{\text{sup}} A \left. \frac{\partial T}{\partial z} \right|_R ; \quad z > L_1, r = R \quad (4)$$

In reality, the temperature is greater on the windward side of the target and probe arm as it travels through the plume because the pressure is greater on this side. However, since the axial flow velocity is expected to be approximately 8,000 ft/sec (2,438 m/sec) and the target transverse velocity is expected to be approximately 100 ft/sec (30 m/sec), this pressure difference between the windward and leeward sides is small. Likewise, the temperature difference is correspondingly small and therefore neglected.

3. On the surfaces of the target touching the support material, the heat flow by conduction is assumed to be equal to the heat flow out of the surface into the arm.

The three boundary conditions are

$$-k_t A \left. \frac{\partial T}{\partial z} \right|_{L_1} = k_{\text{sup}} A \left. \frac{\partial T}{\partial z} \right|_{L_1} ; \quad r > r_1, z = L_1 \quad (5)$$

$$-k_t A \left. \frac{\partial T}{\partial z} \right|_{L_2} = k_{\text{sup}} A \left. \frac{\partial T}{\partial z} \right|_{L_2} ; \quad r < r_1, z = L_2 \quad (6)$$

$$-k_t A \left. \frac{\partial T}{\partial z} \right|_{r_1} = k_{\text{sup}} A \left. \frac{\partial T}{\partial z} \right|_{r_1} ; \quad L_1 < z < L_2, r = r_1 \quad (7)$$

4. A symmetry boundary condition exists along the centerline of the target and steel support because, in this problem, there is no temperature variation with θ . The boundary condition along the centerline is

$$\frac{\partial T}{\partial r} = 0 \quad ; \quad r = 0 \quad (8)$$

5. The area downstream in the steel holder is considered to be insulated. Therefore, the boundary condition is

$$\frac{\partial T}{\partial z} = 0 \quad ; \quad z = 3L_2 \quad (9)$$

6. The initial condition is that the temperature of the target and support materials is initially the ambient temperature which is assumed to be 540°R (300 K).

$$T_i = 540^\circ\text{R} \quad ; \quad 0 \leq r \leq R, \quad 0 \leq z \leq \infty \quad (10)$$

Properties at the Nozzle Exhaust Plane

The Mach number M_1 , temperature T_1 , and pressure P_1 at the exhaust plane were calculated for an exit plane to throat area ratio of 6 (Callens, 1994) using the equations for isentropic flow of a perfect gas (John, 1984):

$$\frac{A_e}{A^*} = \frac{\sqrt{\gamma} \left(\frac{\gamma+1}{2} \right)^{\frac{\gamma+1}{2-2\gamma}}}{M_1 \sqrt{\gamma} \left(1 + \frac{\gamma-1}{2} M_1^2 \right)^{\frac{\gamma+1}{2-2\gamma}}} \quad (11)$$

$$T_1 = \frac{T_{o1}}{1 + \left(\frac{\gamma-1}{2} M_1^2 \right)} \quad (12)$$

$$P_1 = \frac{P_{o1}}{\left(1 + \frac{\gamma-1}{2} M_1^2 \right)^{\frac{\gamma}{\gamma-1}}} \quad (13)$$

where A_e/A^* = cross-sectional area of the exit plane/cross-sectional area of the throat = 6

γ = ratio of specific heats

M_1 = mach number at the exhaust exit plane

T_1 = temperature at the nozzle exit plane

T_{o1} = stagnation temperature at the nozzle exit plane = 6,800° R

P_1 = pressure at the nozzle exit plane

P_{o1} = stagnation pressure at the nozzle exit plane = 473 psia.

The assumed values are taken from Callens (1994). The results are $M_1 = 2.92$, $P_1 = 11.8$ psia (81.4 kPa), and $T_1 = 3404^\circ\text{R}$ (1891 K).

Properties Downstream of the Bow Shock

The properties downstream of the bow shock are determined from the normal shock relations (John, 1984):

$$P_{o2} = P_{o1} \left(\frac{\frac{\gamma+1}{2} M_1^2}{1 + \frac{\gamma-1}{2} M_1^2} \right)^{\frac{\gamma}{\gamma-1}} \left(\frac{1}{\frac{2\gamma}{\gamma+1} M_1^2 - \frac{\gamma-1}{\gamma+1}} \right)^{\frac{1}{\gamma-1}} \quad (14)$$

$$M_2^2 = \frac{M_1^2 + \frac{2}{\gamma-1}}{\frac{2\gamma}{\gamma-1} M_1^2 - 1} \quad (15)$$

$$T_2 = \frac{T_1 \left(1 + \frac{\gamma-1}{2} M_1^2 \right)}{1 + \frac{\gamma-1}{2} M_2^2} \quad (16)$$

$$P_2 = P_1 \left(\frac{1 + \gamma M_1^2}{1 + \gamma M_2^2} \right) \quad (17)$$

The properties behind the shock wave and directly in front of the target are $P_{o2} = 120.5$ psia (830.8 kPa), $M_2 = 0.43$, $P_2 = 108.1$ psia (745.3 kPa), and $T_2 = 6187^\circ\text{R}$ (3437 K).

Properties Behind the Shock Wave Along the Side of the Target

It is assumed that the static pressure on the side of the target is approximately equal to the static pressure at the exit plane of the nozzle ($P_3 = P_1$). The equations for isentropic flow of a perfect gas were used to calculate M_3 and T_3 .

$$P_3 = P_2 \left(\frac{1 + \frac{\gamma-1}{2} M_2^2}{1 + \frac{\gamma-1}{2} M_3^2} \right)^{\frac{\gamma}{\gamma-1}} \quad (18)$$

$$T_3 = T_2 \left(\frac{1 + \frac{\gamma-1}{2} M_2^2}{1 + \frac{\gamma-1}{2} M_3^2} \right) \quad (19)$$

Equation (18) was used to calculate $M_3 = 2.18$ and Eqn. (19) was used to calculate $T_3 = 4,260^\circ\text{R}$ (2,366 K) with $P_3 = P_1 = 11.8$ psia (81.4 kPa). Figure 8 is a summary of the thermodynamic properties in the flow field and around the target.

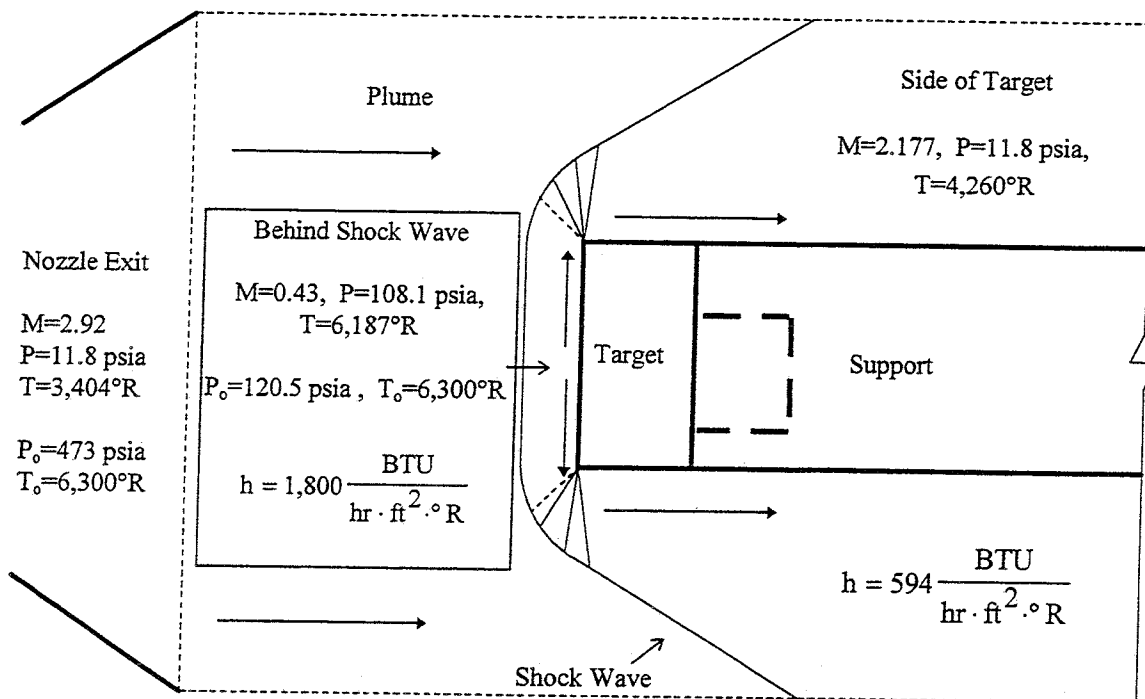


Figure 8. Thermodynamic Conditions in the Flow Field

Semi-Infinite Approximation of Target Material

Since small residence times are expected, a semi-infinite slab approximation of the target material was used to get an estimate of the safe residence time. This estimate assumes that the target and support material are made of the same material and that the curved surfaces are insulated. The approximation is given by Holman (1990):

$$\frac{T_s - T_i}{T_\infty - T_i} = 1 - e^{-\frac{h^2 \alpha t}{k^2}} \left[1 - \operatorname{erf} \left(\frac{h \sqrt{\alpha t}}{k} \right) \right] \quad (20)$$

where T_s = critical temperature

T_i = initial temperature = 540°R

T_∞ = environment temperature = 6,187°R

h = heat transfer coefficient = 1,800 BTU/hr-ft²·°R

α = thermal diffusivity of target material

k = thermal conductivity of target material

t = safe residence time.

Estimates of the safe residence time were made for aluminum and copper. The thermal properties of these materials and the steel probe arm are listed in Table 2. Aluminum and copper were chosen as target materials because of their relatively high thermal diffusivity, low hardness, and low cost. High thermal diffusivity is required because of the high rate of heat transfer and high environment temperature. A high thermal diffusivity allows a material to dissipate heat from a point quickly. Low hardness is required because it is desirable to have deep, distinct craters instead of shallow craters that are difficult to locate. Safe residence times for aluminum and copper were estimated to be 77 ms and 784 ms, respectively. The importance of this calculation is that the safe residence time for the actual probe, with convective heat transfer to the flat and curved surfaces, must be less than 77 ms.

Table 2. Properties of Materials Used in Thermal Calculations

	Density lbm/ft ³	Specific Heat BTU/lbm·°R	Conductivity BTU/hr·ft·°R	Critical Temperature °R
Steel	487	112x10 ⁻³	24.8	1960
Copper	559	917x10 ⁻⁴	223	1830
Aluminum	167	207x10 ⁻³	127	1260

Finite-Difference Formulation of Thermal Response Problem

An exact solution of Eqn. (1) with the boundary conditions and initial condition given by Eqn. (2) through Eqn. (10) is difficult because of the geometry. A finite-difference approximation is used instead with the node geometry shown in Figure 9.

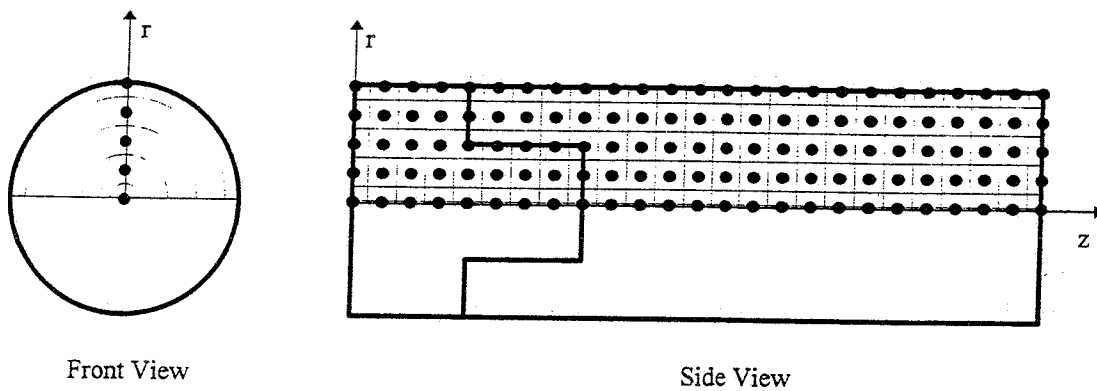


Figure 9. Node Geometry for Finite-Difference Formulation

The approximation uses the electrical analogy wherein thermal resistances between nodes and thermal capacitances of the nodal elements are used to model the flow of heat into or out of the node as if it were a flow of electricity as shown in Figure 10.

Thermal resistance to conduction and convection are modeled as

$$R_{\text{conduction}} = \frac{L}{kA}$$

$$R_{\text{convection}} = \frac{1}{hA}$$

where L = length in the conduction direction

k = thermal conductivity of the conducting material

h = heat transfer coefficient

A = conduction or convection area.

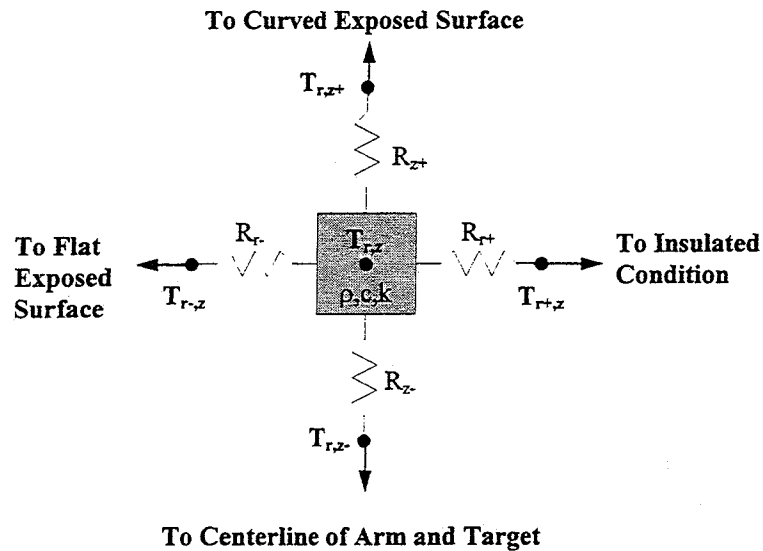


Figure 10. Electrical Analogy for Thermal Conduction Through a Node

Thermal capacitance is modeled as

$$C = \rho c V$$

where ρ = density of the material

c = specific heat of the material

V = volume of the node.

Nodes on a material interface require that the node be separated into a section for each material. Figure 11 illustrates a nodal volume where the z axis is directed perpendicular to the plane of the paper. The radial cross sectional areas for region A and region B are

$$\text{Area}_A = \frac{\pi}{2} \left[r\Delta r + \left(\frac{\Delta r}{2} \right)^2 \right] \quad (21)$$

$$\text{Area}_B = \frac{\pi}{2} \left[r\Delta r - \left(\frac{\Delta r}{2} \right)^2 \right] \quad (22)$$

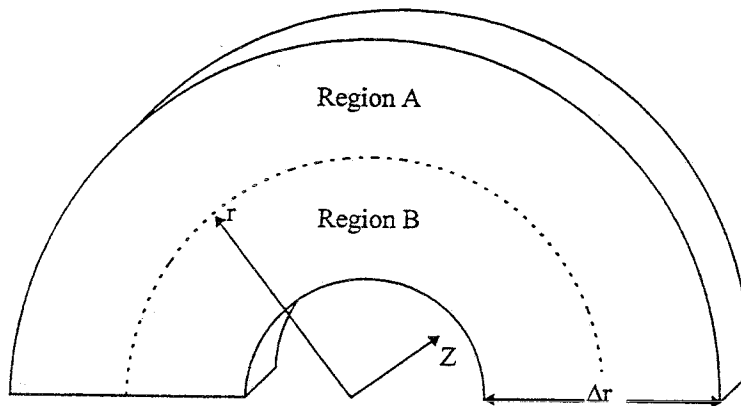


Figure 11. Nodal Volume for Finite-Difference Approximation

The radial cross section area for the entire volume is

$$\text{Area}_{A+B} = \pi r \Delta r \quad (23)$$

The finite-difference formulation for Eqn. (1), written in terms of thermal resistances and thermal capacitances, is (Holman, 1990)

$$T_i^{p+1} = \frac{\sum_j \frac{T_j^{p+1}}{R_{ij}} + \frac{C_i}{\Delta t} T_i^p}{\sum_j \frac{1}{R_{ij}} + \frac{C_i}{\Delta t}} \quad (24)$$

where p = current time

i = current node

j = nodes around node i

R_{ij} = thermal resistance for node ij

C_i = thermal capacitance for node i

Δt = time increment

T_i^p = temperature at node i for the current time step

T_i^{p+1} = temperature at node i for the next time step.

Eqn. (24) is written for each node in the system, and the equations are solved simultaneously for T_i^{p+1} . The equations for R_{ij} and C_i for each node are presented in Table 3. The nomenclature used in Table 3 is defined in Figure 12.

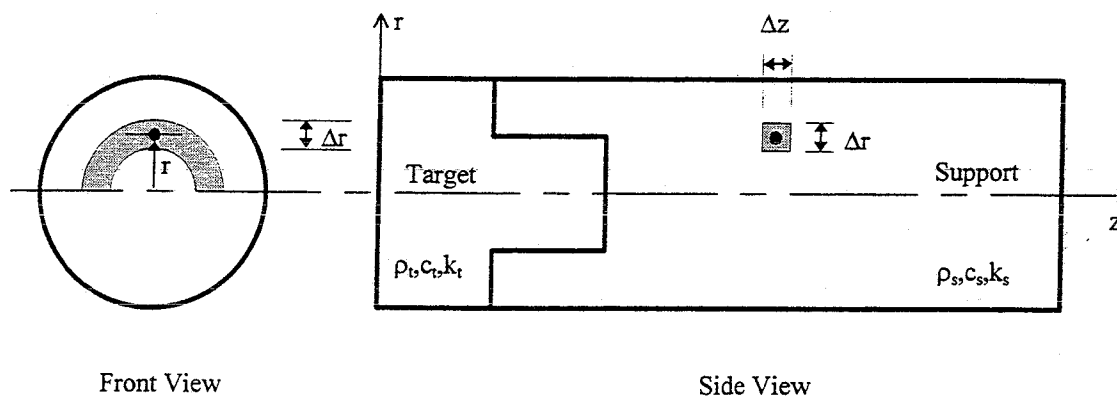
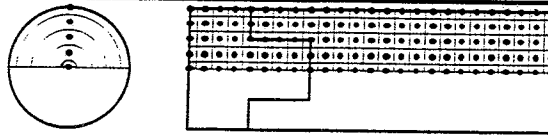


Figure 12. Nomenclature for Finite-Difference Formulation Parameters

The directions of $r+$ (radial directed towards the curved surface), $r-$ (radial directed towards the centerline), $z+$ (axial directed towards the insulated face), and $z-$ (axial directed towards the exposed face) are illustrated in Figure 10.

Table 3. Thermal Resistances and Capacitances for Specified Nodes

a. Centerline Convection Node



$$R_{r+} = \frac{\Delta r}{\pi \left(r + \frac{\Delta r}{2} \right) \frac{\Delta z}{2} k_t}$$

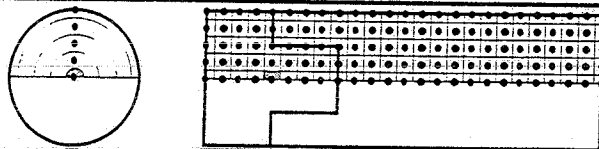
$$R_{z-} = \frac{1}{\frac{\pi}{8} \Delta r^2 h_2}$$

$$C_i = \rho_t c_t \left(\frac{\pi}{8} \Delta r^2 \frac{\Delta z}{2} \right)$$

$$R_{z+} = \frac{\Delta z}{\frac{\pi}{8} \Delta r^2 k_t}$$

$$R_{r-} = \infty$$

b. Centerline Target Node



$$R_{r+} = \frac{\Delta r}{\pi \left(r + \frac{\Delta r}{2} \right) \Delta z k_t}$$

$$R_{z-} = \frac{\Delta z}{\frac{\pi}{8} \Delta r^2 k_t}$$

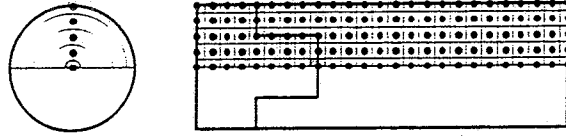
$$C_i = \rho_t c_t \left(\frac{\pi}{8} \Delta r^2 \Delta z \right)$$

$$R_{z+} = \frac{\Delta z}{\frac{\pi}{8} \Delta r^2 k_t}$$

$$R_{r-} = \infty$$

Table 3. (continued)

c. Centerline Target-Support Node



$$R_{r+} = \frac{\Delta r}{\pi \left(r + \frac{\Delta r}{2} \right) \frac{\Delta z}{2}} \left(\frac{1}{k_s} + \frac{1}{k_t} \right)$$

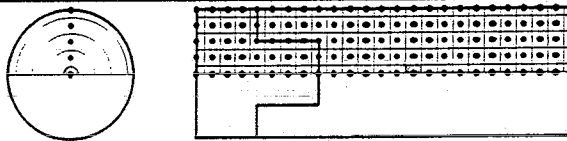
$$R_{z-} = \frac{\Delta z}{\frac{\pi}{8} \Delta r^2 k_t}$$

$$C_i = (\rho_t c_t + \rho_s c_s) \left(\frac{\pi}{8} \Delta r^2 \frac{\Delta z}{2} \right)$$

$$R_{z+} = \frac{\Delta z}{\frac{\pi}{8} \Delta r^2 k_s}$$

$$R_{r-} = \infty$$

d. Centerline Support Node



$$R_{r+} = \frac{\Delta r}{\pi \left(r + \frac{\Delta r}{2} \right) \Delta z k_s}$$

$$R_{z-} = \frac{\Delta z}{\frac{\pi}{8} \Delta r^2 k_s}$$

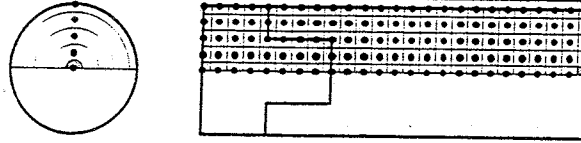
$$C_i = \rho_s c_s \left(\frac{\pi}{8} \Delta r^2 \Delta z \right)$$

$$R_{z+} = \frac{\Delta z}{\frac{\pi}{8} \Delta r^2 k_s}$$

$$R_{r-} = \infty$$

Table 3. (continued)

e. Centerline Insulated Node



$$R_{r+} = \frac{\Delta r}{\pi \left(r + \frac{\Delta r}{2} \right) \frac{\Delta z}{2} k_s}$$

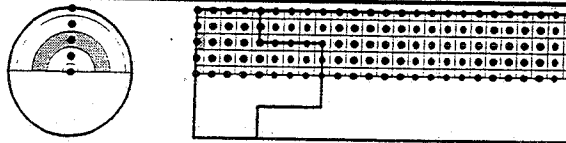
$$R_{zj-} = \frac{\Delta z}{\frac{\pi}{8} \Delta r^2 k_s}$$

$$C_i = \rho_s c_s \left(\frac{\pi}{8} \Delta r^2 \frac{\Delta z}{2} \right)$$

$$R_{z+} = \infty$$

$$R_{r-} = \infty$$

f. Full Node on the Exposed Flat Face



$$R_{r+} = \frac{\Delta r}{\pi \left(r + \frac{\Delta r}{2} \right) \frac{\Delta z}{2} k_t}$$

$$R_{z-} = \frac{1}{\pi r \Delta r h_2}$$

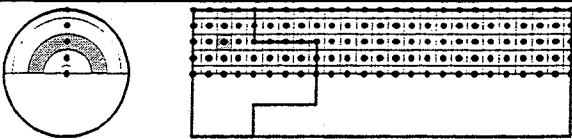
$$C_i = \rho_t c_t \left(\pi r \Delta r \frac{\Delta z}{2} \right)$$

$$R_{z+} = \frac{\Delta z}{\pi r \Delta r k_t}$$

$$R_{r-} = \frac{\Delta r}{\pi \left(r - \frac{\Delta r}{2} \right) \frac{\Delta z}{2} k_t}$$

Table 3. (continued)

g. Full Node in the Target Material



$$R_{r+} = \frac{\Delta r}{\pi \left(r + \frac{\Delta r}{2} \right) \Delta z k_t}$$

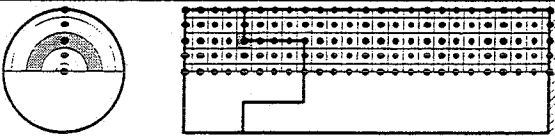
$$R_{z-} = \frac{\Delta z}{\pi r \Delta r k_t}$$

$$C_i = \rho_t c_t (\pi r \Delta r \Delta z)$$

$$R_{z+} = \frac{\Delta z}{\pi r \Delta r k_t}$$

$$R_{r-} = \frac{\Delta r}{\pi \left(r - \frac{\Delta r}{2} \right) \Delta z k_t}$$

h. Front Corner Node Along the Longitudinal Material Interface



$$R_{r+} = \frac{\Delta r}{\pi \left(r + \frac{\Delta r}{2} \right) \frac{\Delta z}{2}} \left(\frac{1}{k_s} + \frac{1}{k_t} \right)$$

$$R_{z-} = \frac{\Delta z}{\pi r \Delta r k_t}$$

$$C_i = \rho_t c_t \pi r \Delta r \frac{\Delta z}{2}$$

$$+ \rho_t c_t \frac{\pi}{2} \left(r \Delta r - \frac{\Delta r^2}{4} \right) \frac{\Delta z}{2}$$

$$+ \rho_s c_s \frac{\pi}{2} \left(r \Delta r + \frac{\Delta r^2}{4} \right) \frac{\Delta z}{2}$$

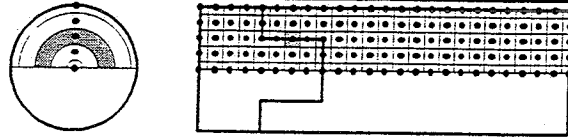
$$R_{z+} = \frac{\Delta z}{\frac{\pi}{2} \left(r \Delta r + \frac{\Delta r^2}{4} \right) k_s}$$

$$+ \frac{\Delta z}{\frac{\pi}{2} \left(r \Delta r - \frac{\Delta r^2}{4} \right) k_t}$$

$$R_{r-} = \frac{\Delta r}{\pi \left(r - \frac{\Delta r}{2} \right) \Delta z k_t}$$

Table 3. (continued)

i. Node Along the Longitudinal Material Interface



$$R_{r+} = \frac{\Delta r}{\pi \left(r + \frac{\Delta r}{2} \right) \Delta z k_s}$$

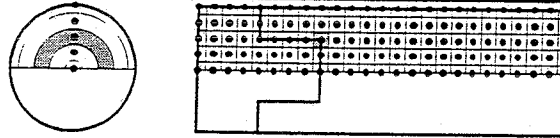
$$R_{z-} = \frac{\Delta z}{\frac{1}{2} \pi \left(\frac{\Delta r^2}{4} + r \Delta r \right) k_s} + \frac{\Delta z}{\frac{1}{2} \pi \left(r \Delta r - \frac{\Delta r^2}{4} \right) k_t}$$

$$C_i = \rho_s c_s \left[\frac{1}{2} \pi \left(\frac{\Delta r^2}{4} + r \Delta r \right) \Delta z \right] + \rho_t c_t \left[\frac{1}{2} \pi \left(r \Delta r - \frac{\Delta r^2}{4} \right) \Delta z \right]$$

$$R_{z+} = \frac{\Delta z}{\frac{1}{2} \pi \left(\frac{\Delta r^2}{4} + r \Delta r \right) k_s} + \frac{\Delta z}{\frac{1}{2} \pi \left(r \Delta r - \frac{\Delta r^2}{4} \right) k_t}$$

$$R_{r-} = \frac{\Delta r}{\pi \left(r - \frac{\Delta r}{2} \right) \Delta z k_t}$$

j. Rear Corner Node Along the Longitudinal Material Interface



$$R_{r+} = \frac{\Delta r}{\pi \left(r + \frac{\Delta r}{2} \right) \Delta z k_s}$$

$$R_{z-} = \frac{\Delta z}{\frac{1}{2} \pi \left(\frac{\Delta r^2}{4} + r \Delta r \right) k_s} + \frac{\Delta z}{\frac{1}{2} \pi \left(r \Delta r - \frac{\Delta r^2}{4} \right) k_t}$$

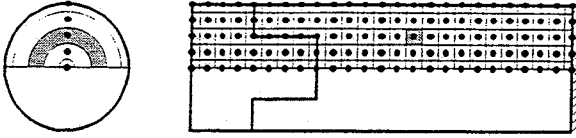
$$C_i = \rho_s c_s \left[\frac{1}{2} \pi \left(r \Delta r + \frac{\Delta r^2}{4} \right) \Delta z \right] + \frac{1}{2} \rho_t c_t \left[\frac{1}{2} \pi \left(r \Delta r - \frac{\Delta r^2}{4} \right) \Delta z \right] + \frac{1}{2} \rho_s c_s \left[\frac{1}{2} \pi \left(r \Delta r - \frac{\Delta r^2}{4} \right) \Delta z \right]$$

$$R_{z+} = \frac{\Delta z}{\pi r \Delta r k_s}$$

$$R_{r-} = \frac{\Delta r}{\pi \left(r - \frac{\Delta r}{2} \right) \frac{\Delta z}{2}} \left(\frac{1}{k_s} + \frac{1}{k_t} \right)$$

Table 3. (continued)

k. Full Node in the Support Material

	$R_{r+} = \frac{\Delta r}{\pi \left(r + \frac{\Delta r}{2} \right) \Delta z k_s}$	
$R_{z-} = \frac{\Delta z}{\pi r \Delta r k_s}$	$C_i = \rho_s c_s (\pi r \Delta r \Delta z)$	$R_{z+} = \frac{\Delta z}{\pi r \Delta r k_s}$
	$R_{r-} = \frac{\Delta r}{\pi \left(r - \frac{\Delta r}{2} \right) \Delta z k_s}$	

l. Node Along the Insulated Boundary

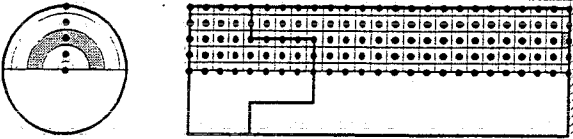
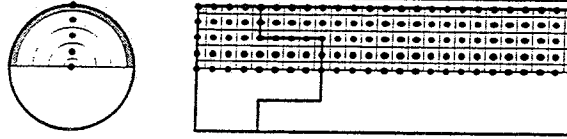
	$R_{r+} = \frac{\Delta r}{\pi \left(r + \frac{\Delta r}{2} \right) \frac{\Delta z}{2} k_s}$	
$R_{z-} = \frac{\Delta z}{\pi r \Delta r k_s}$	$C_i = \rho_s c_s \left(\pi r \Delta r \frac{\Delta z}{2} \right)$	$R_{z+} = \infty$
	$R_{r-} = \frac{\Delta r}{\pi \left(r - \frac{\Delta r}{2} \right) \frac{\Delta z}{2} k_s}$	

Table 3. (continued)

m. Convection Corner Node



$$R_{r+} = \frac{1}{\pi r \frac{\Delta z}{2} h_3}$$

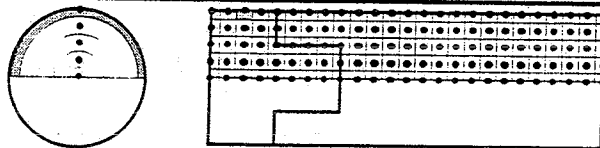
$$R_{z-} = \frac{1}{\frac{\pi}{2} \left(r \Delta r - \frac{\Delta r^2}{4} \right) h_2}$$

$$C_i = \rho_t c_t \left[\frac{\pi}{2} \left(r \Delta r - \frac{\Delta r^2}{4} \right) \frac{\Delta z}{2} \right]$$

$$R_{z+} = \frac{\Delta z}{\frac{\pi}{2} \left(r \Delta r - \frac{\Delta r^2}{4} \right) k_t}$$

$$R_{r-} = \frac{\Delta r}{\pi \left(r - \frac{\Delta r}{2} \right) \frac{\Delta z}{2} k_t}$$

n. Target Node on the Curved Exterior Surface



$$R_{r+} = \frac{1}{\pi r \Delta z h_3}$$

$$R_{z-} = \frac{\Delta z}{\frac{\pi}{2} \left(r \Delta r - \frac{\Delta r^2}{4} \right) k_t}$$

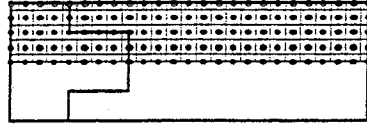
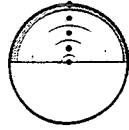
$$C_i = \rho_t c_t \left[\frac{\pi}{2} \left(r \Delta r - \frac{\Delta r^2}{4} \right) \Delta z \right]$$

$$R_{z+} = \frac{\Delta z}{\frac{\pi}{2} \left(r \Delta r - \frac{\Delta r^2}{4} \right) k_t}$$

$$R_{r-} = \frac{\Delta r}{\pi \left(r - \frac{\Delta r}{2} \right) \Delta z k_t}$$

Table 3. (continued)

o. Nodes on the Material Boundary on the Curved Exterior Surface



$$R_{r+} = \frac{1}{\pi r \Delta z h_3}$$

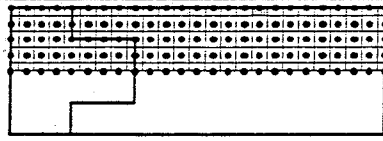
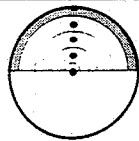
$$R_{z-} = \frac{\Delta z}{\frac{\pi}{2} \left(r \Delta r - \frac{\Delta r^2}{4} \right) k_t}$$

$$C_i = \left[\frac{1}{2} \rho_t c_t + \frac{1}{2} \rho_s c_s \right] \left[\frac{\pi}{2} \left(r \Delta r - \frac{\Delta r^2}{4} \right) \Delta z \right]$$

$$R_{z+} = \frac{\Delta z}{\frac{\pi}{2} \left(r \Delta r - \frac{\Delta r^2}{4} \right) k_s}$$

$$R_{r-} = \frac{\Delta r}{\pi \left(r - \frac{\Delta r}{2} \right) \frac{\Delta z}{2}} \left(\frac{1}{k_s} + \frac{1}{k_t} \right)$$

p. Support Node on the Curved Exterior Surface



$$R_{r+} = \frac{1}{\pi r \Delta z h_3}$$

$$R_{z-} = \frac{\Delta z}{\frac{\pi}{2} \left(r \Delta r - \frac{\Delta r^2}{4} \right) k_s}$$

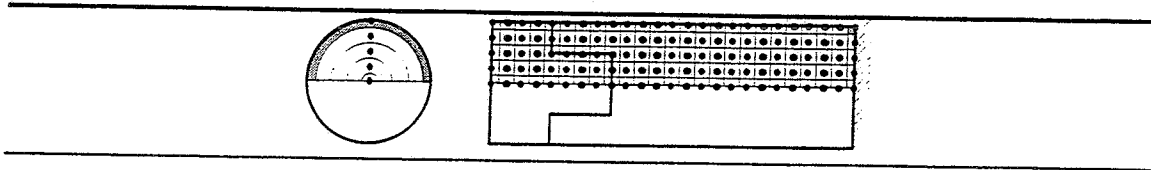
$$C_i = \rho_s c_s \left[\frac{\pi}{2} \left(r \Delta r - \frac{\Delta r^2}{4} \right) \Delta z \right]$$

$$R_{z+} = \frac{\Delta z}{\frac{\pi}{2} \left(r \Delta r - \frac{\Delta r^2}{4} \right) k_s}$$

$$R_{r-} = \frac{\Delta r}{\pi \left(r - \frac{\Delta r}{2} \right) \Delta z k_s}$$

Table 3. (continued)

q. Insulated Node on the Curved Exterior Surface



$$R_{r+} = \frac{1}{\pi r \frac{\Delta z}{2} h_3}$$

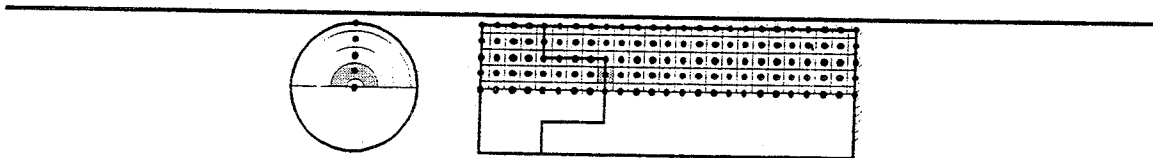
$$R_{z-} = \frac{\Delta z}{\frac{\pi}{2} \left(r \Delta r - \frac{\Delta r^2}{4} \right) k_s}$$

$$C_i = \rho_s c_s \left[\frac{\pi}{2} \left(r \Delta r - \frac{\Delta r^2}{4} \right) \frac{\Delta z}{2} \right]$$

$$R_{z+} = \infty$$

$$R_{r-} = \frac{\Delta r}{\pi \left(r - \frac{\Delta r}{2} \right) \frac{\Delta z}{2} k_s}$$

r. Node Along a Radial Material Boundary



$$R_{r+} = \frac{\Delta r}{\pi \left(r + \frac{\Delta r}{2} \right) \frac{\Delta z}{2}} \left(\frac{1}{k_s} + \frac{1}{k_t} \right)$$

$$R_{z-} = \frac{\Delta z}{\pi r \Delta r k_t}$$

$$C_i = \left(\frac{1}{2} \rho_t c_t + \frac{1}{2} \rho_s c_s \right) (\pi r \Delta r \Delta z)$$

$$R_{z+} = \frac{\Delta z}{\pi r \Delta r k_s}$$

$$R_{r-} = \frac{\Delta r}{\pi \left(r - \frac{\Delta r}{2} \right) \frac{\Delta z}{2}} \left(\frac{1}{k_s} + \frac{1}{k_t} \right)$$

Results of the Finite-Difference Analysis

Temperature profiles for three inches of target and support material were calculated. There are 10 nodes in the radial direction and 120 nodes in the axial direction. The distance between nodes in both the radial and axial directions is 0.025 inches (0.635 cm). There is convection heat transfer into both exposed surfaces as shown in Figure 8. A safe residence time is calculated to be 51 ms as shown in Table 4. Table 4 also shows that the semi-infinite approximation is not acceptable for this problem because of the convection heat transfer into the sides.

Table 4. Safe Residence Times

	Semi-Infinite Approximation (sides insulated)	Finite-Difference Approximation (sides insulated)	Finite-Difference Approximation (actual case)
	ms	ms	ms
Copper	784	754	384
Aluminum	77	79	51

Figures 13 through 21 present the results of the calculations. The temperature increases faster near the corner of the front surface, as shown in Figures 13 and 14, because of the heating of the corner from both the front and the side. Moreover, aluminum heats up faster than copper because of the lower value of thermal diffusivity for aluminum, 1.02×10^{-3} ft²/sec (9.48×10^{-5} m²/sec) compared to 1.21×10^{-3} ft²/sec (1.12×10^{-4} m²/sec) for copper.

Figure 15 indicates that the high temperature region has not penetrated very deeply into the aluminum target when the corner of the front face reaches the critical

temperature. Copper shows greater penetration when the critical temperature is reached, as seen in Figure 16, and the influence of the lower conductivity of steel is seen in the slope at the centerline interface between the target and support materials.

Figure 17 indicates that the exposed curved surface of the aluminum target heats up most at the edge, which agrees with Figure 13. The temperature along the curved exposed surface decreases sharply until the target support interface is reached. This temperature decrease is caused by the lower heat transfer coefficient and the lower temperature on the side of the target. The change in slope at the material interface is caused by the lower conductivity of the steel.

Figure 18 indicates that the heat penetrates deeper into the copper target than the aluminum target (Figure 17) along the exposed curved surface again because of the lower thermal diffusivity of aluminum. Figures 19 and 20 indicate that the outer edge of the aluminum and copper targets heat up faster than the centerline, as would be expected. These figures also indicate that, when the outer edge of the exposed flat face starts to fail, the centerline has not failed. Therefore, if the safe residence time is exceeded, useful data may still be gathered from the interior of the target. Figure 21 further indicates this possibility by showing the difference between the centerline temperature and the corner temperature of the exposed flat face. The finite-difference program is found in Appendix A, and the data represented in the Figures 13 through 21 are tabulated in Appendix B.

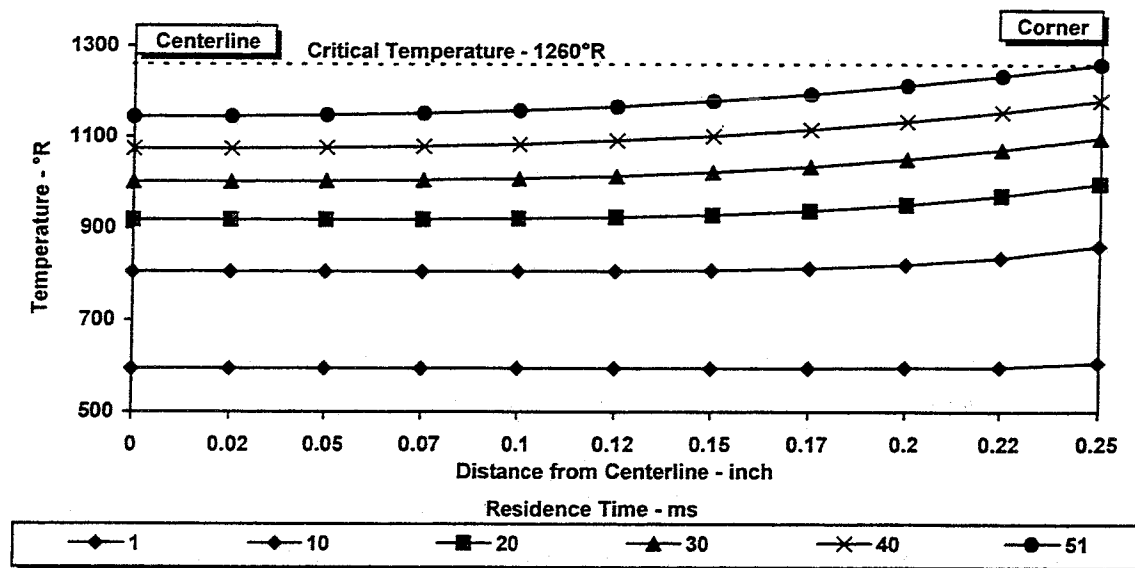


Figure 13. Temperature Profiles Along Exposed Flat Surface of Aluminum Target

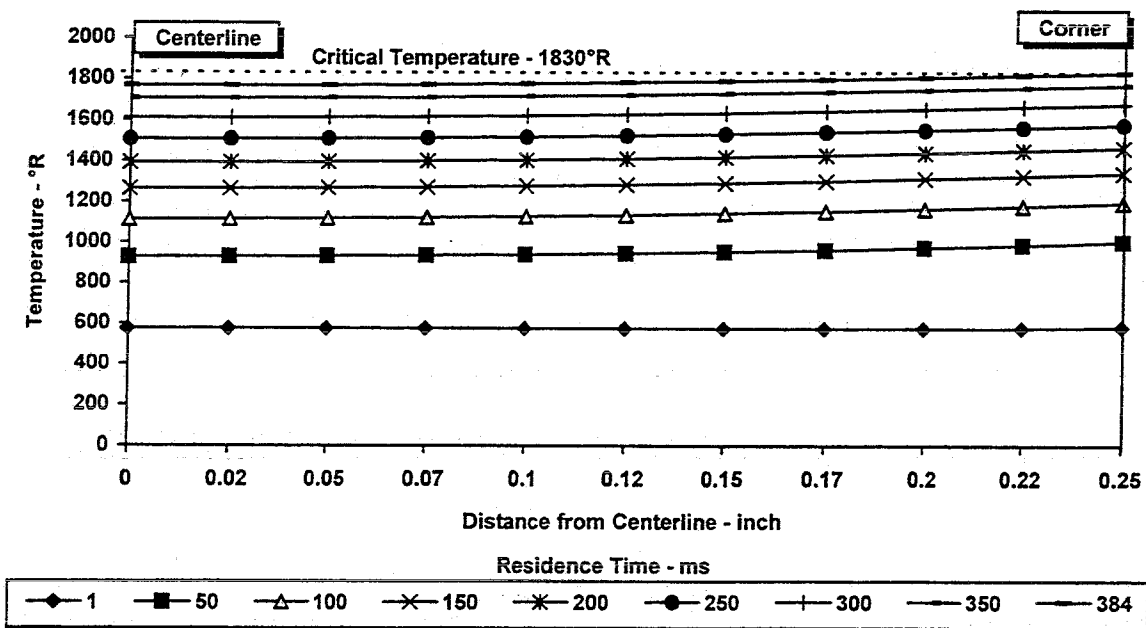


Figure 14. Temperature Profiles Along Exposed Flat Surface of Copper Target

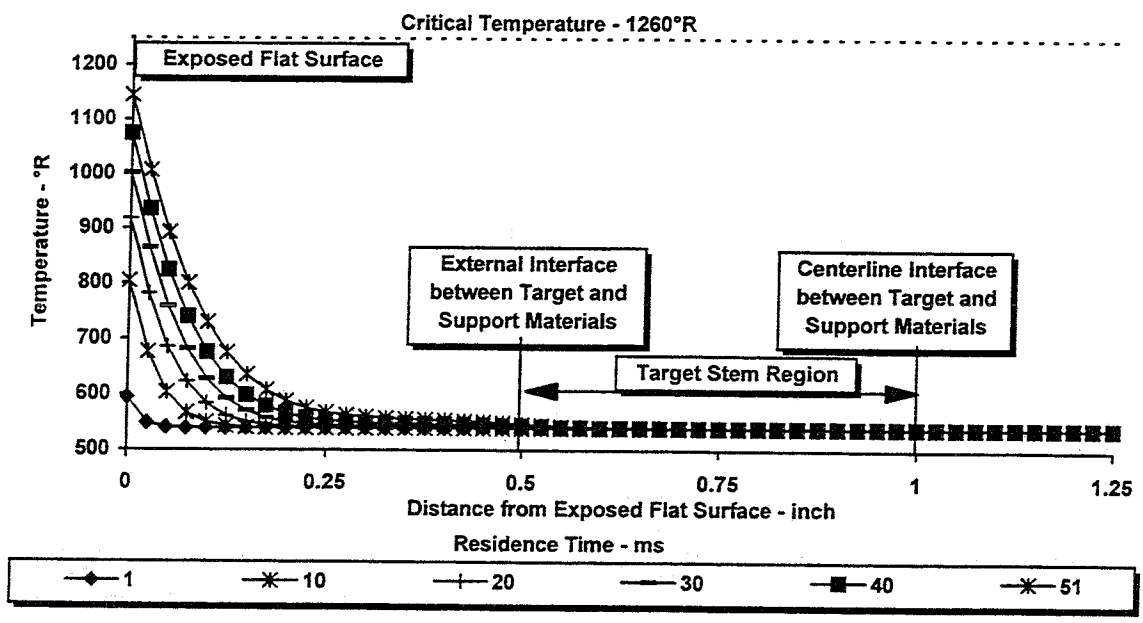


Figure 15. Temperature Profiles Along Centerline of Aluminum Target and Steel Holder

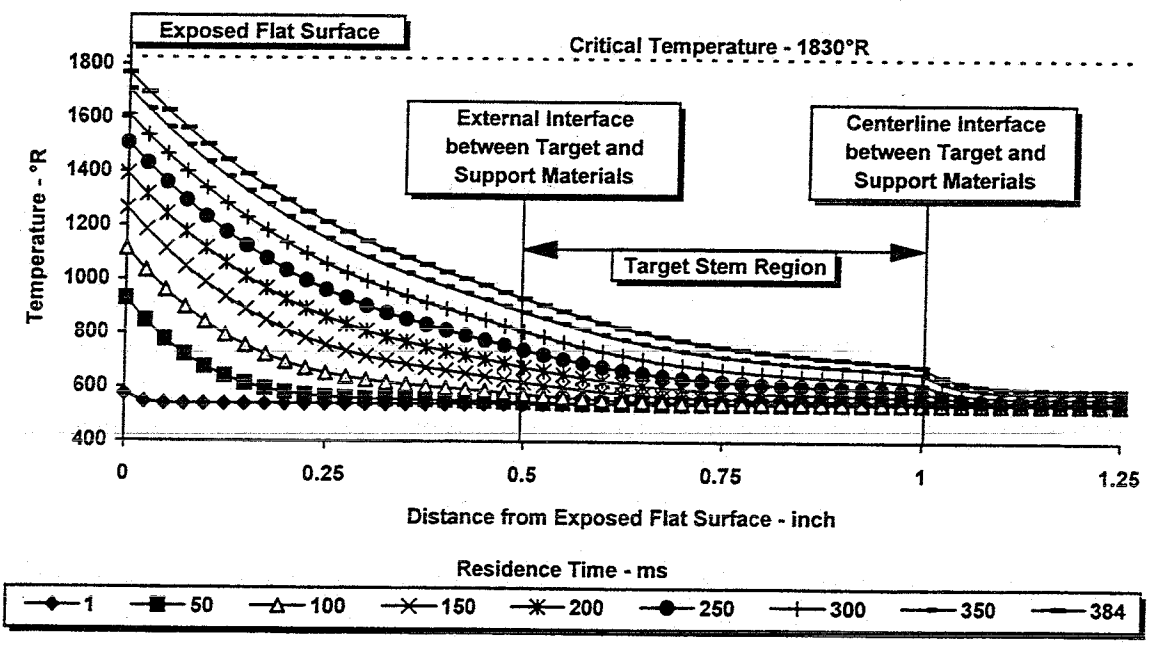


Figure 16. Temperature Profiles Along Centerline of Copper Target and Steel Holder

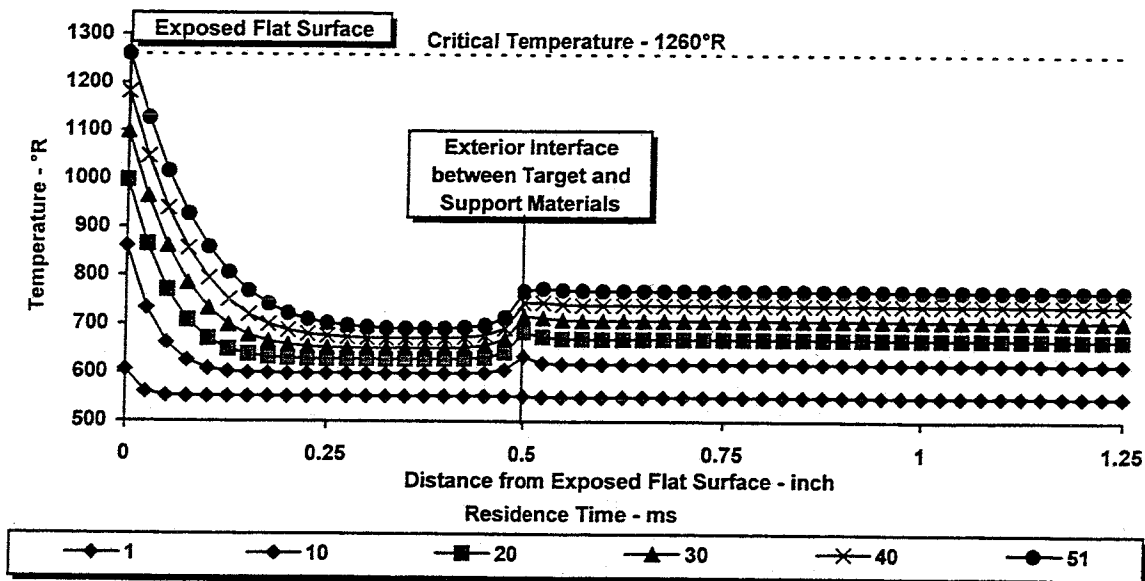


Figure 17. Temperature Profiles Along Exposed Curved Surface of Aluminum Target and Steel Holder

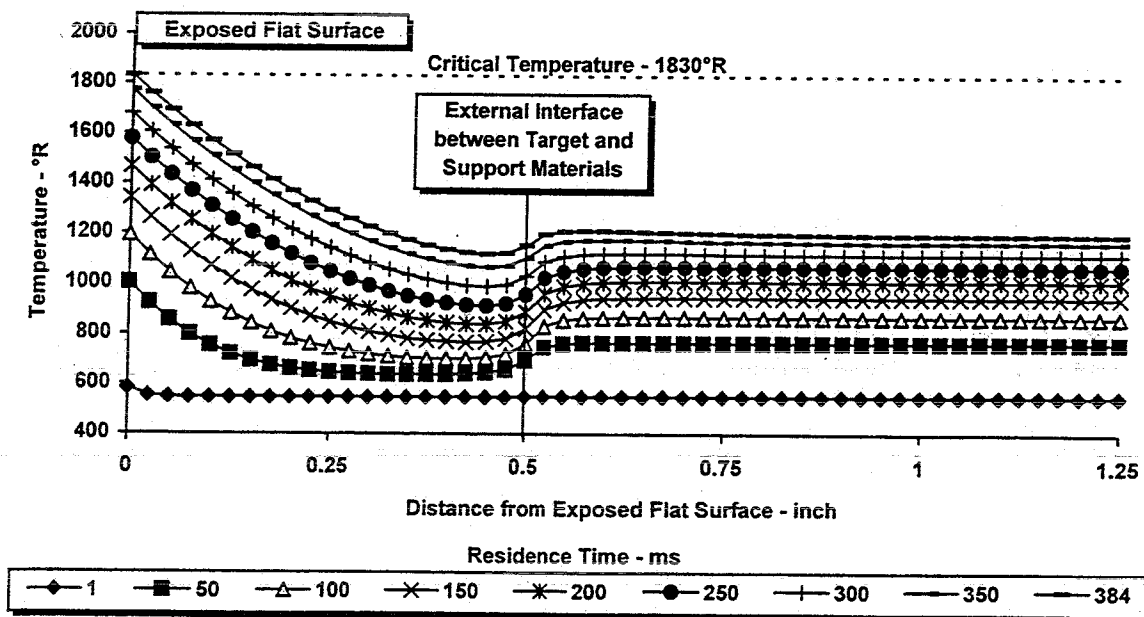


Figure 18. Temperature Profiles Along Exposed Curved Surface of Copper Target and Steel Holder

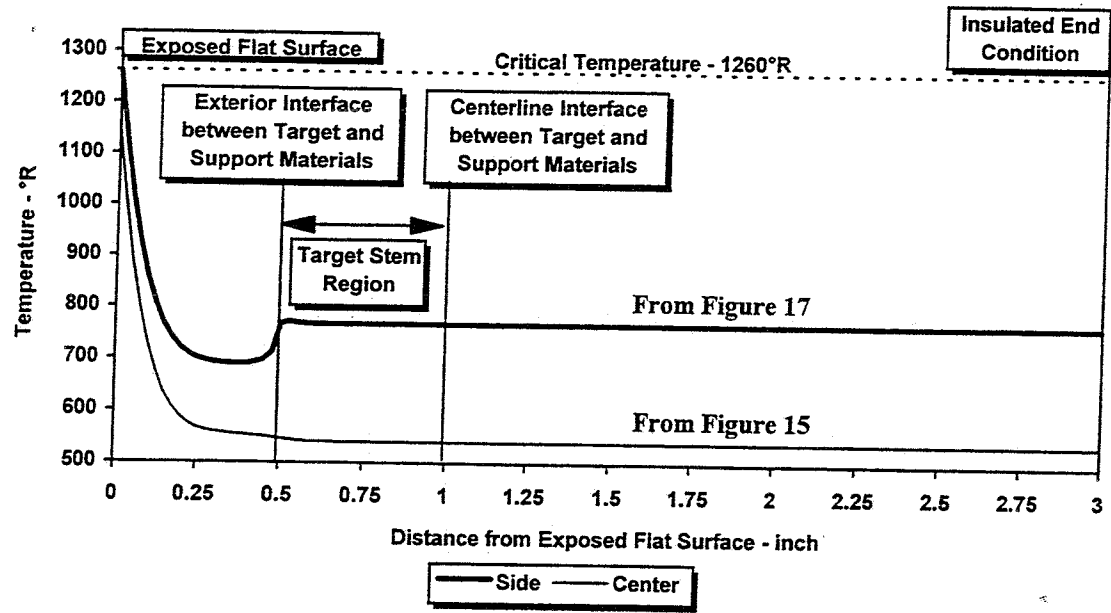


Figure 19. Axial Temperatures for Aluminum Target and Steel Holder at Thermal Failure (t = 51 ms)

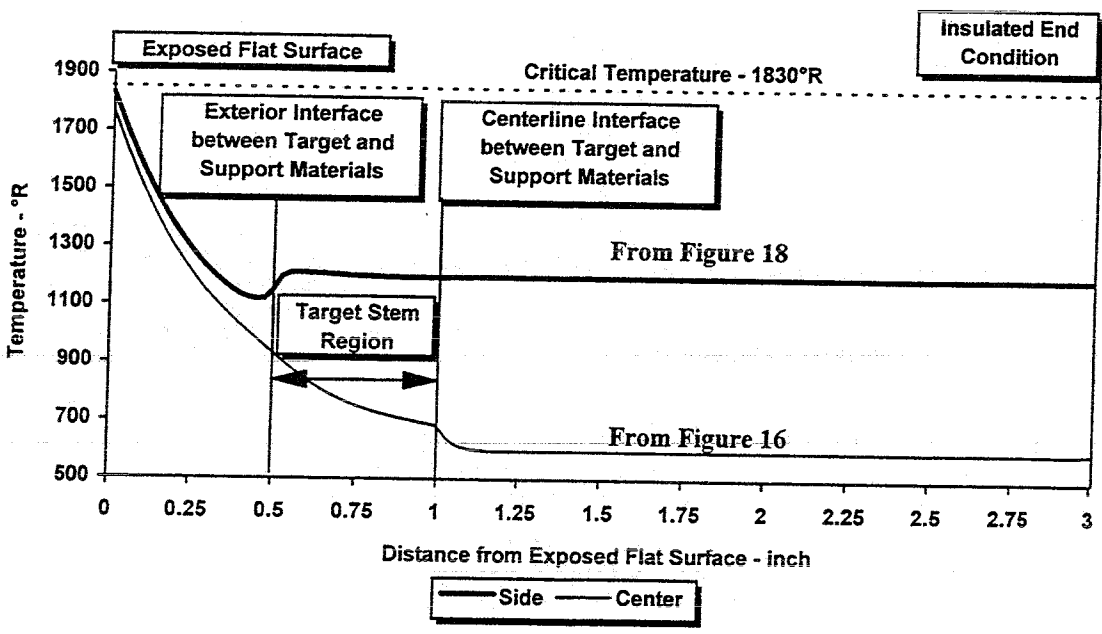


Figure 20. Axial Temperatures for a Copper Target and Steel Holder at Thermal Failure (t = 384 ms)

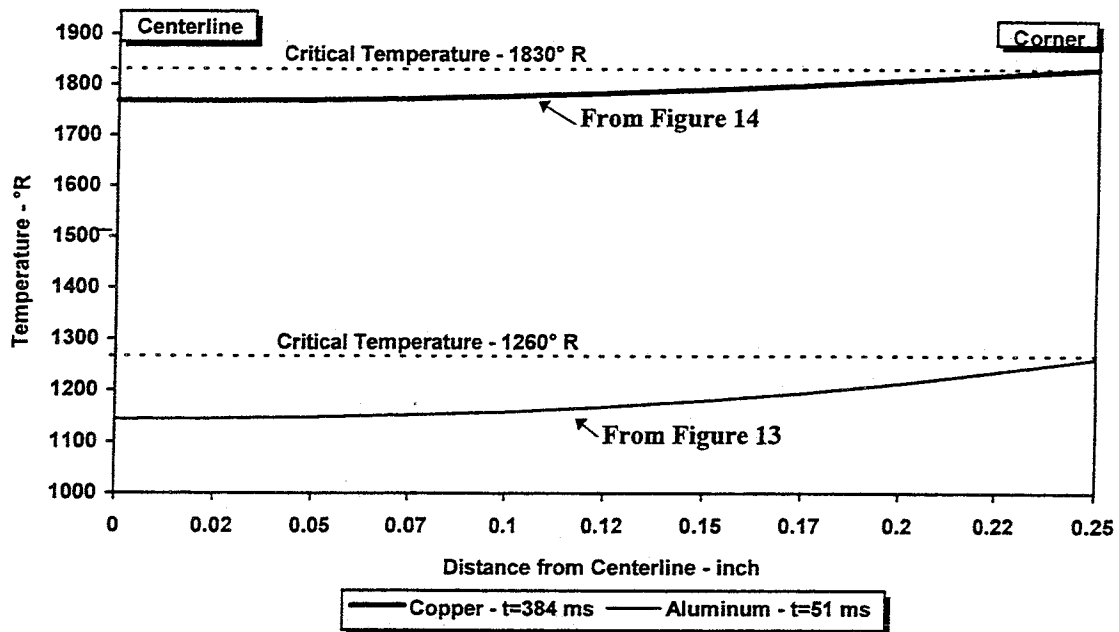


Figure 21. Temperature of Exposed Flat Surface at Thermal Failure

CHAPTER 4

KINETIC RESPONSE OF PARTICLES IN THE EXHAUST

Development of Particle Velocity Governing Equations

The flow near the exit plane will typically be supersonic so that a near-normal bow shock will be present upstream of the target as shown in Figure 22.

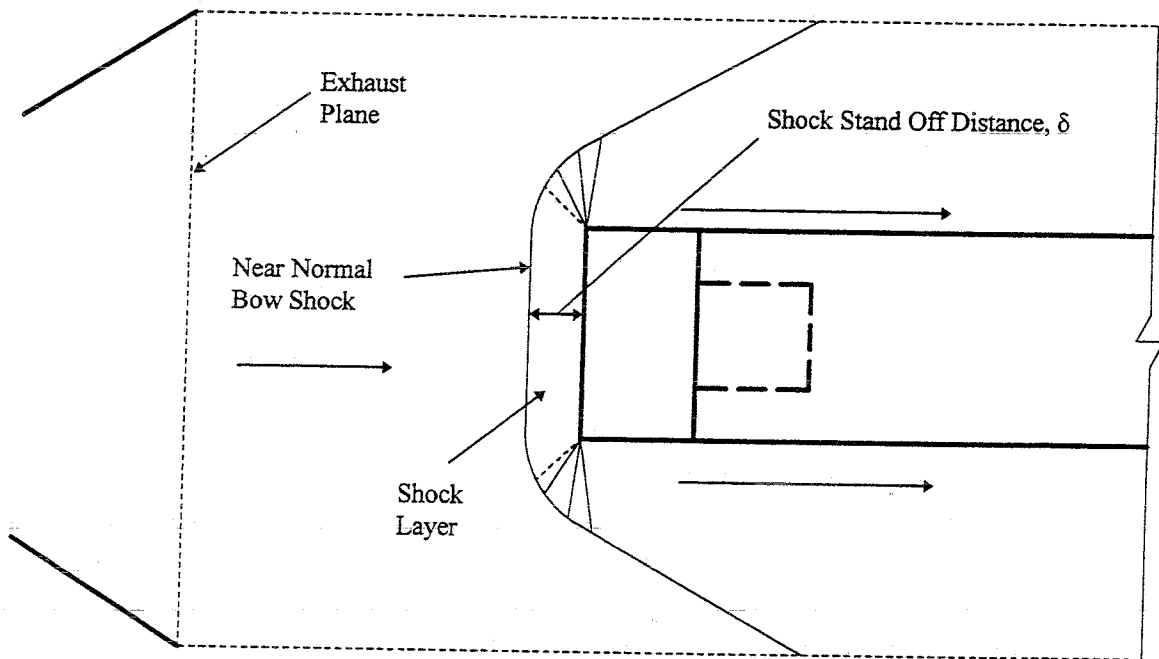


Figure 22. Bow Shock in Front of Target

The particles that impact the surface of the target will experience some deceleration in the shock layer between the bow shock and the surface. It is expected that the deceleration

will be large for sufficiently small particles and negligible for sufficiently large particles.

It is necessary to model the velocities of the particles in the plume both before and after they encounter the shock. The particle velocity immediately upstream of the shock serves as a boundary condition for the determination of the velocity of the particle in the shock layer. This boundary condition allows the calculation of the particle impact velocity, which is an input to the ballistic impact computer code used to calculate the expected impact crater depth and diameter.

The force on the particle is given by

$$F = \frac{1}{2} C_d \rho_g A_p V_r^2 \quad (25)$$

where F = force on the particle

C_d = coefficient of drag for the particle

ρ_g = gas density

A_p = cross-sectional area of the particle

V_r = velocity of particle relative to gas.

Newton's second law of motion also gives the force on the particle as

$$F = m_p V_p \frac{dV_p}{dx} \quad (26)$$

where m_p = mass of the particle

V_p = particle velocity

x = axial distance.

These two equations are combined to give the particle velocity before it enters the bow shock (Callens, 1994):

$$\frac{dV_p}{dx} = \frac{C_d \rho_g A_p}{2m_p} \left(V_p - 2V_g + \frac{V_g^2}{V_p} \right) \quad (27)$$

where V_g = gas velocity. After manipulation, Eqn. (27) becomes

$$\frac{2\rho_p v_p}{C_d \rho_g A_p} V_p \frac{dV_p}{dx} - V_p^2 - 2V_g V_p - V_g^2 = 0 \quad (28)$$

where ρ_p = particle density

v_p = particle volume.

By making the substitutions

$$\begin{aligned} a &= \frac{2\rho_p v_p}{C_d \rho_g A_p} & b &= -1 \\ c &= 2V_g & d &= -V_g^2 \end{aligned} \quad (29)$$

Eqn. (28) becomes

$$aV_p \frac{dV_p}{dx} + bV_p^2 + cV_p + d = 0 \quad (30)$$

This equation is used to model the particle velocity in the plume.

Solution Method for the Particle Velocity Equation

A finite difference approximation of Eqn. (30) is obtained by replacing V_p and the derivative by their finite difference equivalents. The result is

$$a \left(\frac{V_{P_{i+1}} + V_{P_i}}{2} \right) \left(\frac{V_{P_{i+1}} - V_{P_i}}{\Delta x} \right) + b \left(\frac{V_{P_{i+1}} + V_{P_i}}{2} \right)^2 + c \left(\frac{V_{P_{i+1}} + V_{P_i}}{2} \right) + d = 0 \quad (31)$$

Through manipulation, Eqn. (31) becomes the quadratic equation

$$\left(\frac{a}{\Delta x} + \frac{b}{2} \right) V_{P_{i+1}}^2 + (bV_{P_i} + c)V_{P_{i+1}} + \left[V_{P_i}^2 \left(\frac{b}{2} - \frac{a}{\Delta x} \right) + cV_{P_i} + 2d \right] = 0 \quad (32)$$

The values for a and d should also be replaced with

$$a = \frac{2\rho_p v_p}{C_d \left(\frac{\rho_{g_{i+1}} + \rho_{g_i}}{2} \right) A_p} \quad d = \frac{V_{g_{i+1}} + V_{g_i}}{2} \quad (33)$$

to make the finite difference approximation valid.

Before Eqn. (32) can be solved, ρ_g and V_g must be known at node i and $i+1$.

Determining these values requires the assumption of a typical nozzle shape. One-half of the nozzle is assumed to be of the shape shown in Figure 23. This shape is defined by the relations

$$\frac{A}{A^*} = \frac{\left(A_c - \frac{A_c + A^*}{2} \right) \cos\left(\frac{\pi x}{x^*} \right) + \frac{A_c + A^*}{2}}{A^*} \quad 0 \leq \frac{x}{x^*} \leq 1 \quad (34)$$

$$\frac{A}{A^*} = \frac{\left(A_e - \frac{A_e + A^*}{2} \right) \cos\left(\frac{\pi(x - x_e)}{x^* - x_e} \right) + \frac{A_e + A^*}{2}}{A^*} \quad 1 \leq \frac{x}{x^*} \leq \frac{x_e}{x^*}$$

where x = distance from the combustion chamber to the point of interest

x_e = distance from the combustion chamber to the exhaust plane

x^* = distance x from the combustion chamber to the throat

A = cross-sectional area at x

A_c = cross-sectional area in the combustion chamber

A_e = cross-sectional area at the exhaust plane

A^* = cross-sectional area at the throat.

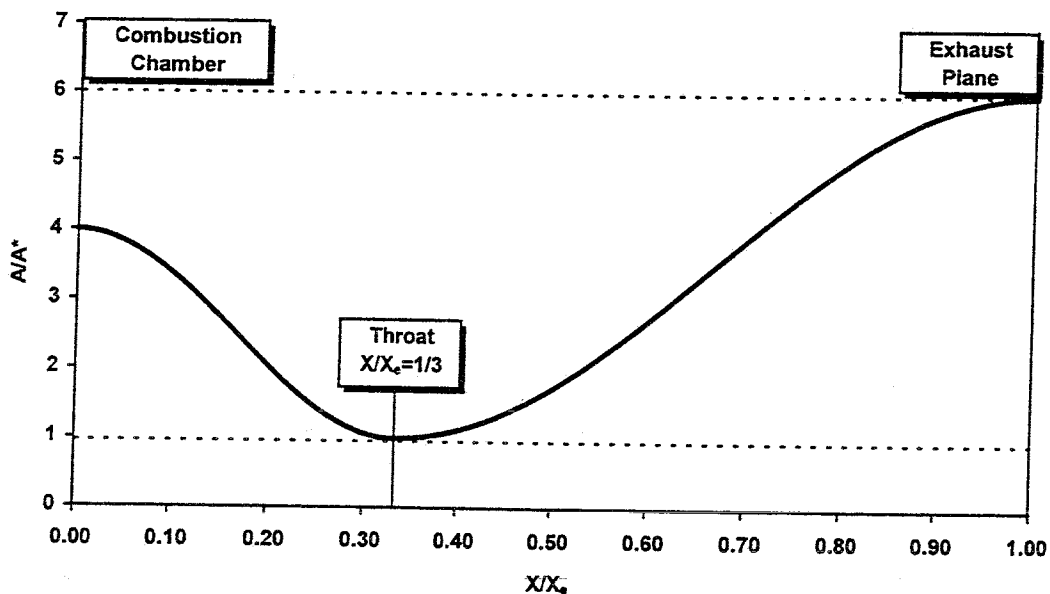


Figure 23. Assumed Nozzle Shape

The value of A/A^* is assumed to be 6 (Callens, 1994) because this value is typical for hybrid rocket engines.

The nodal values for M , V_g , and ρ_g are determined from the relations (John, 1984)

$$\frac{A^*}{A} = \left(\frac{\gamma + 1}{2} \right)^{\frac{\gamma + 1}{2(\gamma - 1)}} M \left(1 + \frac{\gamma - 1}{2} M^2 \right)^{-\frac{\gamma + 1}{2(\gamma - 1)}} \quad (35)$$

$$\left(\frac{V_g}{a^*} \right)^2 = \frac{\gamma + 1}{2} M^2 \left(1 + \frac{\gamma - 1}{2} M^2 \right)^{-1} \quad (36)$$

$$\frac{\rho_g}{\rho_t} = \left(1 + \frac{\gamma - 1}{2} M^2\right)^{-\frac{1}{\gamma - 1}} \quad (37)$$

where M = mach number of the gas

γ = ratio of specific heats for the gas

a^* = speed of sound at the throat

ρ_t = stagnation density of the gas.

Speed of sound at the throat is calculated from (John, 1984)

$$a^* = \sqrt{\gamma R T^*} \quad (38)$$

where R = exhaust gas constant = 2,093 ft²/sec²·°R (350 m²/sec²·K) (Callens, 1994)

T^* = stagnation temperature at the exit plane from Eqn. (12) evaluated at $M^*=1$.

The particle velocity impacting the probe is given by (Callens, 1994)

$$V_p = V_{pe} e^{\frac{-C_d \delta \rho_g A_p}{2m_p}} \quad (39)$$

where C_d = coefficient of drag

V_p = impact velocity of particle

V_{pe} = particle velocity at the nozzle exit plane (beginning of the shock layer)

δ = shock stand-off distance.

The shock stand-off distance is approximately (Anderson, 1989)

$$\delta = 0.143r \exp\left(\frac{3.24}{M^2}\right) \quad (40)$$

where r = radius of the probe. The shock stand-off distance, δ , is shown in Figure 22.

The computational procedure which solves Eqn. (32) through Eqn. (40) to determine the mach number, gas velocity, gas density, particle velocity at the exit plane, and particle impact velocity at the target surface is as follows:

1. Divide the flow region from the combustion chamber to the exhaust plane into N regions Δx apart.
2. For each x_{i+1} , calculate A/A^* from Eqn. (34), starting with known values at the combustion chamber.
3. Calculate M_{i+1} corresponding to the area ratios from Eqn. (35).
4. Calculate $(V_g)_{i+1}$ corresponding to the mach numbers from Eqn. (36).
5. Calculate $(\rho_g)_{i+1}$ from Eqn. (37).
6. For an assumed particle size, calculate $(V_p)_{i+1}$ from Eqn. (32), using the above values of V_g and ρ_g . C_d is given in Figure 24 (White, 1994).
7. Once the exit velocity is known, calculate impact velocity from Eqn. (39).

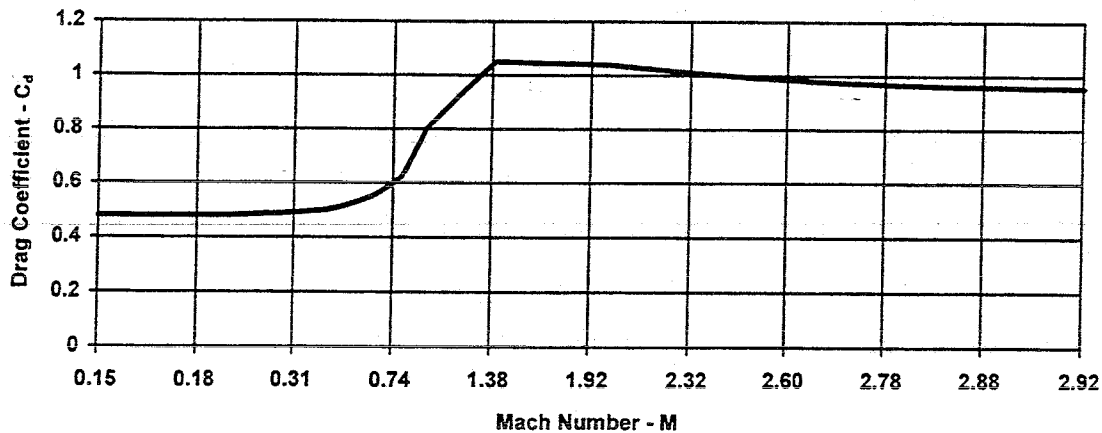


Figure 24. Drag Coefficient of a Smooth Sphere

Results of the Analysis

Figures 25 through 27 show the mach number, gas velocity, and gas density, respectively, for the assumed nozzle shape. These graphs are valid for any length nozzle of the assumed shape as long as $A/A^* = 6$ and $x^*/x_e = 1/3$. Figures 28 through 32 show the velocities of various sized particles of hydroxyl-terminated polybutadiene ($\rho_p = 115.5 \text{ lbm/ft}^3, 1850 \text{ kg/m}^3$) exiting nozzles of lengths of 1, 6, 12, 24, and 48 inches (2.54, 15.24, 30.48, 60.96, and 121.9 cm). This material was chosen for the particles because it is the least dense material likely to be present in solid form in the exhaust. Therefore, if a particle of this material will create a usable crater, so will a particle of a denser material. The velocities at the exhaust plane are the only values of interest. It is evident from Figure 28 that particles larger than approximately $500 \mu\text{m}$ may not have enough momentum exiting a 1-inch (2.54 cm) nozzle to create a useful crater. Evaluation of the craters formed by these particles will be required to determine if this situation constitutes an operational limit of the PICS. All other particles on the various graphs in Figures 29 through 32 appear to have sufficient velocity entering the shock to form usable craters.

Figure 33 shows the approximate impact velocity of particles up to $3,000 \mu\text{m}$ in diameter exiting from nozzles 1 to 48 inches in length. It is evident that particles less than approximately $0.1 \mu\text{m}$ in diameter will not make usable craters because of deceleration in the shock layer. Impact velocities are low for particles larger than $3,000 \mu\text{m}$ because of lower acceleration in the nozzle. It is concluded that the PICS has

the capability of characterizing particles between $0.1 \mu\text{m}$ and $3,000 \mu\text{m}$ in diameter in nozzles greater than 1 inch (2.54 cm) in length. The particle dynamics program is in Appendix C, and the data represented in the graphs are found in Appendix D.

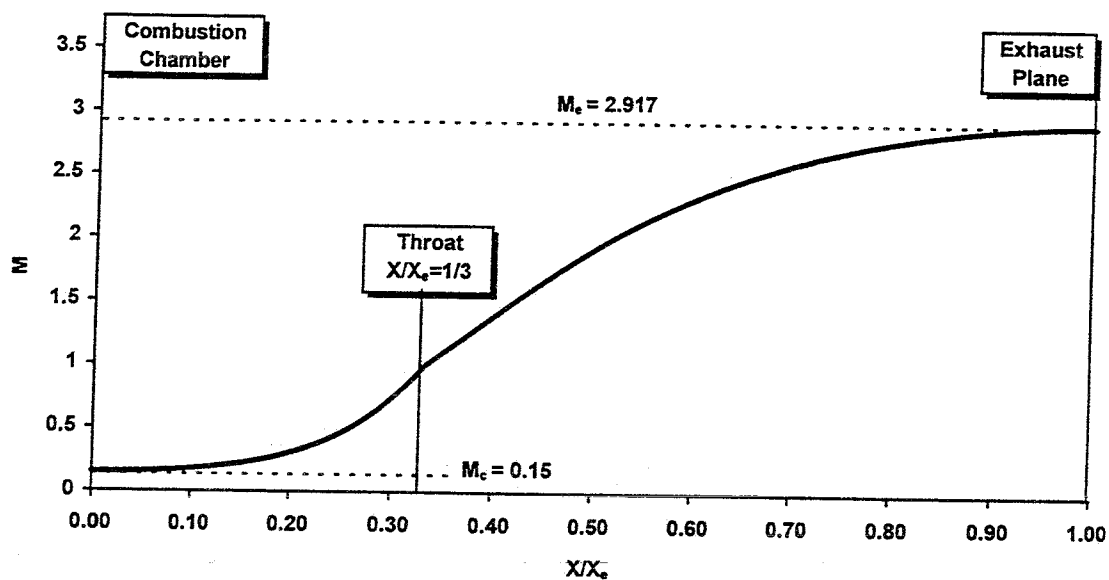


Figure 25. Mach Number in the Nozzle

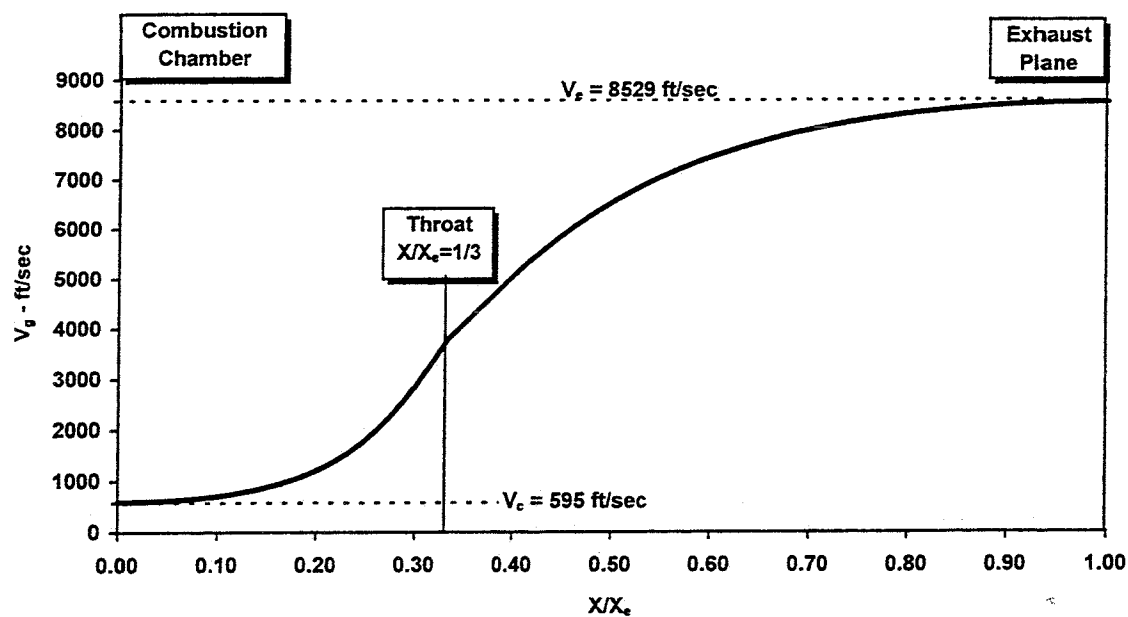


Figure 26. Gas Velocity in the Nozzle

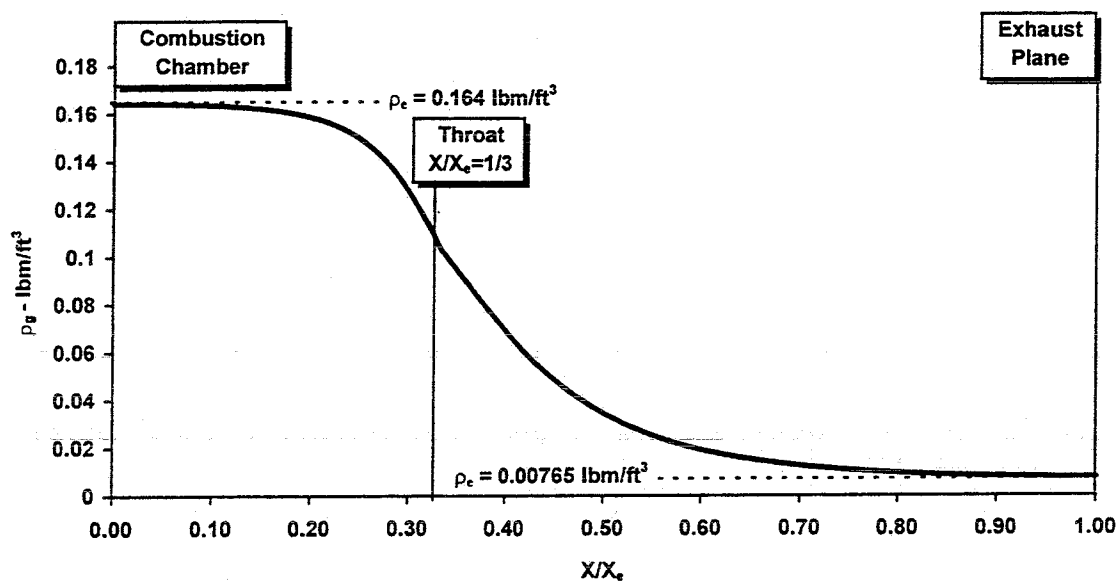


Figure 27. Gas Density in the Nozzle

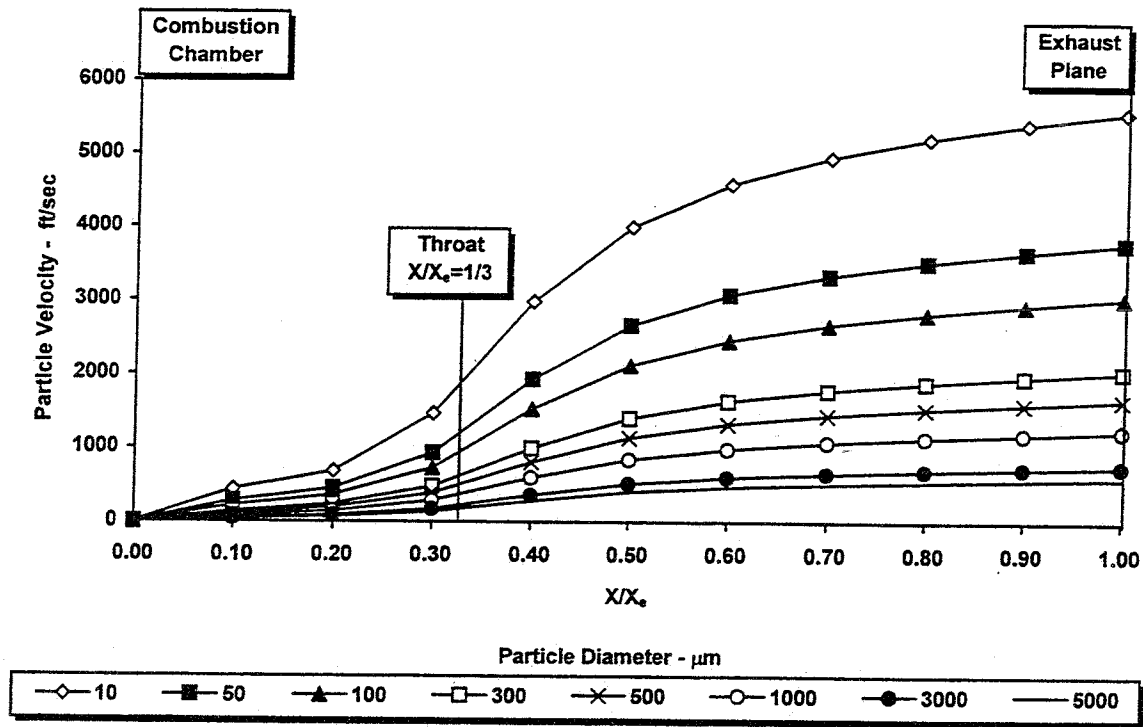


Figure 28. Particle Velocity in the Nozzle for $X_e = 1$ inch

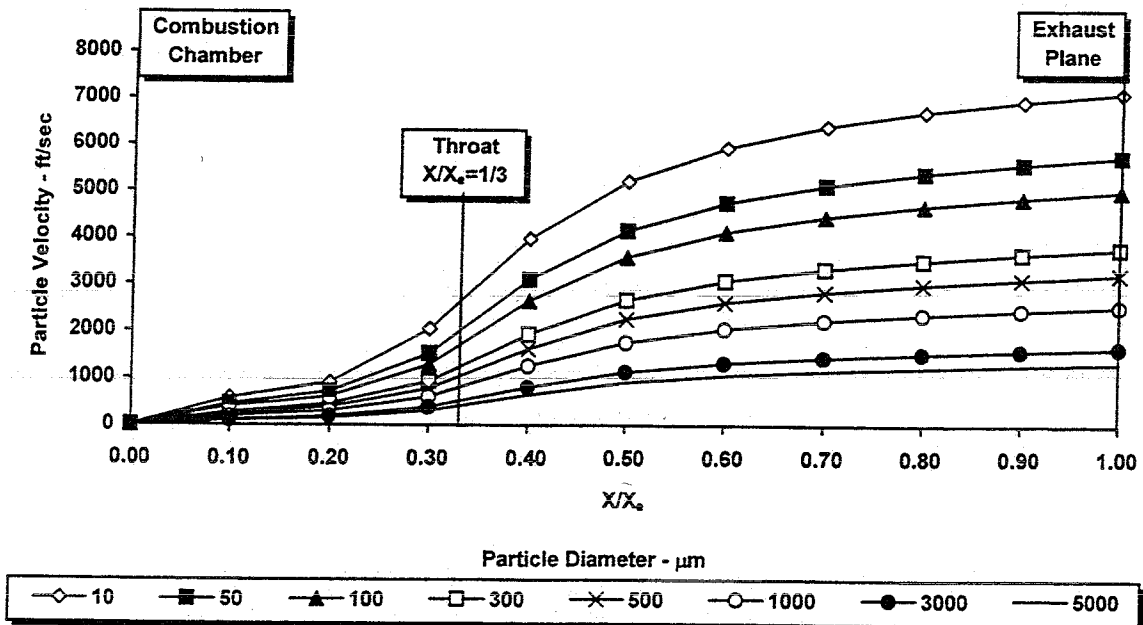


Figure 29. Particle Velocity in the Nozzle for $X_e = 6$ inch

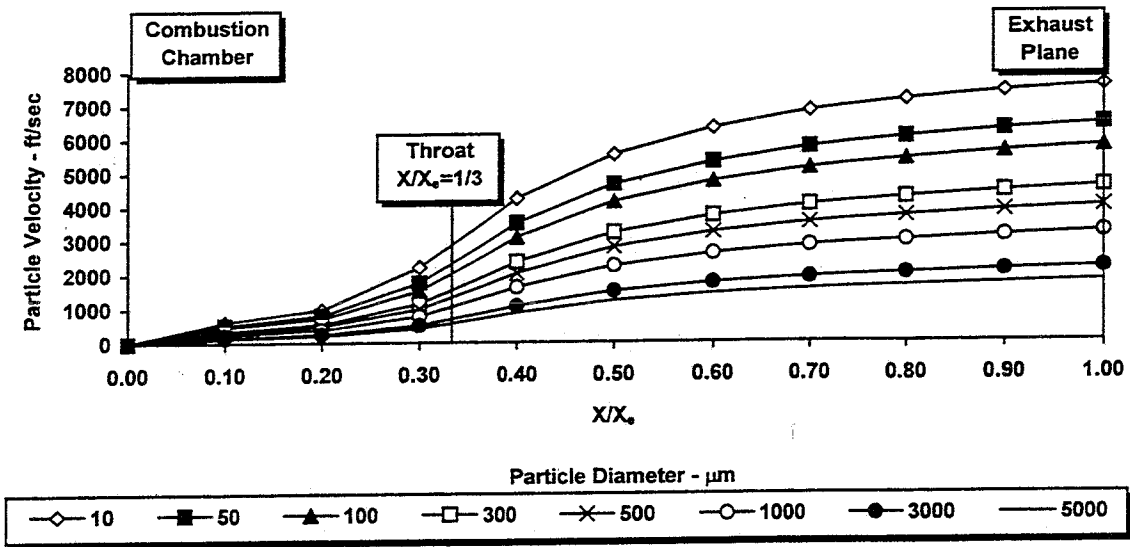


Figure 30. Particle Velocity in the Nozzle for $X_e = 12$ inch

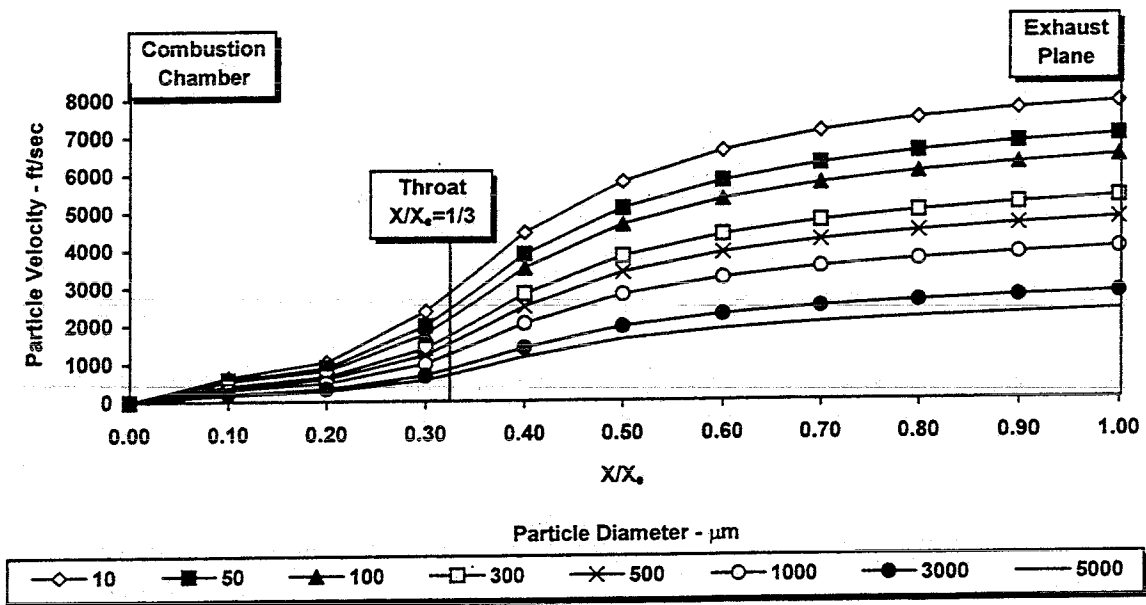


Figure 31. Particle Velocity in the Nozzle for $X_e = 24$ inch

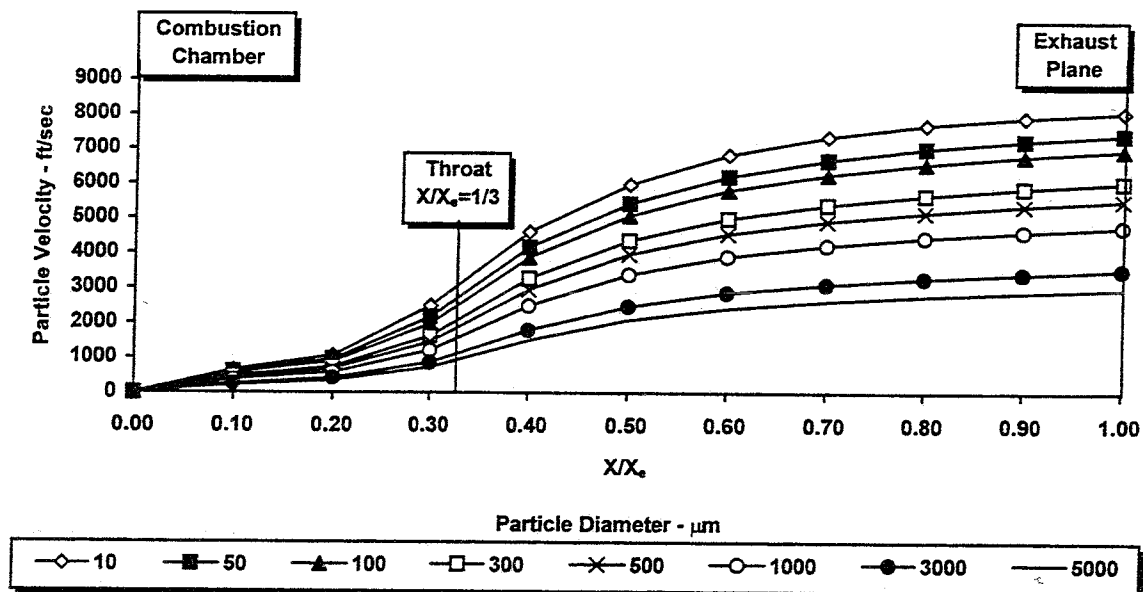


Figure 32. Particle Velocity in the Nozzle for $X_e = 48$ inch

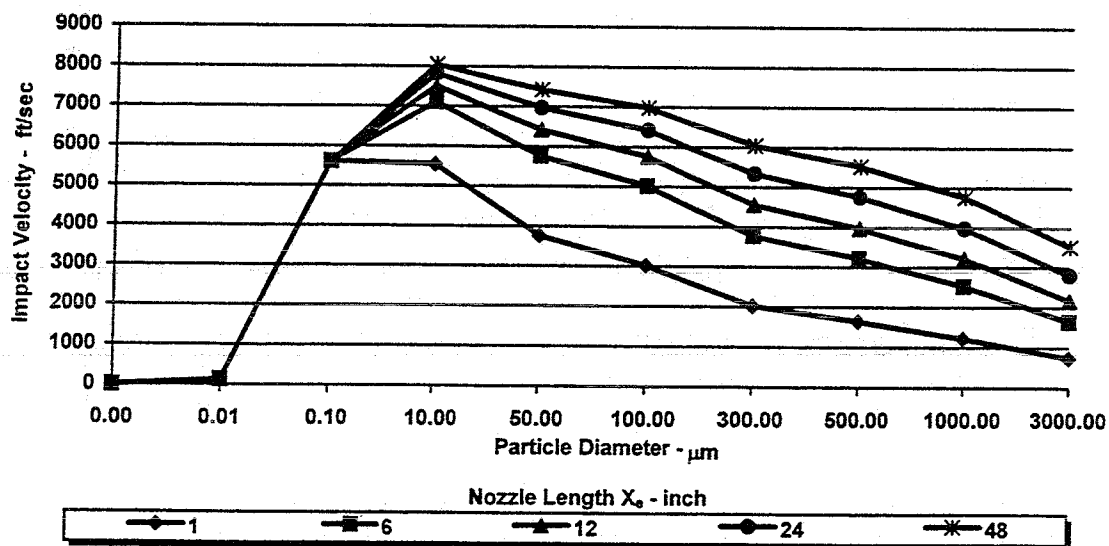


Figure 33. Impact Velocity Versus Particle Diameter for Various Size Nozzles

Estimation of Crater Depth and Diameter

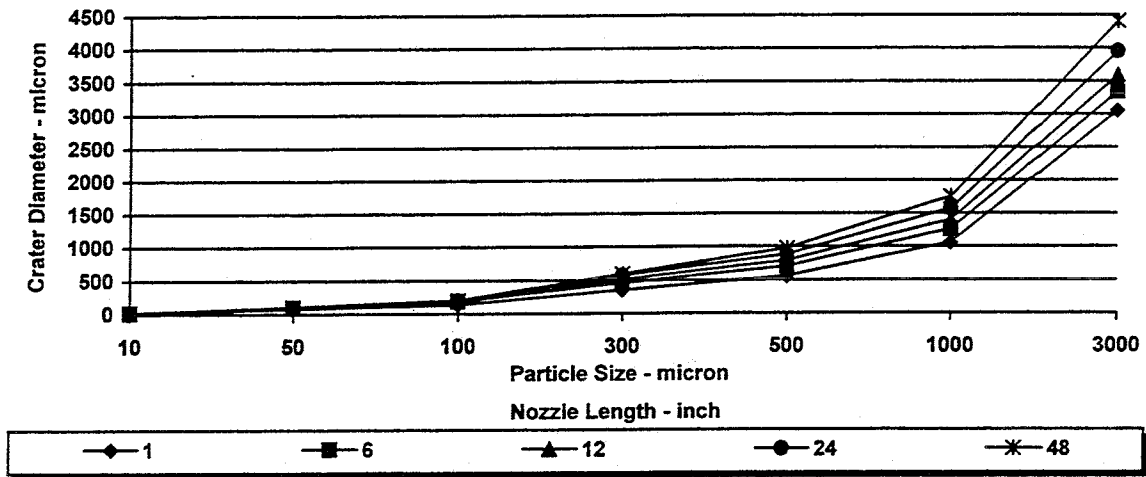
Crater depths and diameters, as estimated by McMurtry's projectile penetration computer code (McMurtry, 1997), for various HTPB particle sizes are given in Figures 34 through 37. This application of McMurtry's code assumes that the particles are spherical. Small particles are roughly spherical in the plume because the flow field around these particles, coupled with the high heat in the plume, tends to mold the particles into a sphere. As particle size increases, this spherical assumption is less accurate. Fortunately, only relatively small particles are expected to be in the exhaust plume. Table 5 gives the penetrator and target material data used for the crater analysis (Beer and Johnston, 1992). The HTPB data is an estimate of the properties of a hard rubber. Impact velocities for the various size particles are given in Figure 33.

Table 5. Properties of Materials for Penetration Code

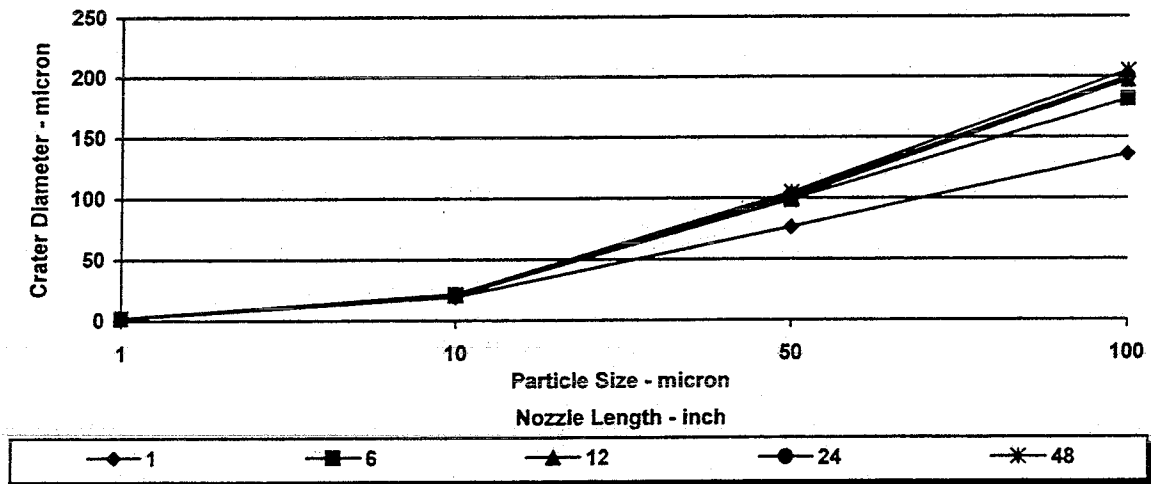
	HTPB (penetrator)	6061-T651 Aluminum (target)	Copper 99.9% (target)
Density (lbm/ft³)	74.9	169	537
Compressive Strength (ksi)	7.3	45	56.6
Lateral Speed of Sound (ft/sec)	8,169	17,480	12,927
Transverse Speed of Sound (ft/sec)	4,921	10,007	9,268
Poisson's Ratio	0.35	0.33	0.33
Hugoniot Constant	1.577	1.338	1.489

Figures 34 through 37 show that the diameter of the crater formed in 6061-T651 aluminum by a particular size HTPB particle is unique for a given nozzle length. However, error introduced by the measurement process requires the measurement of both the crater depth and diameter. The particle velocity then can be determined from graphs similar to Figures 28 through 32 for the known nozzle configuration. Longer nozzles allow particles to accelerate more before exiting the engine, enabling particles to create larger craters as shown in Figures 34 through 37.

Figures 35 and 37 indicate that some particles in the shorter nozzles do not generate sufficient velocity to form a crater. This condition creates an operational limit, which is a function of nozzle length, on the size of the particles which can be characterized by the PICS. Figures 36 and 37 indicate the same trends for impact with copper that are seen in impact with aluminum (Figures 34 and 35). Crater depth and diameter are slightly higher in aluminum than they are in copper because of the higher compressive strength of copper.

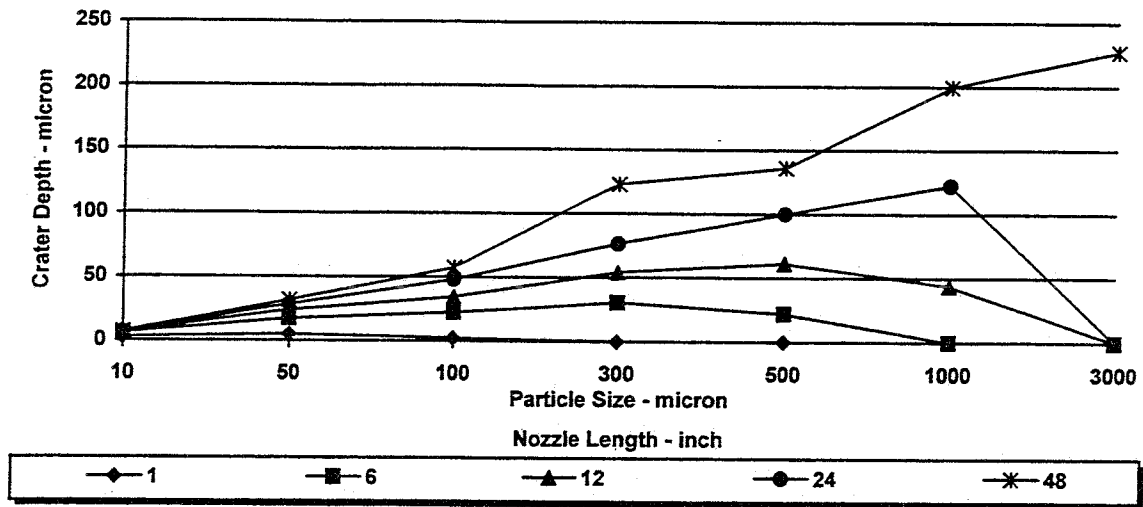


a. Particle Size Range 10 to 3,000 μm

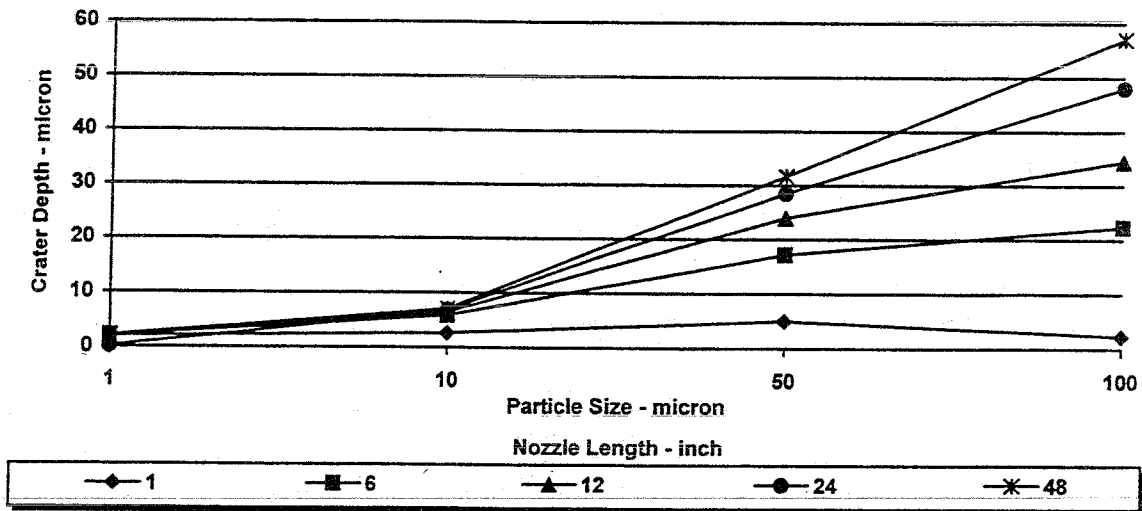


b. Particle Size Range 1 to 100 μm

Figure 34. Crater Diameter in 6061-T651 Aluminum as a Function of HTPB Particle Size

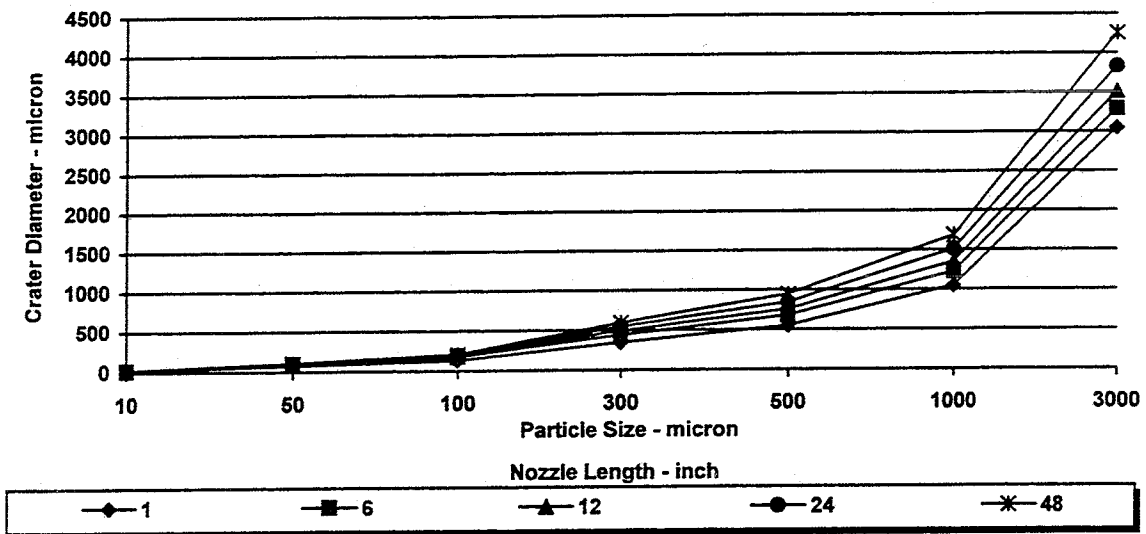


a. Particle Size Range 10 to 3,000 μm

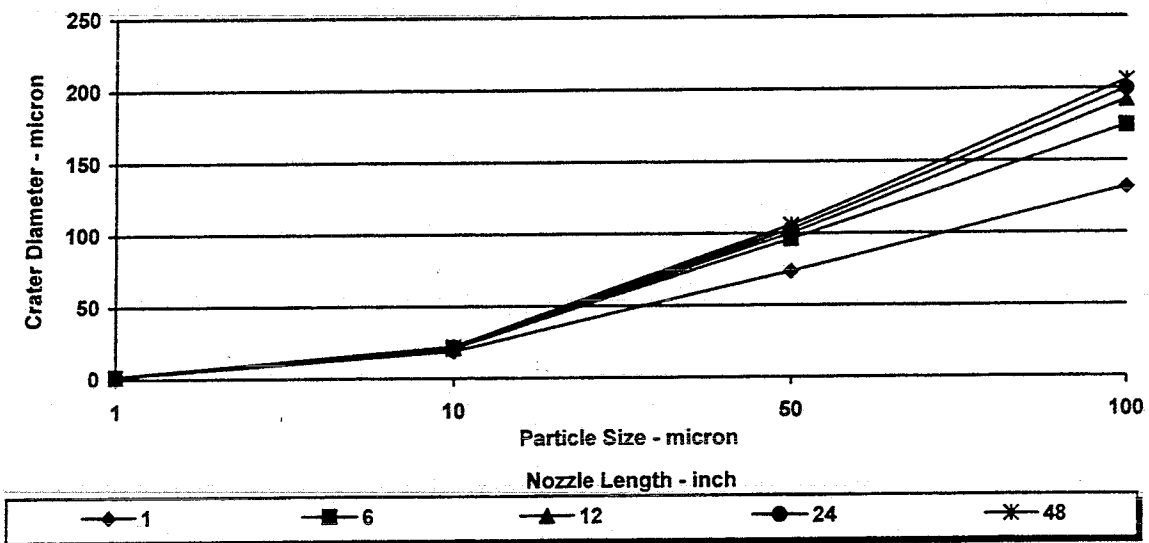


b. Particle Size Range 1 to 100 μm

Figure 35. Crater Depth into 6064-T651 Aluminum as a Function of HTPB Particle Size



a. Particle Size Range 10 to 3,000 μm



b. Particle Size 1 to 100 μm

Figure 36. Crater Diameter in Copper as a Function of HTPB Particle Size

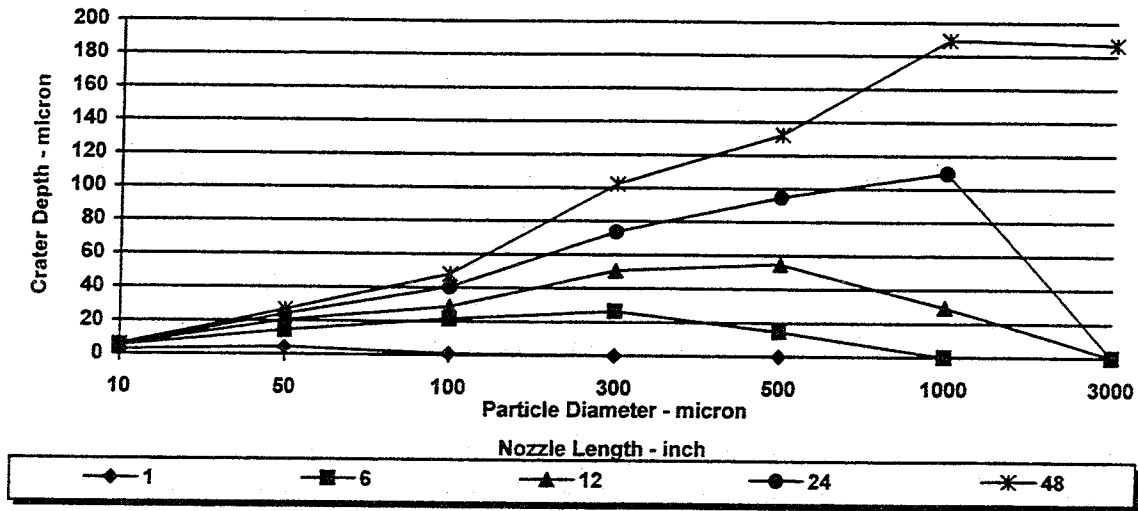
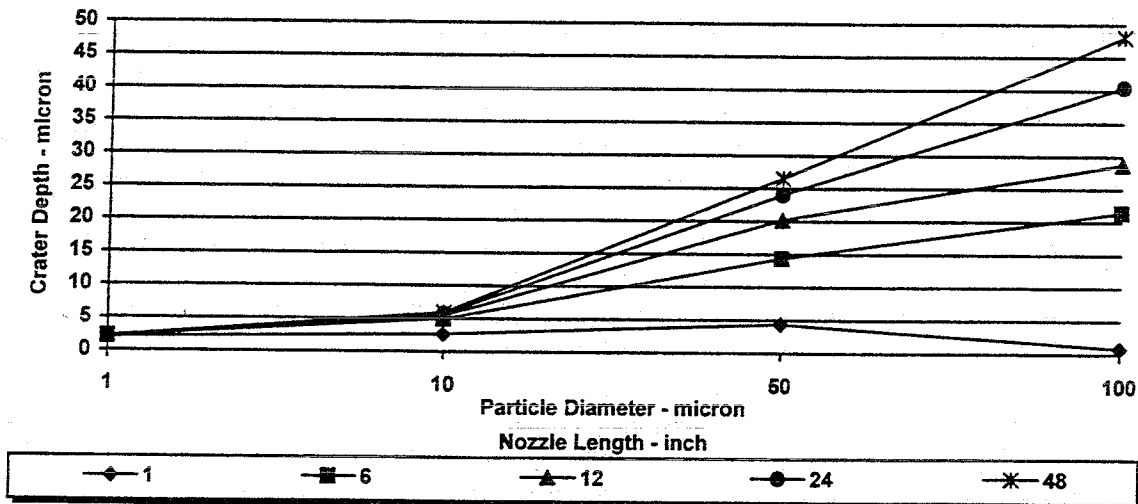
a. Particle Size Range 10 to 3,000 μm b. Particle Size Range 1 to 100 μm

Figure 37. Crater Depth into Copper as a Function of HTPB Particle Size

CHAPTER 5

DESIGN OF PROTOTYPE

Energy Analysis of the Probe

For the design residence time in the plume of 20 ms, a target velocity of approximately 100 ft/sec (30.5 m/sec) is required. The target launch velocity should be higher than this to correct for aerodynamic drag and pressure resistance upon entrance to the plume. To determine the correct arm rotational launch velocity, it is required to calculate the kinetic energy of the arm E_1 , the energy of the arm lost in the entrance to the plume E_2 , and the energy of the arm lost to drag inside the plume E_3 for a target translational velocity $V_T = r_T \omega$ where r_T is the radius of curvature for the path of the target and ω is the arm rotational velocity.

The kinetic energy of the arm is

$$E_1 = \frac{1}{2} I \omega^2 \quad (41)$$

where I = mass moment of inertia of the arm

ω = angular velocity of the arm.

The energy change in the entrance to the plume is given by

$$E_2 = \int_0^{2R} (P_{\text{gas}} - P_{\text{atm}}) A(t) dS \quad (42)$$

where R = radius of the probe at the entrance to the plume

P_{gas} = gas pressure in the plume

P_{atm} = atmospheric pressure

$A(t)$ = probe profile area as a function of time

V_t = probe translational velocity

$dS = V_t dt.$

In Eqn. (42) $P_{gas} - P_{atm}$ and V_t are both constant. Figure 38 illustrates the probe entering the plume. An expression for $x(t)$ is required to determine $A(t)$.

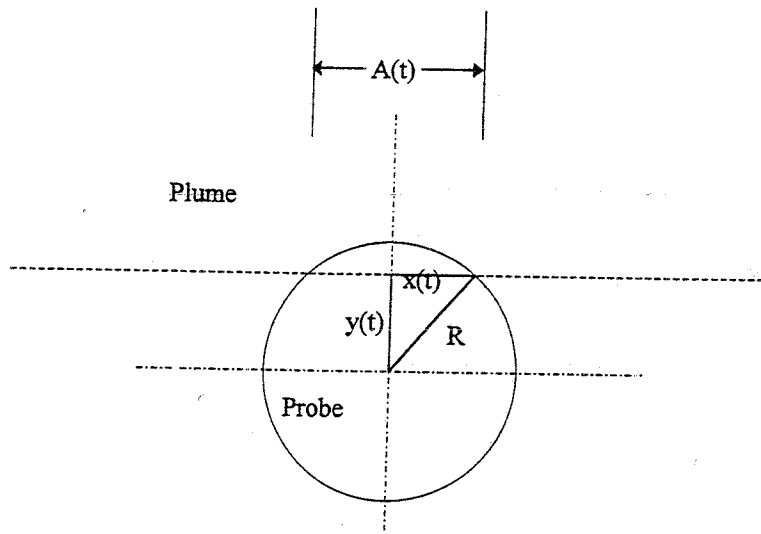


Figure 38. Probe Entering the Plume

The distance from the probe centerline to the plume, $y(t)$, is $y(t) = R - V_t t$. From the Pythagorean theorem,

$$x(t) = \sqrt{R^2 - (R - V_t t)^2} \quad (43)$$

which reduces to

$$x(t) = \sqrt{2V_t R t - V_t^2 t^2} \quad (44)$$

Substituting $A(t) = 2 x(t) L_p$, where L_p is the length of probe entering the plume, into Eqn. (42) yields

$$E_2 = 2L_p V_t (P_{\text{gas}} - P_{\text{atm}}) \int_0^{\frac{2R}{V_t}} \sqrt{2V_t R t - V_t^2 t^2} dt \quad (45)$$

which reduces to

$$E_2 = \pi L_p R^2 (P_{\text{gas}} - P_{\text{atm}}) \quad (46)$$

The probe actually gains energy entering the plume because the pressure in the plume is 11.8 psia (8.1 kPa) which is less than the atmospheric pressure of 14.7 psia (10.1 kPa).

Assuming a plume width of 6 inches (15.24 cm), the energy lost to drag inside the plume is

$$E_3 = \int_0^6 \frac{1}{2} C_d \rho_{\text{gas}} A_{\text{profile}} V_t^2 dS \quad (47)$$

where C_d = coefficient of drag of the arm (conservatively assumed to be 2)

ρ_{gas} = gas density in the plume

A_{profile} = probe profile area = $2RL_p$

V_t = probe translational velocity.

The launch energy is given by

$$\frac{1}{2} I \omega_L^2 = \frac{1}{2} I \omega_p^2 + E_2 + E_3 \quad (48)$$

where ω_L = rotational velocity of the arm at launch

ω_p = rotational velocity of the arm in the plume.

The last two terms are highly sensitive to the orientation of the probe arm when it enters the plume. If the arm enters the plume at a negative angle of attack, it will experience much higher energy losses than this analysis assumes. The energy lost to drag E_2 is also highly sensitive to whether the nozzle is underexpanded or overexpanded. These nozzles produce regions of high and low pressure in the plume which will affect the drag on the probe. Calibration of the PICS is required to correct for energy loss caused by these two problems.

The mass moment of inertia of the arm is required for the calculation of the launch rotational velocity of the arm. The mass moment of inertia of an object about an axis is defined as

$$I = \int_0^L r^2 dm \quad (49)$$

To evaluate this equation, the arm is divided into several sections as shown in Figure 39.

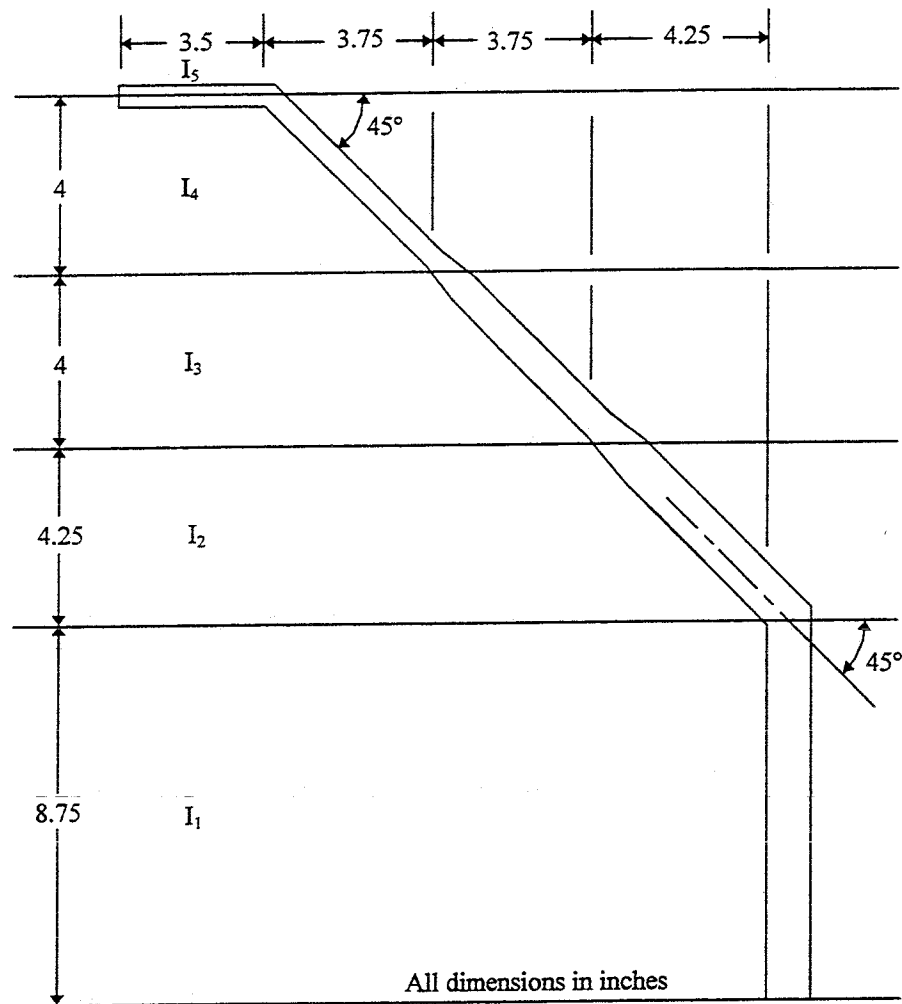


Figure 39. Sections of Arm Used in Mass Moment of Inertia Calculation

The mass moment of inertia of each section is found, and these moments are summed.

The moments of inertia are

$$I_1 = \int_0^{8.75} r^2 \rho \pi (.5)^2 dr$$

$$I_2 = \int_{-8.75}^3 r^2 \rho \pi (.5)^2 \cos(45^\circ)^{-1} dr$$

$$I_3 = \int_3^{17} r^2 \rho \pi (.325)^2 \cos(45^\circ)^{-1} dr \quad (50)$$

$$I_4 = \int_7^{21} r^2 \rho \pi (.25)^2 \cos(45^\circ)^{-1} dr$$

$$I_5 = \frac{1}{2} \rho \pi (.25)^2 (3.5)(.25)^2 + \rho \pi (.25)^2 (3.5)(21)^2$$

where ρ = density of steel

r = distance from the axis of rotation.

Summing these moments of inertia yields 527 lbm·in² (1.52 kg·m²/sec²).

The launch energy is calculated to be 185.8 lbf·ft (251.9 kg·m²/sec²). This energy corresponds to an arm rotational velocity of 57.1 rad/sec and a target translational launch velocity of 101.3 ft/sec (30.9 m/sec).

A similar analysis can be made for the minimum safe residence time of 50 ms and is calculated to be 29.6 lbf·ft (40.1 kg·m²/sec²). This energy corresponds to an arm rotational velocity of 22.8 rad/sec and a target translational launch velocity of 39.9 ft/sec (12.2 m/sec). The results of this analysis for the design condition are listed in Table 6. It is observed that the calculated losses are negligible for the assumed conditions.

Design of the Spring

The spring is viewed as a deflected beam where the energy in is given by (Juvinall and Marshek, 1991):

$$\text{Energy} = \int_0^L \frac{T^2}{2EI} dx \quad (51)$$

where L = length of the beam

E = Young's modulus

I = area moment of inertia

T = torque applied to the beam

x = distance along the centerline of the beam.

Table 6. Velocities and Energies the Probe Encounters During Operation

Rotational Velocity at Launch ω_L	57 rad/sec	Energy of the arm at Launch E_L	185.8 lbf-ft
Rotational Velocity in the Plume ω_p	57 rad/sec	Energy Change Entering the Plume E_{pe}	0.17 lbf-ft
Translational Velocity of Target Launch V_L	99.9 ft/sec	Energy Change to Drag for the Entire Path E_{pd}	-0.033 lbf-ft
Translational Velocity of Target in the Plume V_p	100 ft/sec	Kinetic Energy of the Arm in the Plume E_p	185.7 lbf-ft

Ebsco Spring Company, Inc., produces software which calculates, among other things, the torque a torsion spring will produce as a function of the angular displacement of the spring arm. It also calculates the safe stress, which includes an empirically determined safety factor, for a particular spring and the stress in the spring as a function of angular displacement. The program is called Spring Calculation Program and is available on the Internet at "<http://www.tulsaweb.com/ebsco>." Inputs and outputs, used in the spring design, for Spring Calculation Program are given in Table 7.

Table 7. Inputs and Outputs for Spring Calculation Program

Inputs	Outputs
1. Spring Material (The program lists material choices and their relevant properties)	1. Unbended Length, L in Eqn. (51), of the Spring Wire
2. Mean Diameter of Coils	2. Torque, T in Eqn. (51), in the Spring for Each of the Deflection Angles
3. Leg Length	3. Stress in the Spring for Each of the Deflection Angles
4. Number of Coils	4. Safe Working Stress in the Spring
5. Spring Deflection Angles	

Iteration between Eqn. (51) and the Spring Design Program is required to design the torsion spring. A spring is acceptable if the unbended length L of spring wire and the torque T produced by the spring satisfies Eqn. (51) when Energy = 186 lbf-ft (252 kg·m²/sec²). The design torque is calculated to be 2275 lbf·in (169.5 kg·m²/sec²) and the unbended length of wire is 195 inches (495.3 cm). This spring fails when the stress in the spring exceeds 176,250 psi (1.215 GPa). The specified spring is given in Table 8.

Figure 40 indicates the torque of the specified spring versus angular deflection of the spring arm. The design angular deflection of the spring arm to produce the required 20 ms residence time is approximately 106°. Figure 41 indicates that the spring can theoretically be calibrated to produce target launch velocities between 0 and 140 ft/sec (61.0 m/sec) by varying the angular deflection of the spring arm. It is evident from

Figure 42 that no test requirement will require a deflection which will exceed the safe working stress of the spring.

Table 8. Specifications for Required Torsion Spring

Number of Coils	11.125
Wire Size	0.625 inch
Mean Diameter	5 inch
Material	Chrome Silicon
Leg Length	6 inch
Body Length	Min 7.813 inch Max 8.273 inch
Max Shaft Size	4.021 inch
Safe Working Stress	176,250 psi

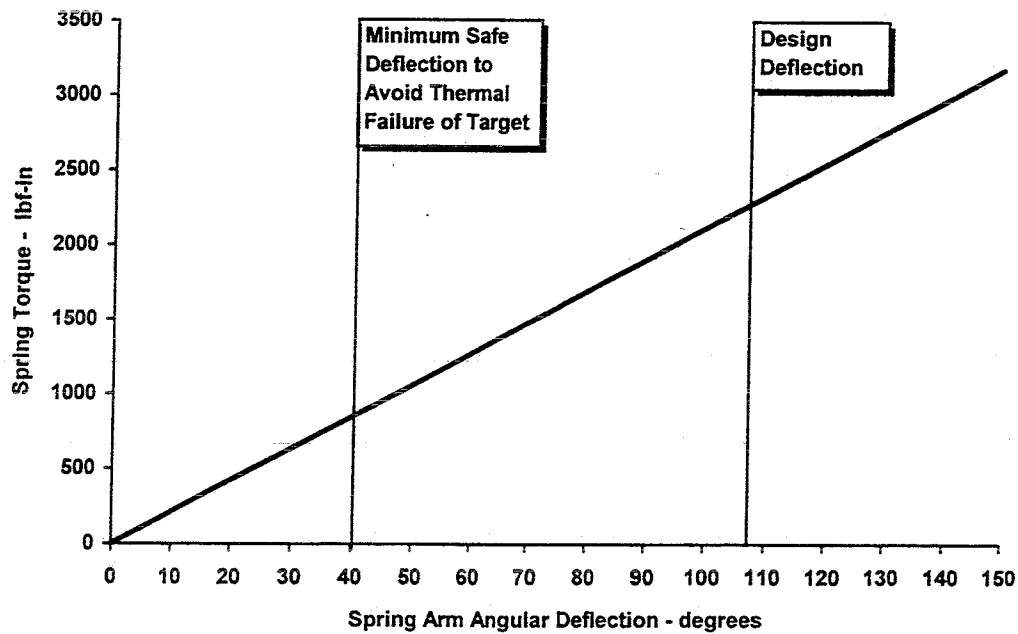


Figure 40. Spring Torque Versus Spring Arm Deflection

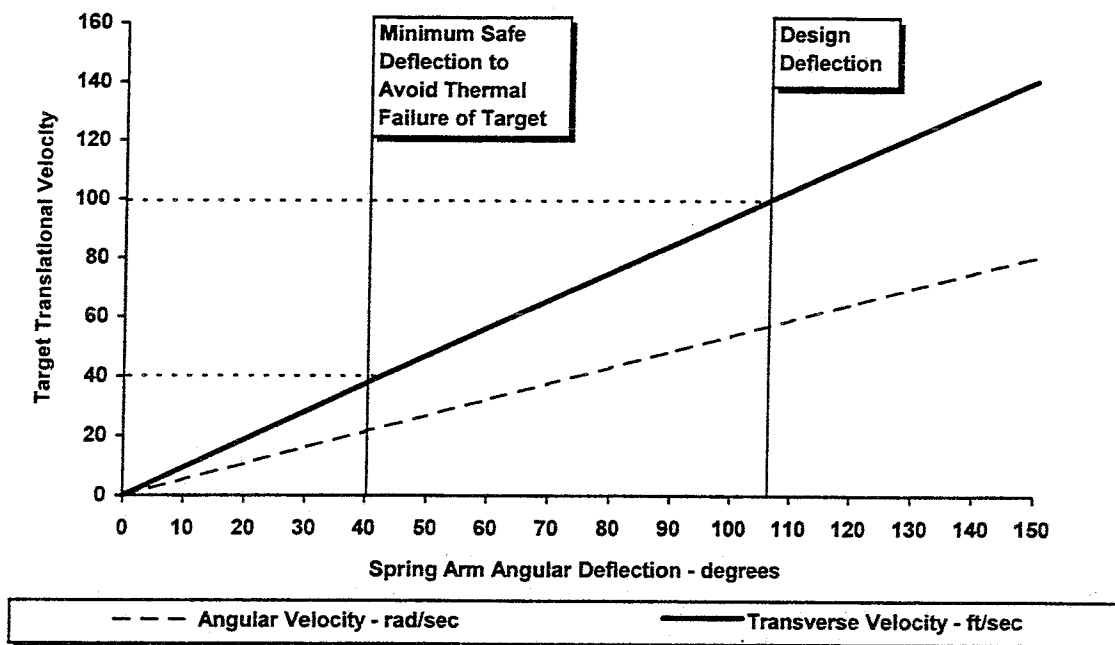


Figure 41. Target Translational and Rotational Velocity Versus Spring Arm Deflection

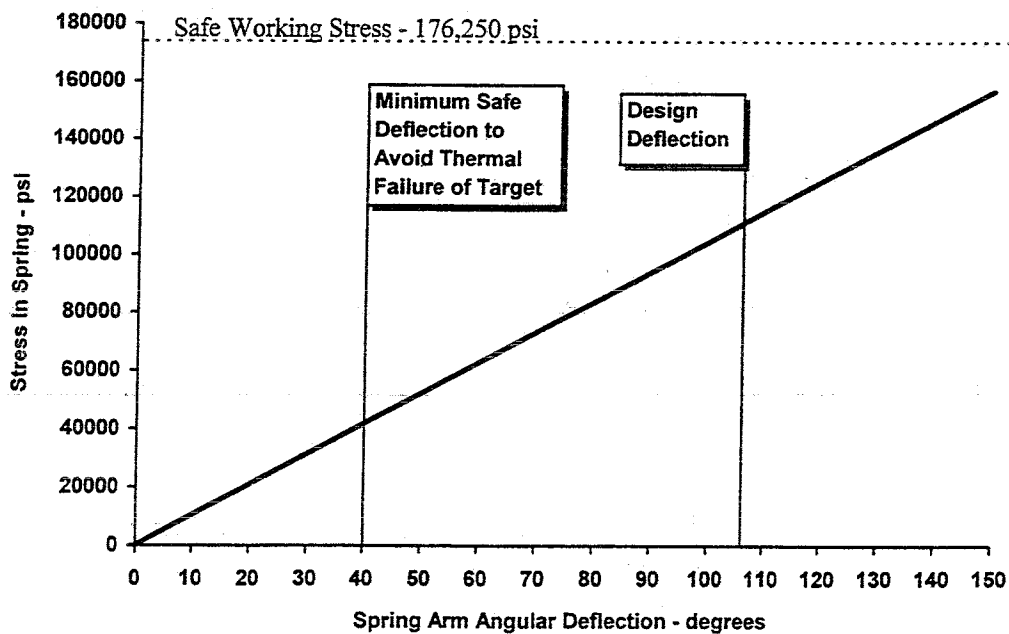


Figure 42. Stress in Spring Versus Spring Arm Deflection

Parts List and Shop Drawings

Table 9 is a list and description of parts required to build the PICS.

Table 9. Parts List

Figure	Description of Part
	<p>Figures 43 through 52 are Required to Manufacture the Probe and Spring Structure</p>
	<p>Probe Arm</p>
<p>43 44 45</p>	<p>Figure 43 is a drawing of the unbended length of rod required to produce the probe arm, and Figure 44 shows the required bends to produce the final shape of the probe arm. The 0.25-inch (0.635 cm) hole which holds the target is shown in Figure 45. ASTM A-514 steel is specified for this part because of its hardness.</p>
	<p>Probe Collar</p>
<p>46</p>	<p>The probe collar attaches the probe arm to the shaft. It is suggested that the vertical and horizontal sections of the probe collar be manufactured separately and welded together. Weld size is not critical on this component since it is a pinned joint and has little mass moment of inertia of its own. ASTM A-36 steel is specified for this part. The probe arm should be inserted into the probe collar and welded in place. This was not done on the prototype because the probe collar was designed after the probe arm was built. It was later realized that welding the parts would create a mechanism with less play than a threaded arm and probe collar would create.</p>
	<p>Shaft</p>
<p>47</p>	<p>The shaft holds the spring mandrel and probe collar in place. Nuts are required on this part only to keep the shaft from slipping out of the vertical supports. Material is ASTM A-36 steel.</p>
	<p>Vertical Support</p>
<p>48</p>	<p>Vertical supports hold the shaft in place. The distance between the bottom of the vertical support and the hole is critical. This distance is chosen because it allows the spring to sit on the mandrel properly. Material is ASTM A-36 steel.</p>
	<p>Baseplate</p>
<p>49</p>	<p>The baseplate holds the vertical supports, horizontal supports, and spring arm holder in place. Material is ASTM A-36 steel.</p>

Table 9. (continued)

Figure	Description of Part
	Mandrel
50	The mandrel provides support for the spring while it is deflected. A 4-inch (10.16 cm) outer diameter steel pipe may be used to manufacture the mandrel shown in Figure 50. The mandrel end plugs, Figure 51, are inserted into the ends of the mandrel and spot welded in place. They allow the mandrel to sit properly on the shaft. Material is ASTM A-36 steel.
51	
	Spring Arm Holder
52	The spring arm holder keeps the spring from rotating around the mandrel. Material is ASTM A-36 steel.
	Figures 53 through 61 are Required to Manufacture the Pneumatic Clip
	Horizontal Support
53	Horizontal supports hold the pneumatic clip in place. Material is ASTM A-36 steel.
	Slider Holder
54	The slide holder creates a pocket which the slider slips into before the clip is pressurized. Material is ASTM A-36 steel.
	Pin Holder
55	The pin holder holds the pin in place above the slider. Material is ASTM A-36 steel.
	Pin
56	The pin keeps the slider from slipping out of the slider holder while the pneumatic clip is pressurized. Material is ASTM A-514 steel.
	Bottom Plate
57	The bottom plate holds the pin, pin holder, and slider holder in place. A 0.0625-inch (15.8 mm) rubber gasket is placed in the outer groove. Material is ASTM A-36 steel.
	Top Plate
58	The top plate holds the pressure inlet and electric valve in place. A 0.0625-inch (15.8 mm) rubber gasket is placed in the outer groove. Material is ASTM A-36 steel.

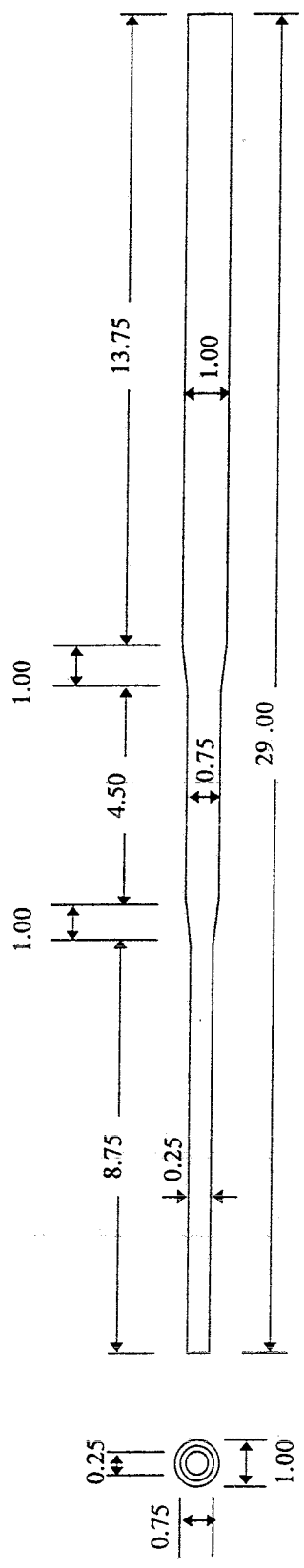
Table 9. (continued)

Figure	Description of Part
	Pressure Vessel
59	The pressure vessel is made of 4-inch (10.16 cm) pipe. Material is ASTM A-36 steel.
	Plunger
60	The plunger pushes the pin down so that it interferes with the slider and holds it in place while the pneumatic clip is pressurized. The two pieces should be made separately and welded together. A 0.0625-inch (15.8 mm) rubber gasket is placed on the outer race between the plunger and bottom plate. Material is ASTM A-36 steel.
	Slider
61	The slider holds the arm back when the pneumatic clip is pressurized. Material is ASTM A-36 steel.

Miscellaneous Parts Which Do Not Require Part Drawings

- torsion spring with specifications listed in the previous section (one part)
 0.375-inch (0.953 cm) diameter bolts, each 4 inches (10.16 cm) in length (five parts)
 0.375-inch nuts (five parts)
 0.375-inch washers (five parts)
- 0.25-inch (0.635 cm) diameter bolt, each 2 inches (5.08 cm) in length (one part)
 0.25-inch nut (one part)
- 3-inch (7.62 cm) spring clip (one part)
 4-inch (10.16 cm) quick link (one part)
 24 inches (60.96 cm) of 0.375-inch (0.953 cm) chain
 1.5-inch (3.81 cm) width x 3.5-inch (8.89 cm) height x 0.12-inch (0.3175 cm) wire diameter compression spring (one part)
- 0.125 inch (0.3175 cm) threaded air inlet (one part)
 0.125-inch nipple (one part)
 12 V DC, 0.125-inch connector, electric valve (75 psig = 517 kPa max) (one part)
- 0.125-inch (0.3175 cm) thick rubber gasket,
 ID: 4.00 inches (10.16 cm) OD: 4.25 inches (10.795 cm) (one part)
 0.125-inch thick rubber gasket,
 ID: 3.50 inches (8.89 cm) OD: 4.00 inches (10.16 cm) (one part)

Figures 62 through 64 indicate which parts must be welded together to complete the fabrications of the individual pieces of the PICS. Figure 62 shows how to weld the slider holder, pin holder, and bottom plate together. The pin must be placed inside the pin holder before the parts are welded together. Figures 63 and 64 indicate how to weld the horizontal and vertical supports, and the spring arm holder to the baseplate.



All dimensions in inches

All tolerances in this drawing are +/- 0.01

1 part is required

Figure 43. Section Required to Manufacture Probe Arm

All dimensions in inches
All tolerances in this drawing are +/-0.01

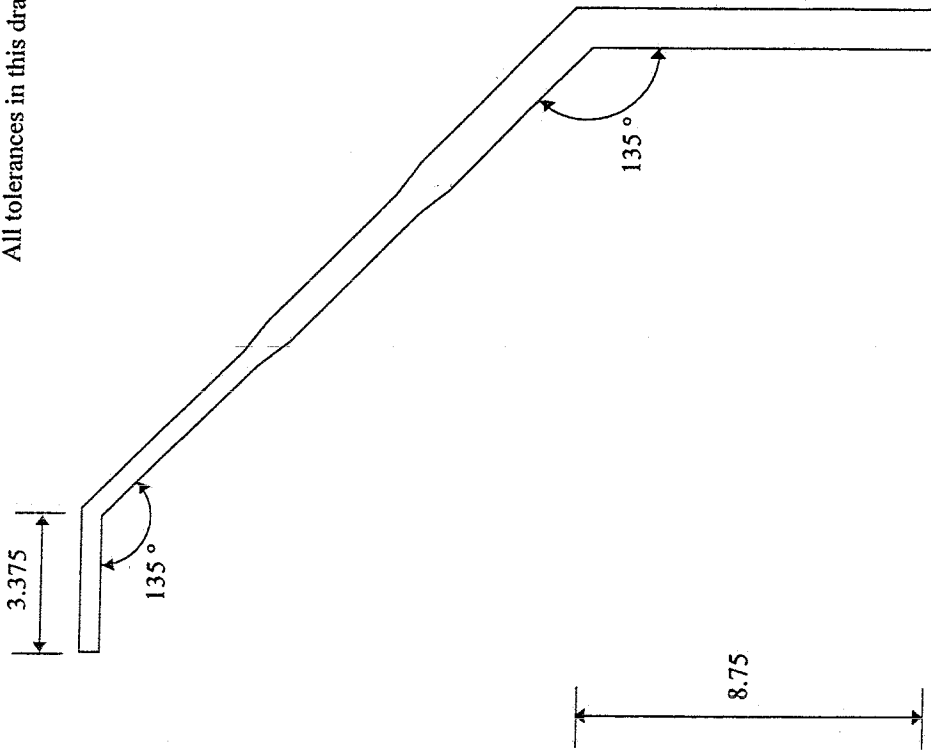
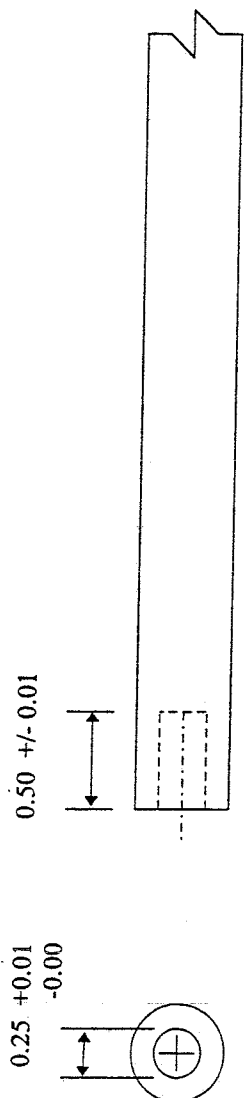


Figure 44. Bends Required in Section to Manufacture Probe Arm



All dimensions in inches

Figure 45. Call-Out of Hole in Tip of Probe Arm

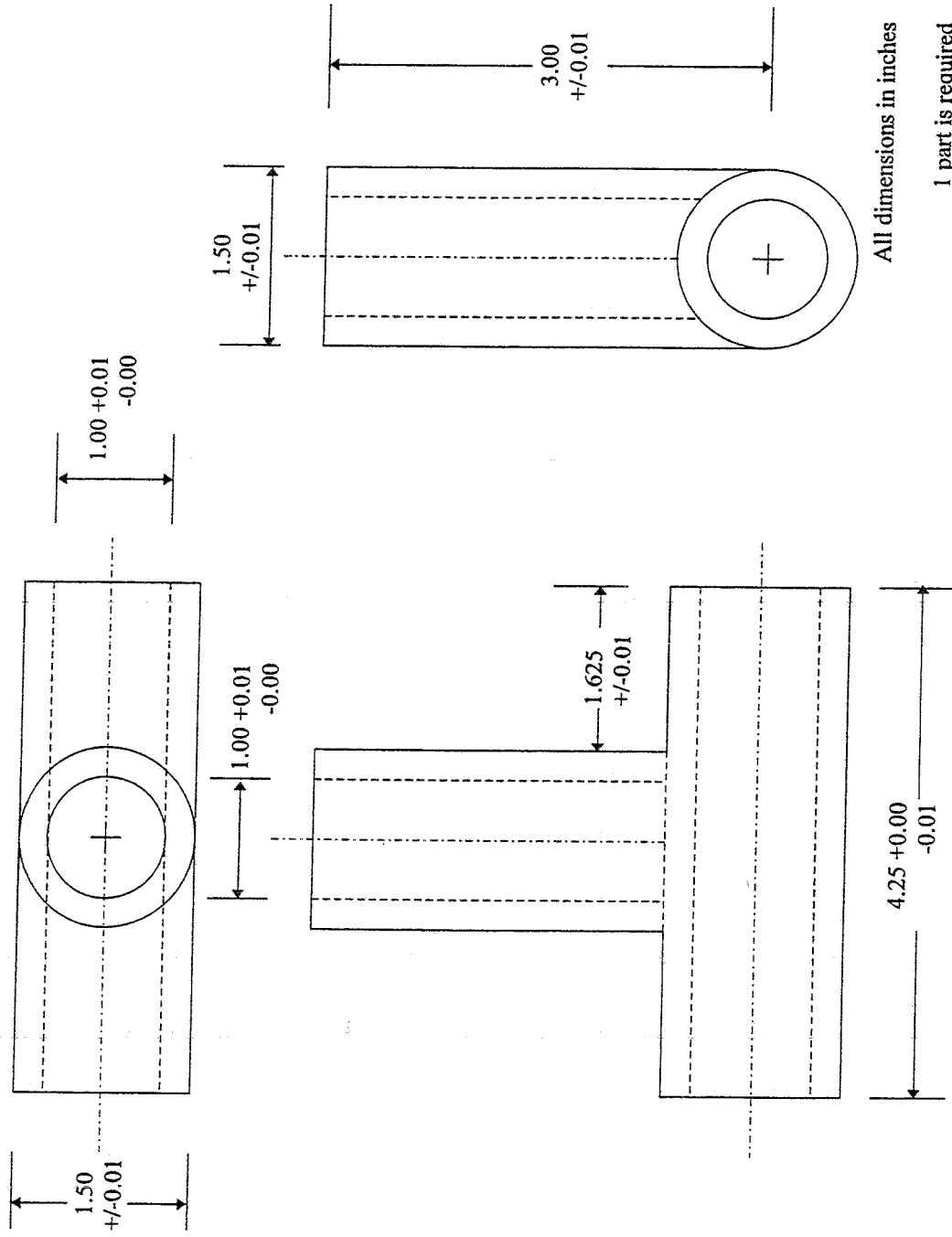
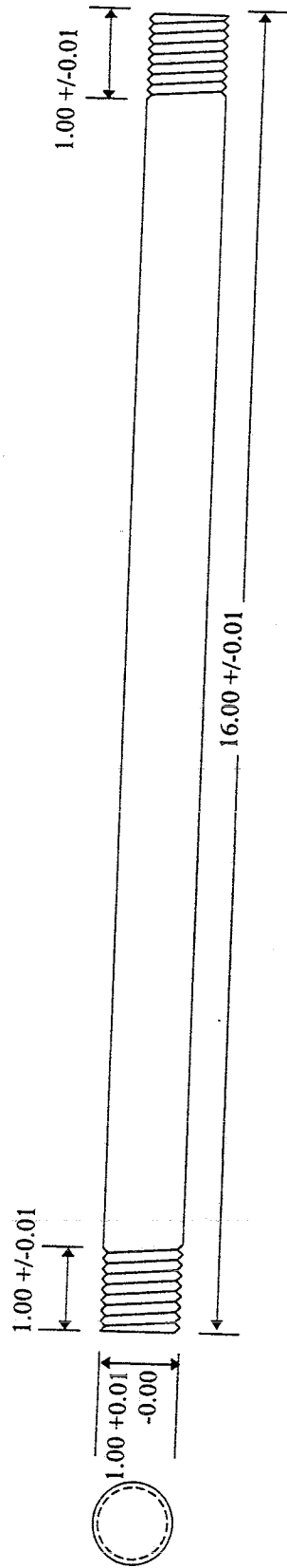


Figure 46. Probe Collar

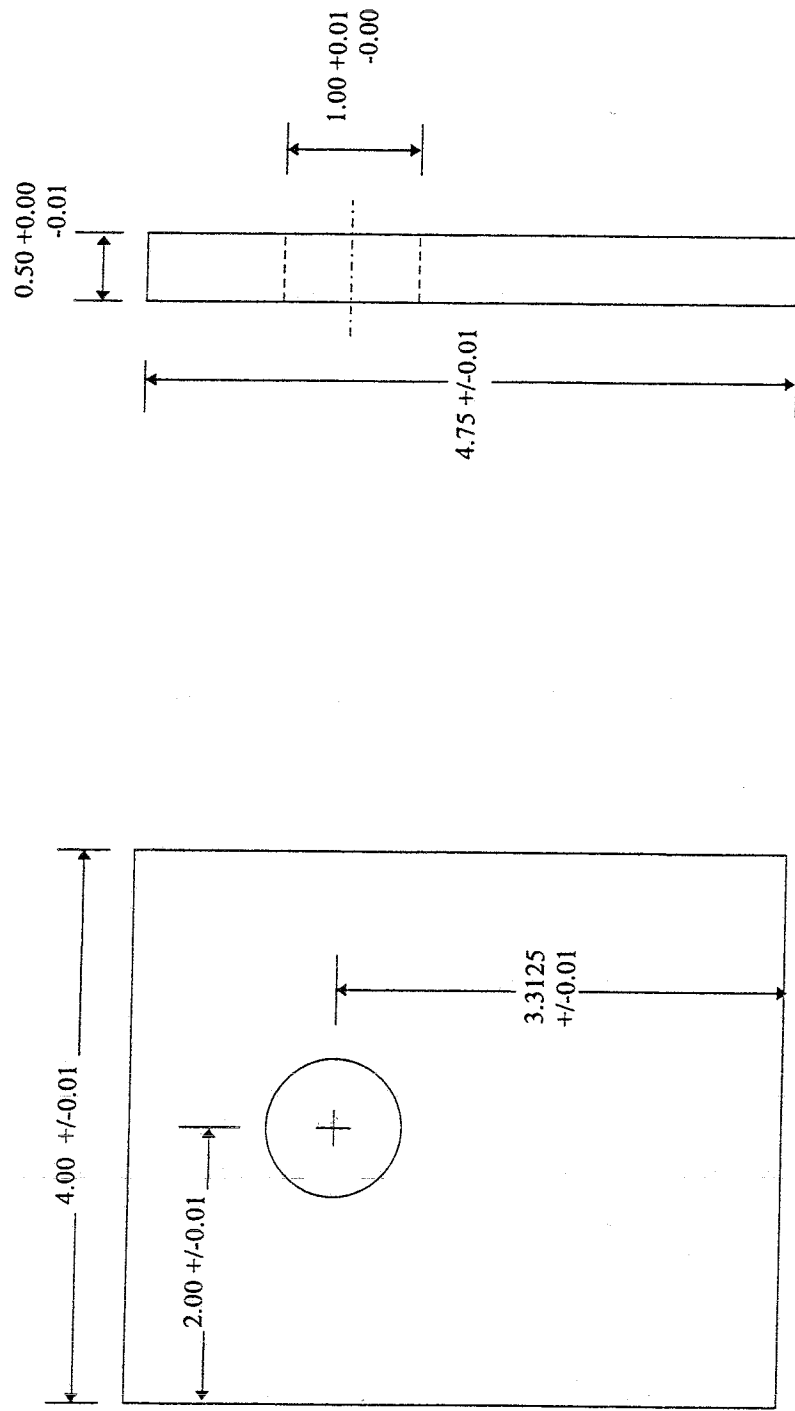


All dimensions in inches

All threads are "1 in-12UNF"

1 part is required

Figure 47. Shaft



All dimensions in inches

3 parts are required

Figure 48. Vertical Support

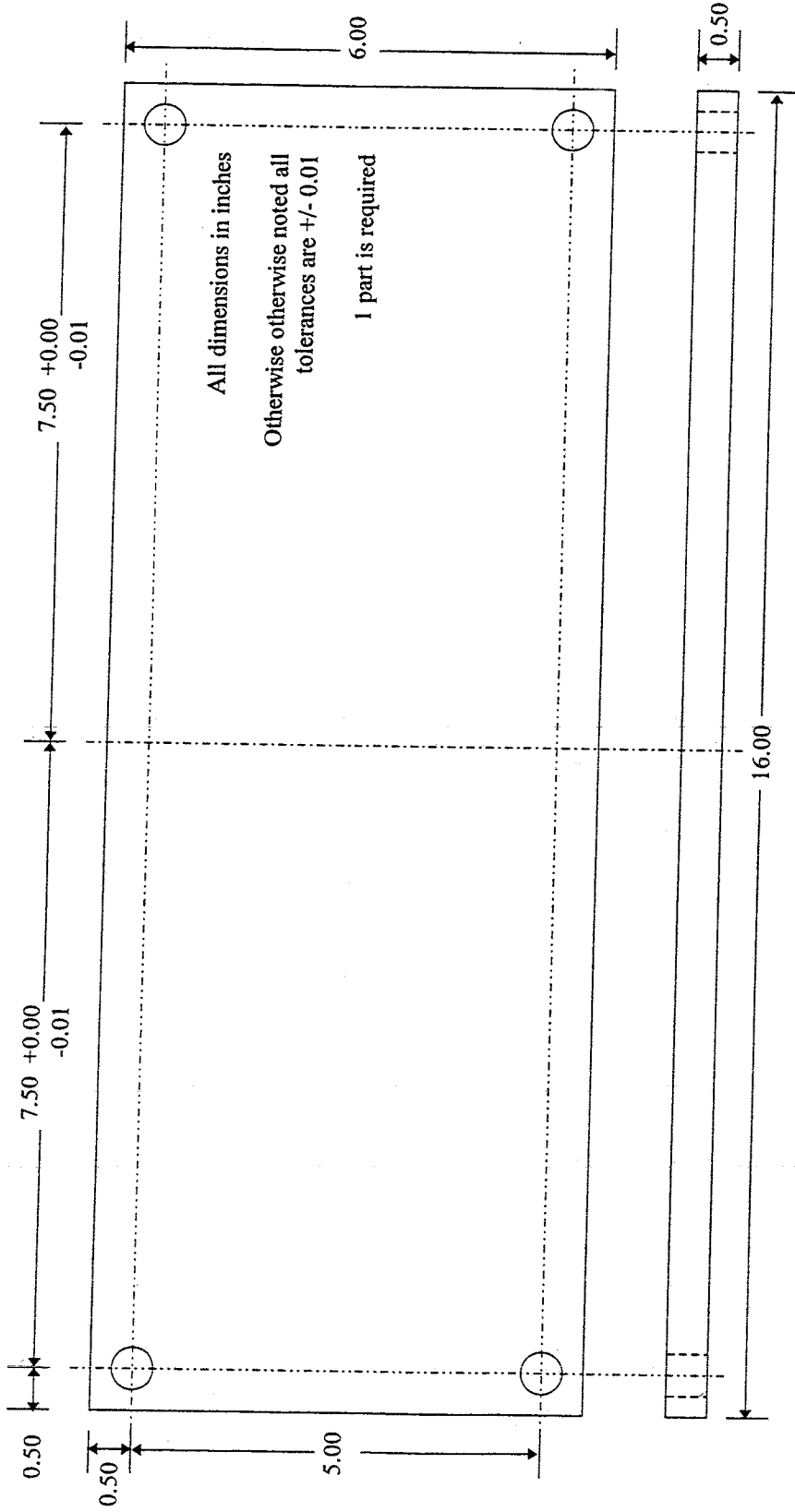
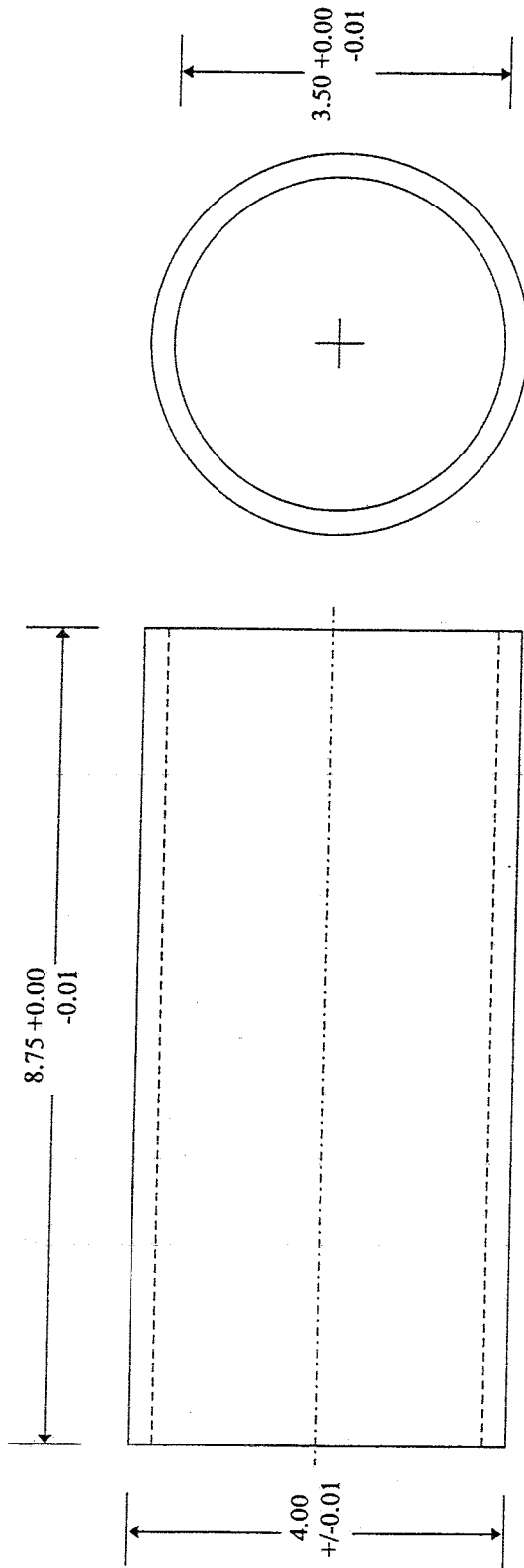


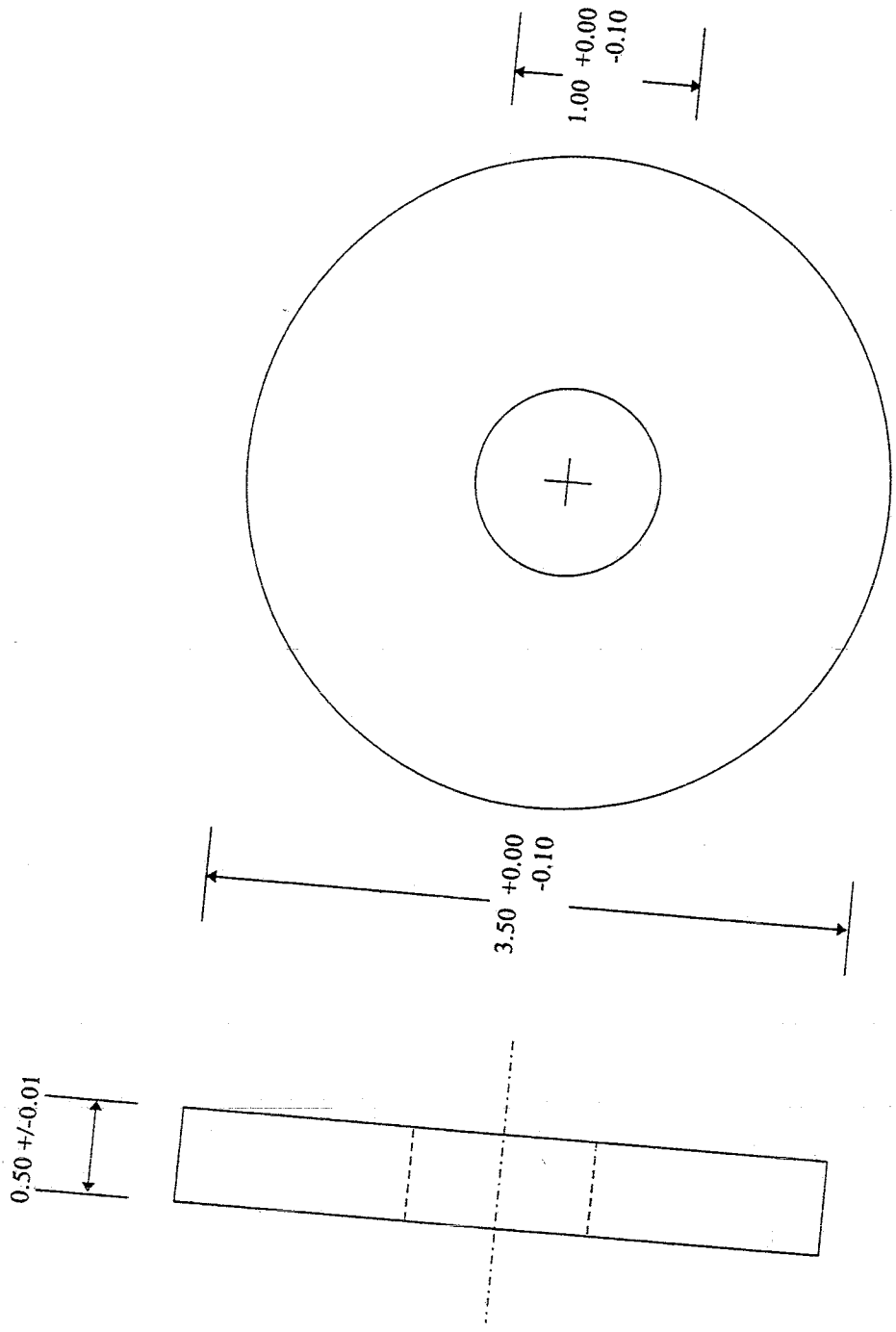
Figure 49. Baseplate



All dimensions in inches

1 part is required

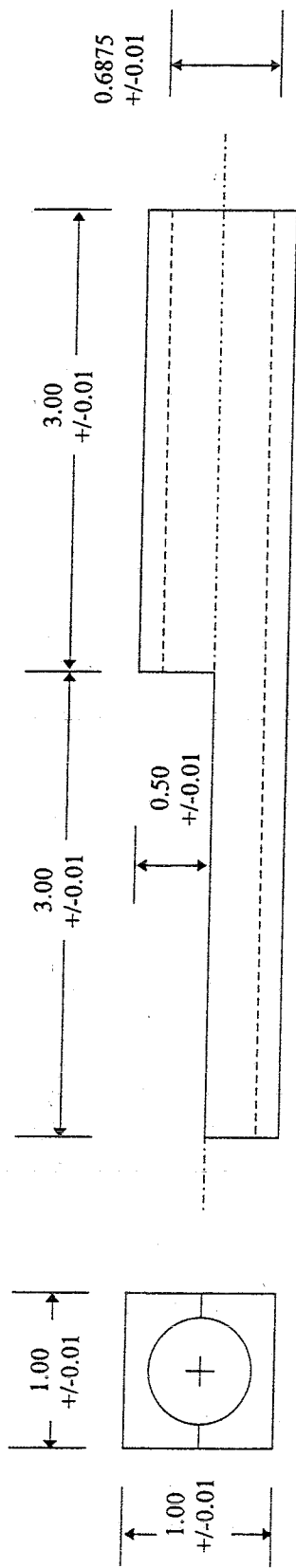
Figure 50. Pipe Section Required to Manufacture Mandrel



All dimensions in inches

2 parts are required

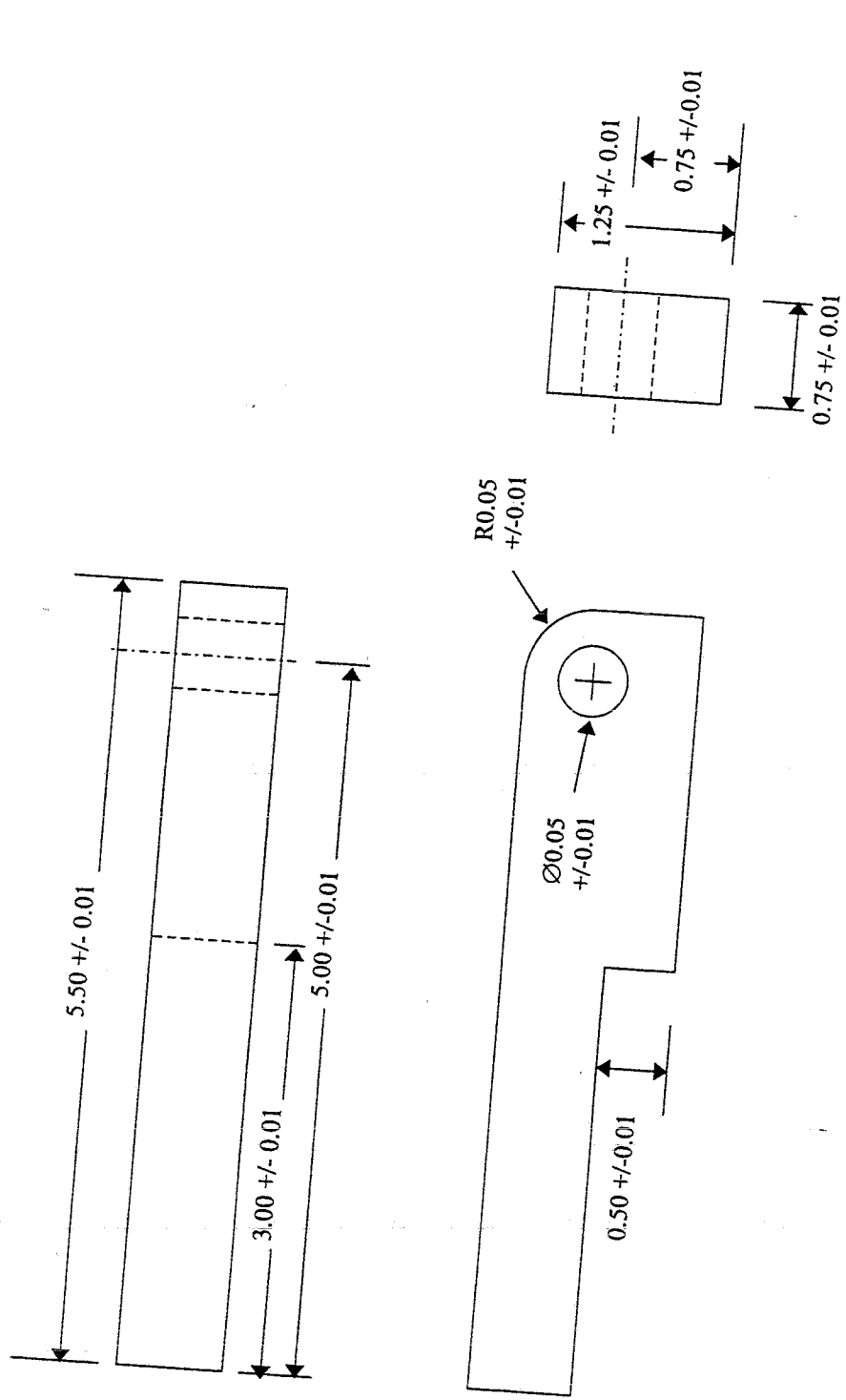
Figure 51. End Plugs Required to Manufacture Mandrel



All dimensions in inches

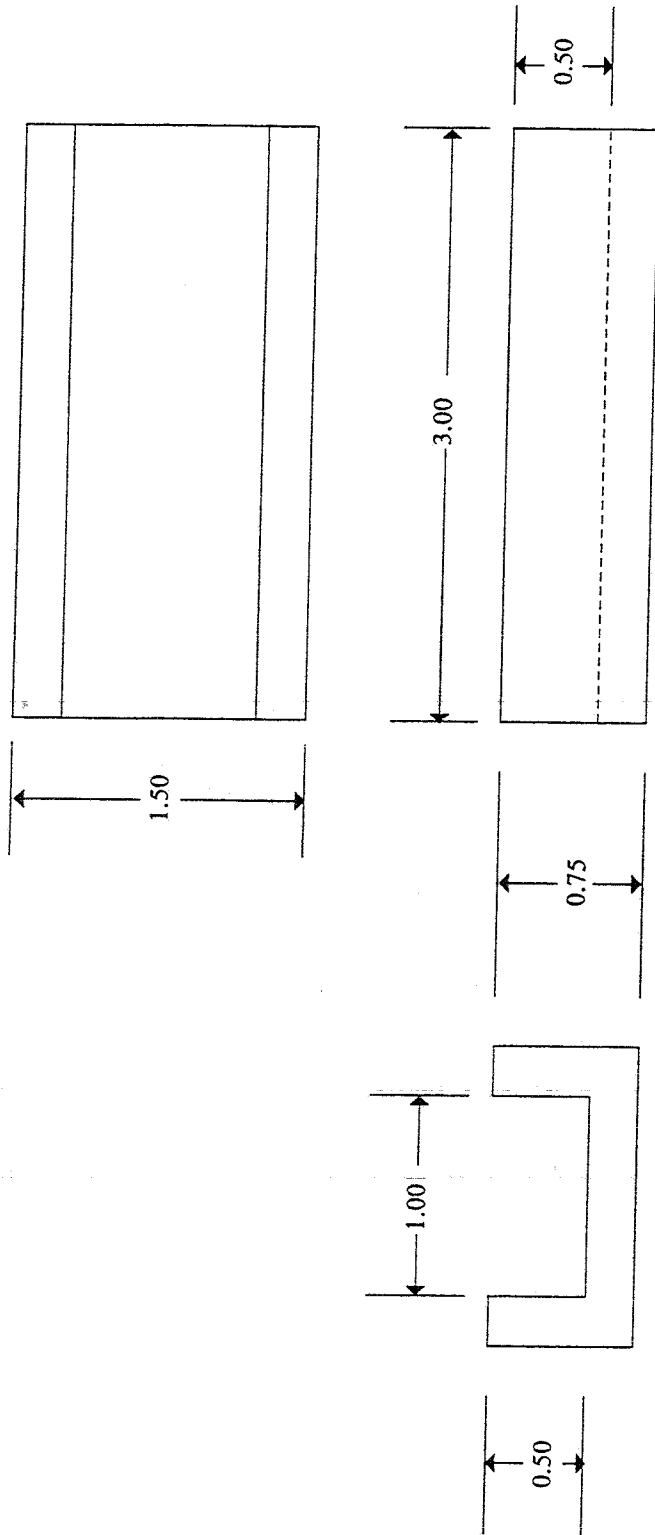
1 part is required

Figure 52. Spring Arm Holder



All dimension in inches
2 parts are required

Figure 53. Horizontal Support



All dimensions in inches

All tolerances are ± 0.01

1 part is required

Figure 54. Slider Holder

All dimensions in inches

Unless otherwise noted all tolerances are +/- 0.01

1 part is required

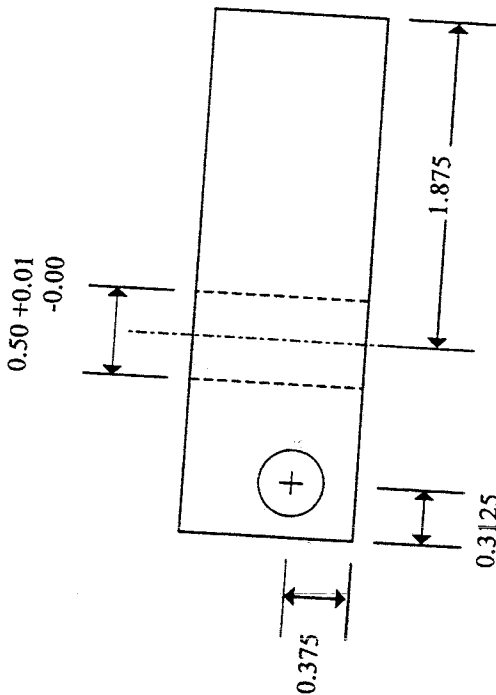
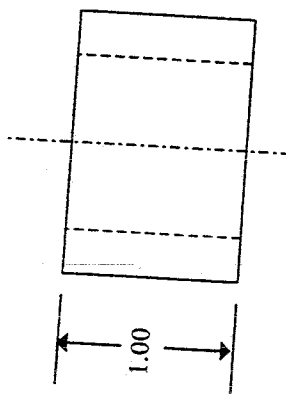
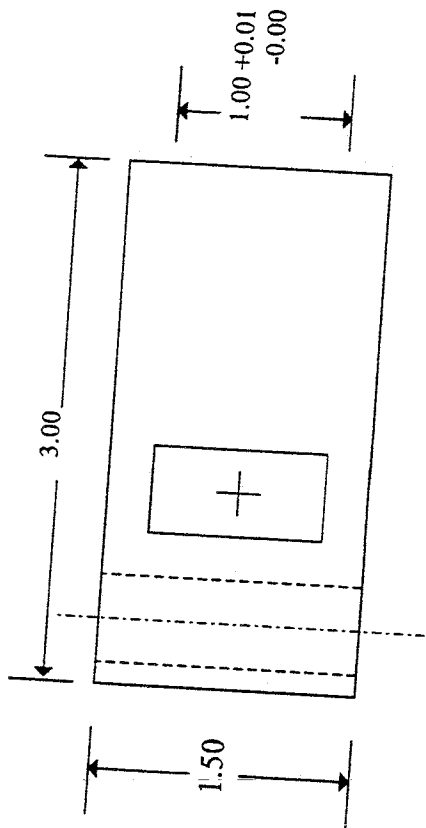


Figure 55. Pin Holder

All dimensions in inches

Unless otherwise noted all tolerances are ± 0.01

1 part is required

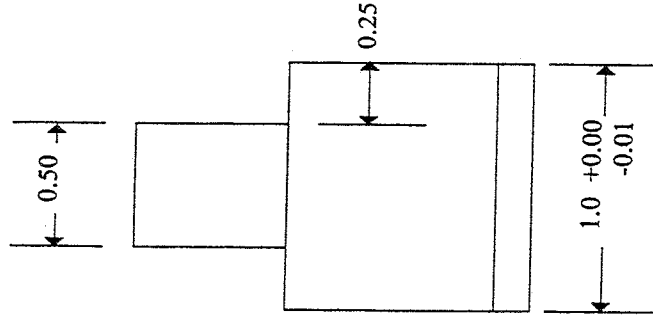
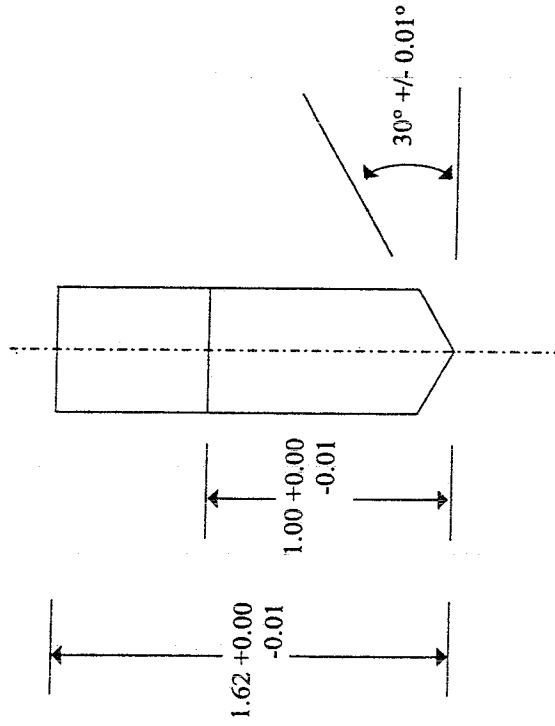
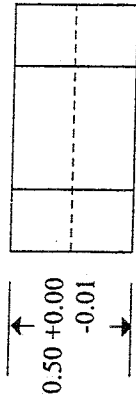


Figure 56. Pin

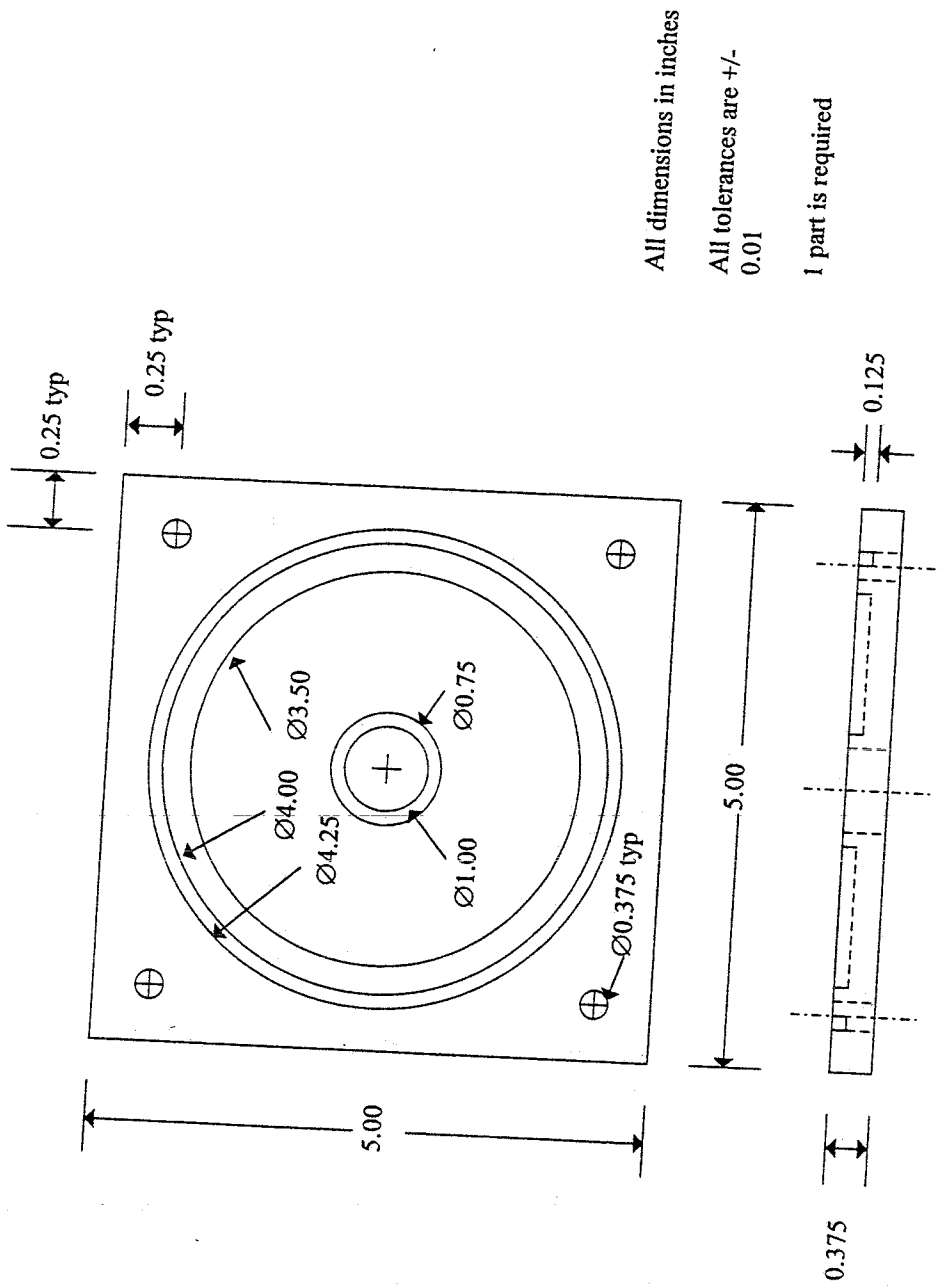
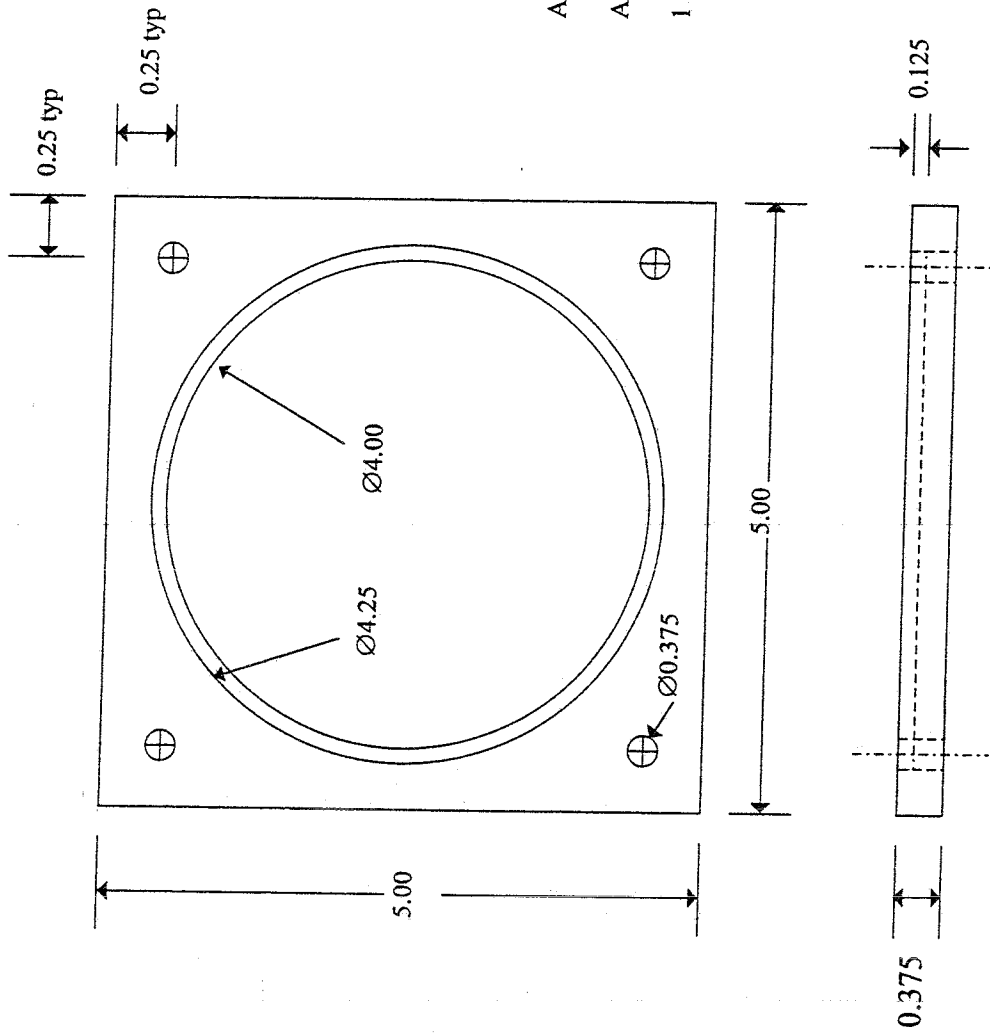


Figure 57. Bottom Plate

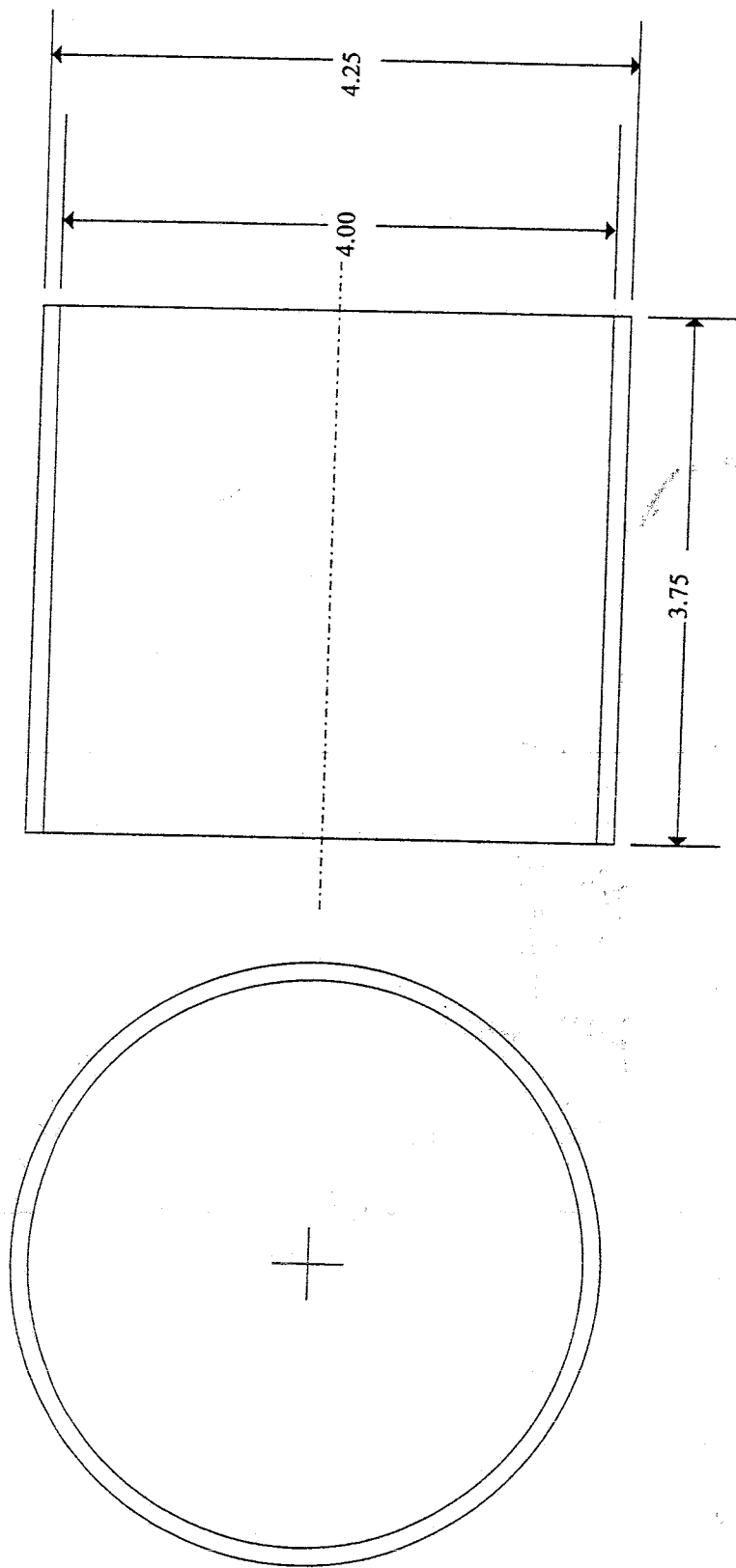


All dimensions in inches

All tolerances are +/- 0.01

1 part is required

Figure 58. Top Plate

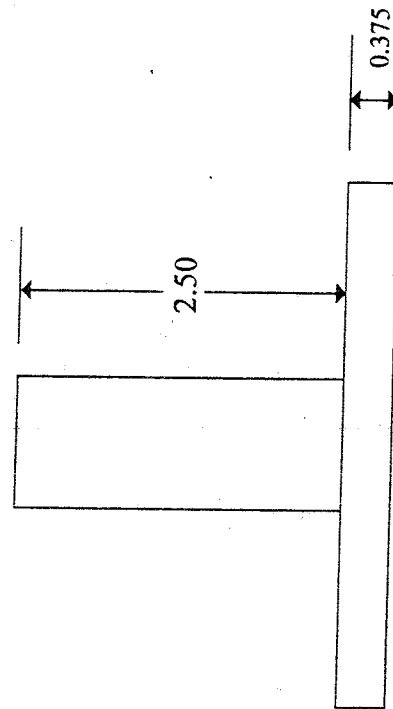
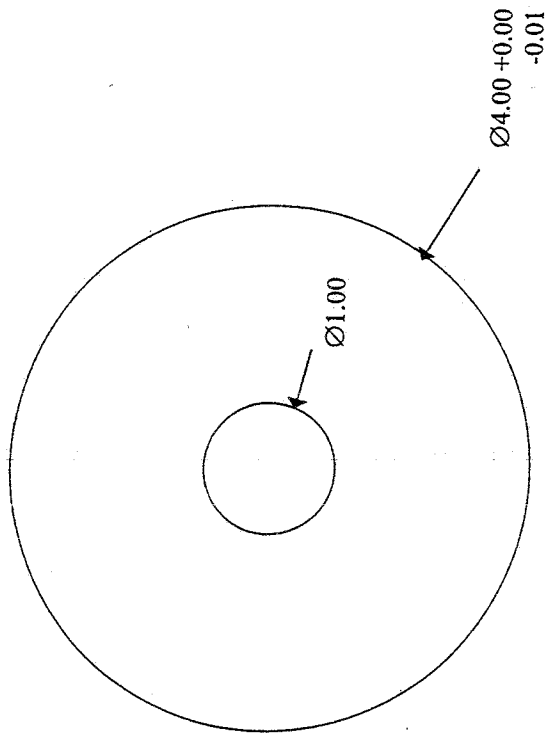


All dimensions in inches

All tolerances are +/-0.01

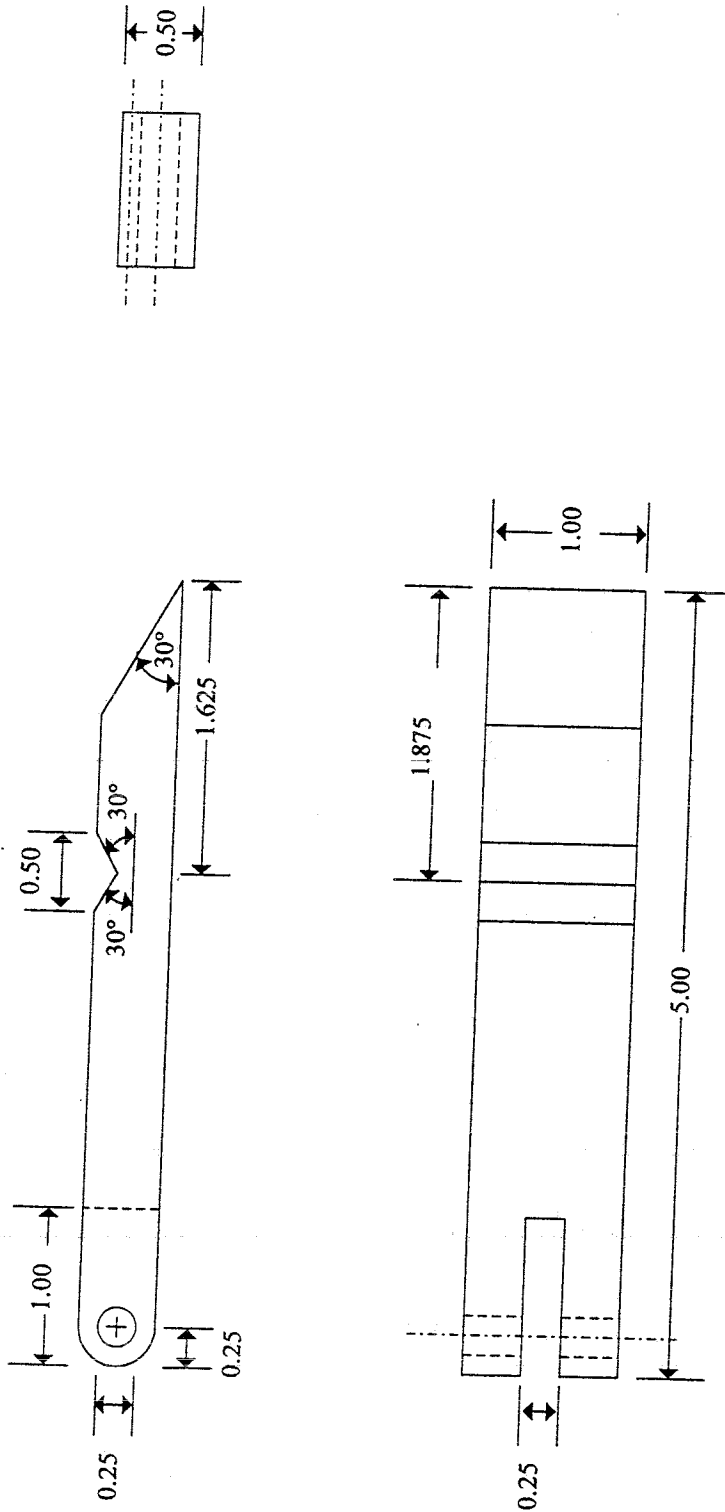
1 part is required

Figure 59. Pressure Vessel



All dimensions in inches
 Unless otherwise noted
 tolerances +/-0.01
 1 part is required

Figure 60. Plunger



All dimensions in inches
All tolerances are +/- 0.01

1 part is required

Figure 61. Slider

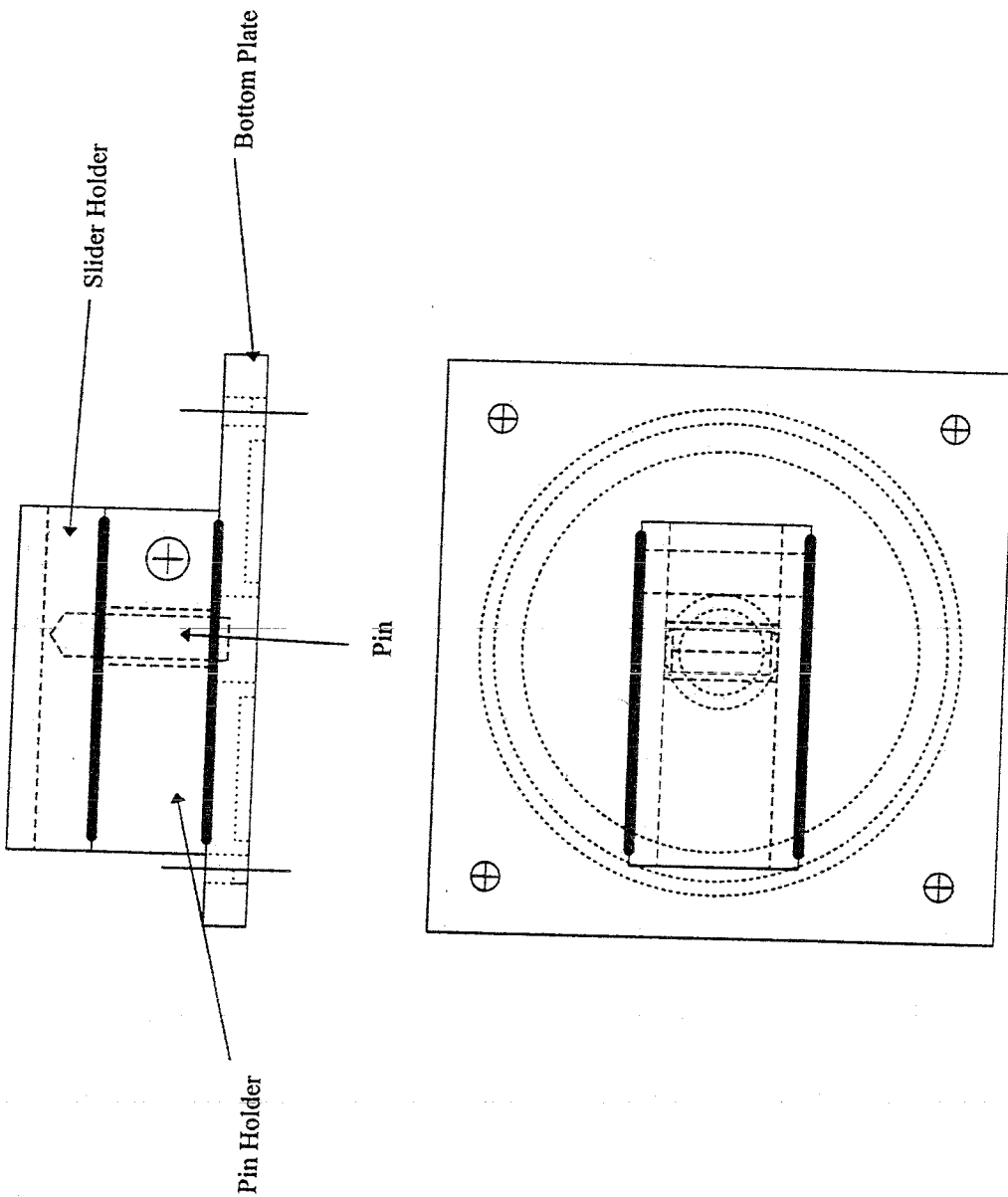


Figure 62. Welds on Bottom Plate, Slider Holder, and Pin Holder

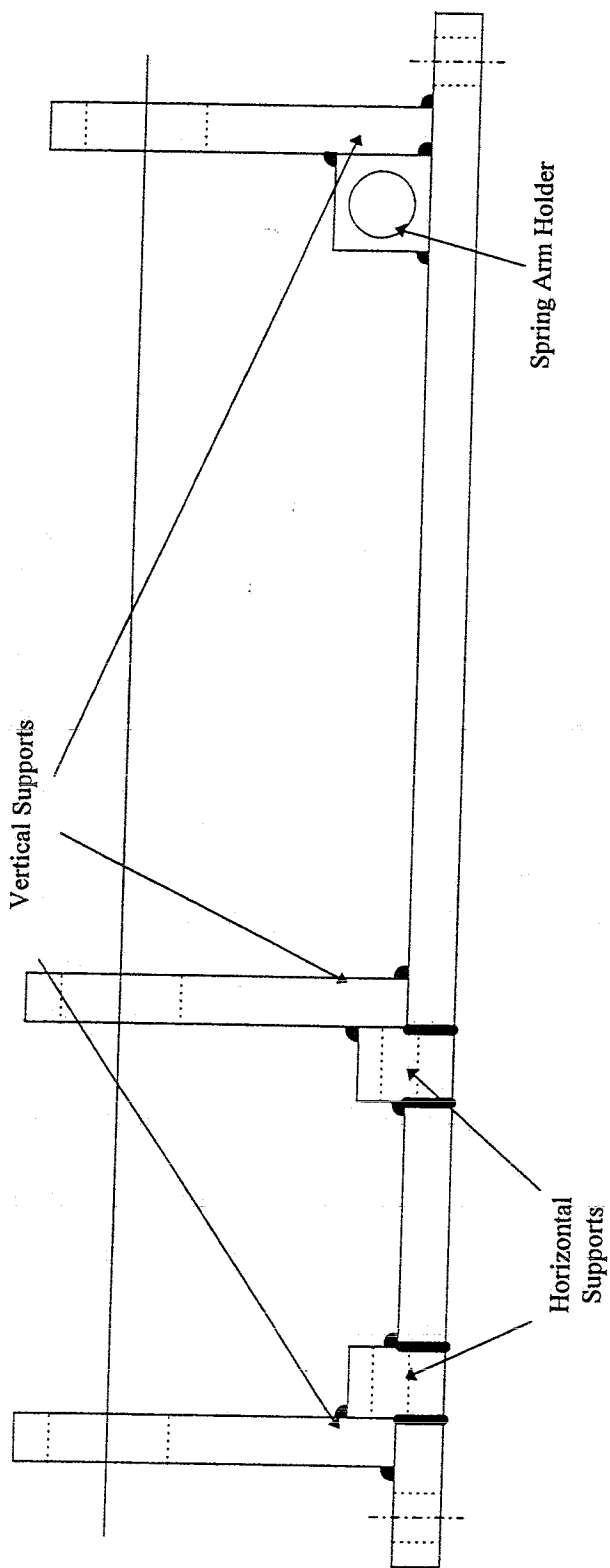


Figure 64. Welds Required to Attach Vertical Supports and Spring Arm Holder to Baseplate (Front View)

Prototype Assembly

Once all parts are welded together, they must be assembled. The first step in assembly is to place the mandrel into the spring as shown in Figure 65. Then, insert the shaft through the left vertical support, through the probe collar, and into the middle vertical support (Figure 66). Next, insert the straight spring arm into the spring arm holder (Figure 67), and push the spring into place. Then, insert the shaft through the mandrel and into the right vertical support.

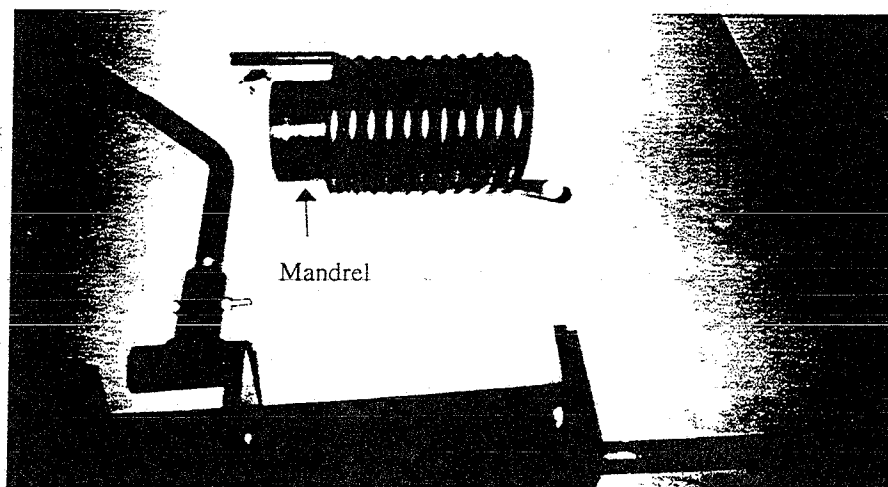


Figure 65. Spring with Mandrel Partially Inserted

The pneumatic clip must now be assembled. First, place the 4-inch OD gaskets into the outer grooves in the top and bottom plates (Figure 68). Then, place the pressure vessel into the outer groove of the bottom plate. Place the remaining gasket into the pressure vessel, followed by the plunger and the compression spring (Figure 69). The top plate now can be attached to the bottom plate by means of the 0.375-inch (0.9525 cm)

bolts, washers, and nuts (Figure 70). Tighten the nuts, making sure that the pressure vessel mates with the outer groove of the top plate.

The pneumatic clip is now ready to be attached to the baseplate. Insert the remaining bolt through one end of the chain. Next, insert the bolt through a link on the chain, through one hole on the horizontal support, through the hole in the pin holder, and into the hole in the other horizontal support (Figure 71). Put a nut on the other end of this bolt. Put the quicklink onto the other end of the chain. The PICS is now assembled.

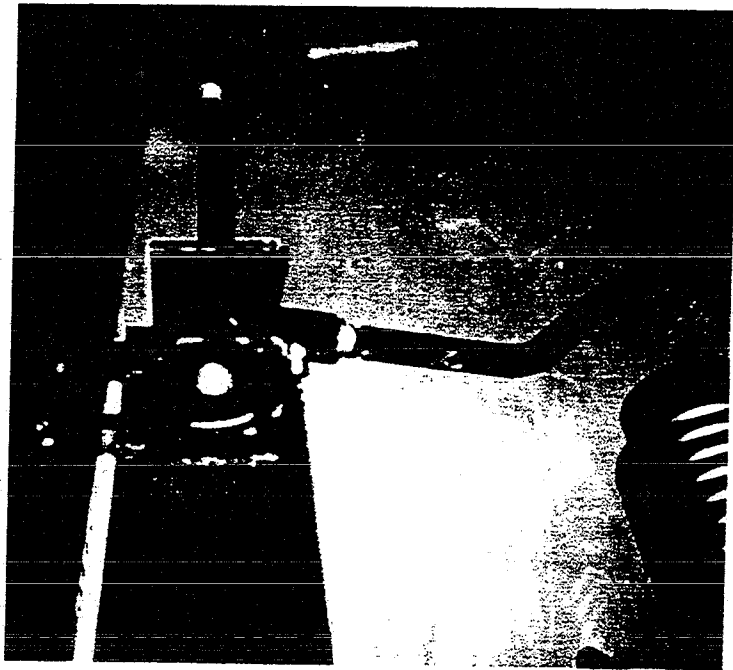


Figure 66. Shaft Inserted Through the Probe Arm Collar

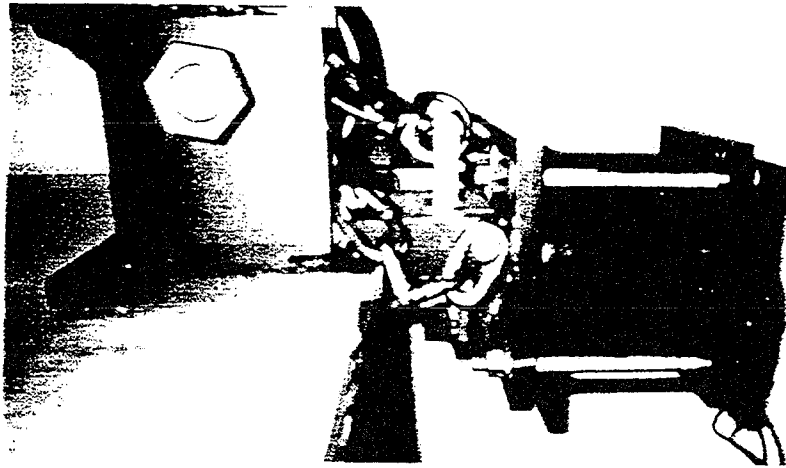


Figure 71. Pneumatic Clip Attached to Baseplate

Prototype Testing

The prototype was tested in the Louisiana Tech University Mechanical Laboratory to determine the velocity of the probe arm as a function of angular displacement of the spring arm from the launch position to plume. The velocity was measured with a digital chronograph designed to measure the velocity of a bullet which passes over two sensors. When the bullet passes over the first sensor, the chronograph activates; as the bullet passes over the second sensor, the chronograph deactivates. The chronograph divides the distance between the sensors by the time of activation to determine the velocity of the bullet. Since the probe arm has an angular velocity which consists of both x and y components, the velocity was measured while the probe arm was vertical (Figure 72). This configuration eliminated the y -component of velocity and resulted in a direct reading of the translational velocity of the probe arm. This configuration also limited measurable data to between the angles of 0° and 90° . The sensors were separated by 1.5 inches

This moment provides extra energy to the system. However, at full deflection this moment adds only 7 lbf-ft of energy to the system.

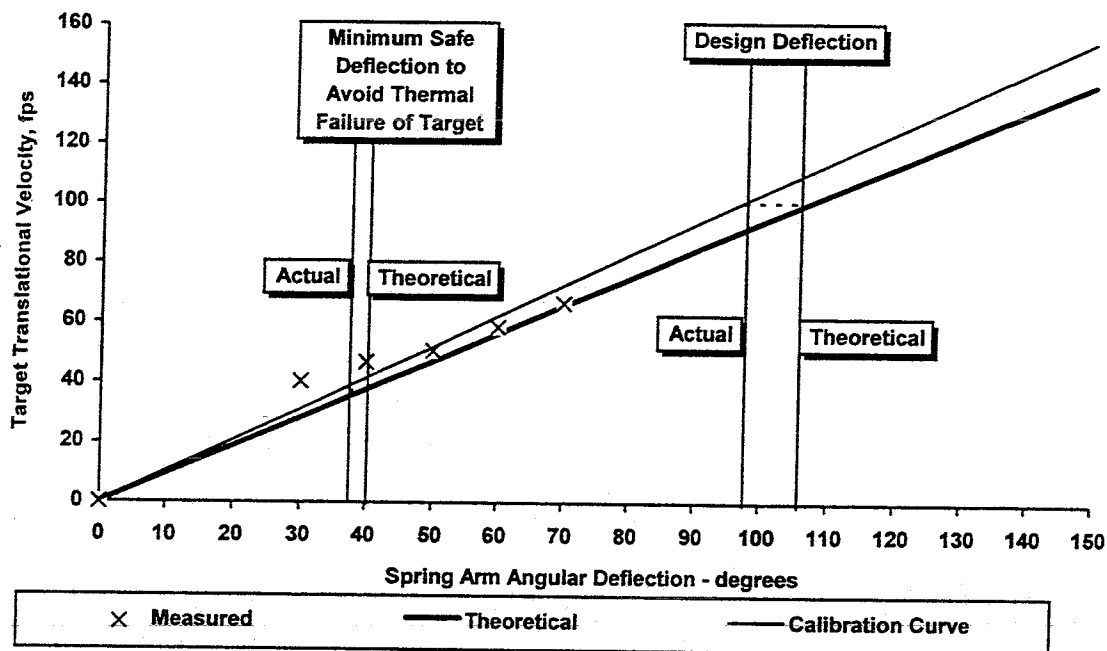


Figure 73. Experimental and Theoretical Probe Velocity

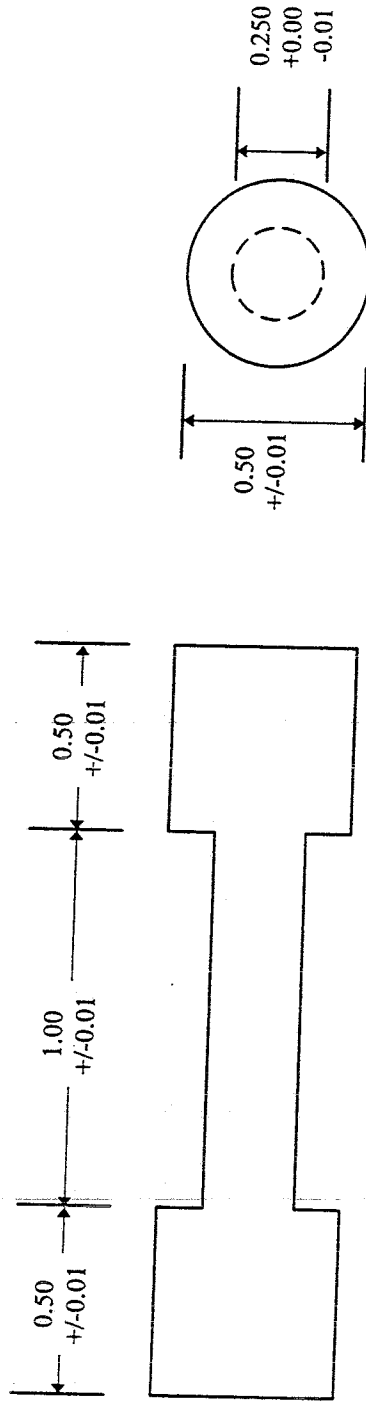
Operation of the PICS

1. Before the test firing of the rocket, mount the PICS in a position which allows the probe arm to pass perpendicularly to the exhaust flow. The probe should not be in the plume before launch nor should it be in the plume after launch, and the hole in the 0.5-inch (1.27 cm) section of the probe arm should be facing the rocket exhaust. The PICS should be firmly secured to the substrate with either bolts or clamps.
2. Push the slider into the pneumatic clip until it clicks into place.
3. Pressurize the pneumatic clip to 70 psig (482.6 kPa).

with the jig. At this point, the 0.5-inch diameter section will be a half-cylinder.

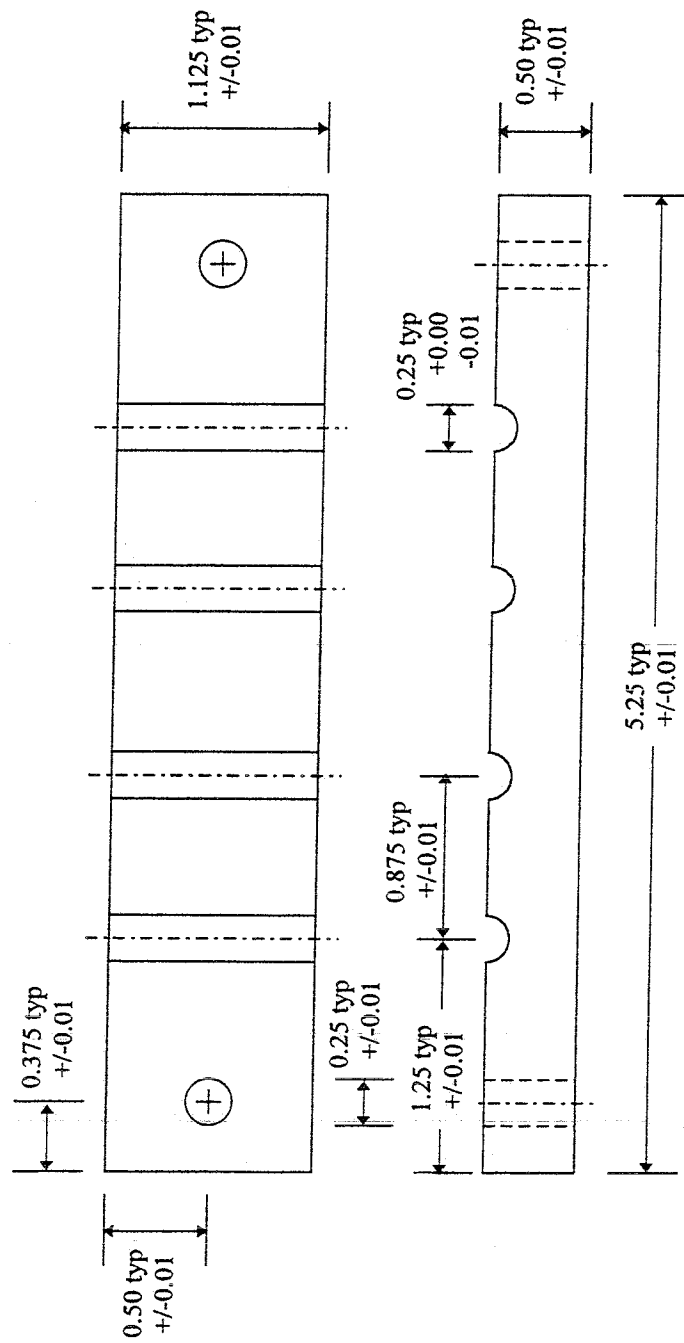
6. Remove jig part 2, place jig part 3 (Figure 77) over the flat surfaces of the target, and secure it to jig part 1.
7. At this point, the 0.25-inch (0.635 cm) diameter should be exposed in the center on the jig. Use an endmill to remove the exposed areas of the target so that the target is flush with the jig.
8. The aluminum half of the target is now fabricated. Remove it from the jig.
9. Repeat steps 1-8 with a copper (pure) cylinder.

The jig manufactured in the Louisiana Tech machine shop and shown in Figures 75 through 77 allows for up to four target halves to be manufactured at one time. It is a simple matter to increase this number by making the jig longer and adding more cradles for targets, if needed. Because of differences in the machining properties of aluminum and copper, it is suggested that only one material type be placed in the jig at one time.



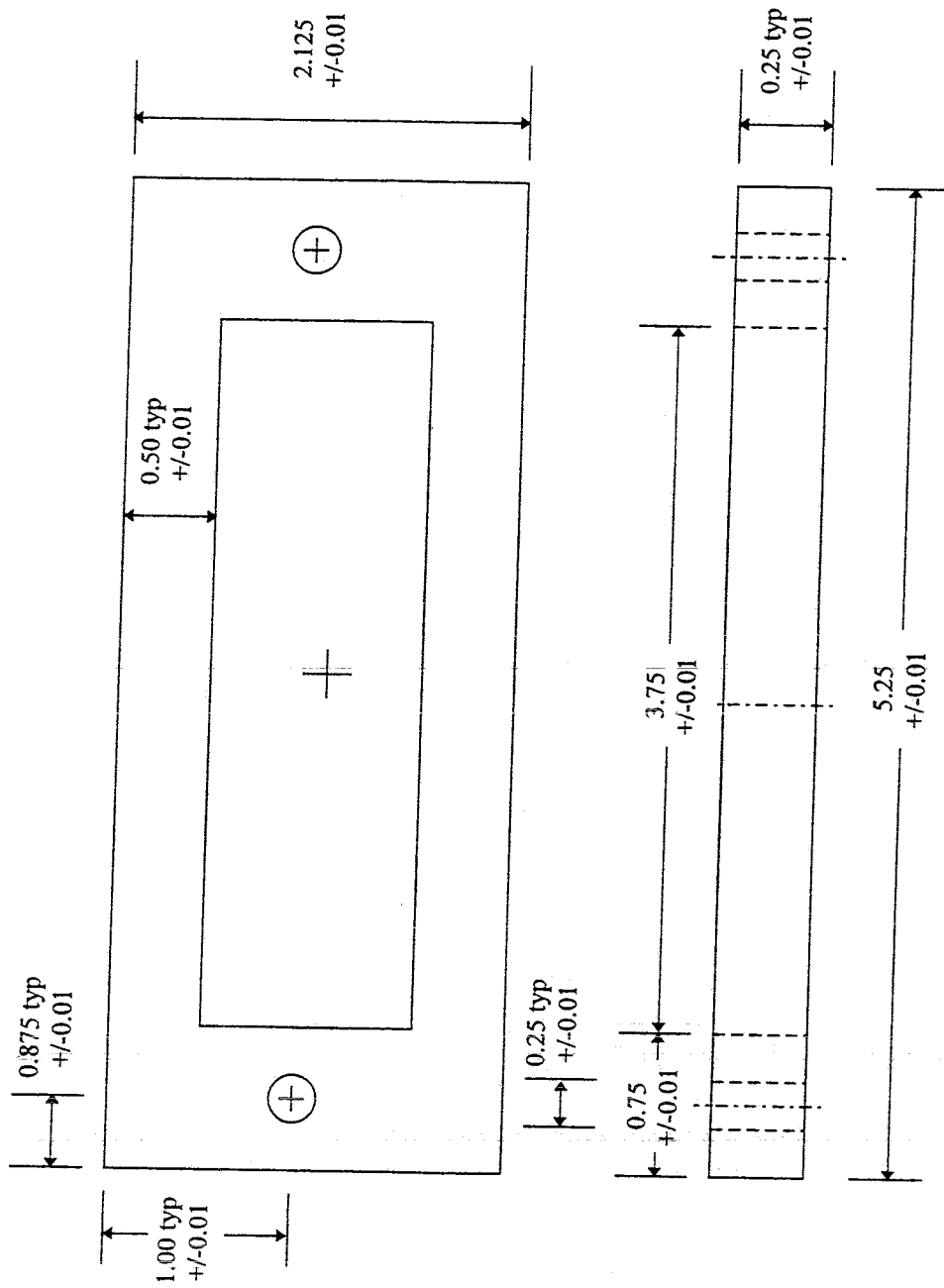
All dimensions in inches

Figure 74. Insert Required to Manufacture Targets



All dimensions in inches

Figure 76. Jig Part 2



All dimensions in inches

Figure 77. Jig Part 3

```

/* This program calculates the safe residence time of the target and probe. If
SEMI_INFINITE is defined the calculation assumes that the sides are insulated. Either
AL (aluminum) or CU (copper) must be defined for the program to work correctly.*/

```

```

#include <stdio.h>
#include <conio.h>
#include <math.h>
#include <stdlib.h>
#include <string.h>

```

```

#define INFINITE 1.0e+300

```

```

#define NUMR 11
#define NUMZ 121
#define EPS 0.01

```

```

#define dSEMI_INFINITE
#define CU

```

```

double T[NUMR][NUMZ],Told[NUMR][NUMZ],To;
double Rip,Rim,Rjp,Rjm,SumR,SumTR;
double dt,dr,dz,t,C;
int i,j,converged;

```

```

void main(void){
    double h1,h2,T1,T2;
    int p1,p2,p3,l;
    double cs,denss,ks,Tcrits;
    double ct,denst,kt,Tcritt;
    double dq,dv;
    double pi,q,r;
    char target[12],FrontTemp[20],SideTemp[20],CenterTemp[20],Dim[3];
    FILE *Side,*Center,*Front;
    void CheckForCritical(double,double,int,int);
    void CalculateNode(double,double,double,double);

    clrscr();
    _setcursortype(_NOCURSOR);
    pi=4*atan(1);
    t=0;
    dt=.001;           /* s */
    dr=.00635/(NUMR-1); /* m */
    dz=.0762/(NUMZ-1); /* m */

```

```

p1=(NUMZ-1)/6.0;
p2=(NUMR-1)/2.0;
p3=(NUMZ-1)/3.0;

```

```

/**** load environment data ****/
T1=3437;          /* K */
T2=2224;          /* K */
h1=10220;         /* W/m^2*C */
h2=3371;          /* W/m^2*C */

```

```

/**** load material data ****/
#ifdef AL
strcpy(target,"Al");
strcpy(FrontTemp,"alfront.dat");
strcpy(SideTemp,"alside.dat");
strcpy(CenterTemp,"alcenter.dat");
denst=2700;        /* kg/m^3 */
ct=866;           /* J/kg*C */
kt=220;           /* W/m*C */
Tcritt=700;       /* K */
#endif

```

```

#ifdef CU
strcpy(target,"Cu");
strcpy(FrontTemp,"cufront.dat");
strcpy(SideTemp,"cuside.dat");
strcpy(CenterTemp,"cucenter.dat");
denst=8954;        /* kg/m^3 */
ct=384;           /* J/kg*C */
kt=386;           /* W/m*C */
Tcritt=1017;      /* K */
#endif

```

```

#ifdef STEEL
strcpy(target,"Steel");
denst=7800;        /* kg/m^3 */
ct=470;           /* J/kg*C */
kt=43;            /* W/m*C */
Tcritt=1360;      /* K */
#endif

```

```

denss=7800;       /* kg/m^3 */
cs=470;           /* J/kg*C */

```

```

ks=43;                /* W/m*°C */
Tcrits=1360;         /* K */

Front=fopen(FrontTemp,"wt");
Side=fopen(SideTemp,"wt");
Center=fopen(CenterTemp,"wt");

fprintf(Side," ");
fprintf(Center," ");
fprintf(Front," ");
for(i=0;i<NUMZ;i++){
    fprintf(Side,"%4.2lf ",i*dz*39.37);
    fprintf(Center,"%4.2lf ",i*dz*39.37);
}
for(j=0;j<NUMR;j++) fprintf(Front,"%4.2lf ",j*dr*39.37);

strcpy(Dim,"2D");
#ifdef SEMI_INFINITE
strcpy(Dim,"1D");
#endif

printf("target material: %s - %s conduction\n",target,Dim);
printf("dr=%1.2e in, dz=%1.2e in, dt=%1.2e sec\n",dr*39.37,dz*39.37,dt);

for(i=0;i<NUMR;i++)
for(j=0;j<NUMZ;j++){
    T[i][j]=300;        /* K */
    Told[i][j]=T[i][j];
}

do{
t+=dt;
do{
    converged=1;
    for(j=NUMZ-1;j>=0;j--){
        for(i=NUMR-1;i>=0;i--){
            r=i*dr;
            To=T[i][j];
            if(i==0){ /* along the centerline */
                if(j==0){ /* flat exposed surface */
                    Rip=dr/((r+dr/2)*pi*(dz/2)*kt);
                    Rim=INFINITE;
                    Rjm=1/((pi/8)*dr*dr*h1);
                }
            }
        }
    }
}

```



```

Rjp=dz/((pi/8)*dr*dr*kt);
dv=(pi/8)*dr*dr*(dz/2);
C=denst*ct*dv;
CalculateNode(T[i+1][j],T[i+1][j],T[i][j+1],T1);
}else if(j==NUMZ-1){ /* insulated surface */
Rip=dr/((r+dr/2)*pi*(dz/2)*ks);
Rim=INFINITE;
Rjm=(dz)/((pi/8)*dr*dr*ks);
Rjp=INFINITE;
dv=(pi/8)*dr*dr*(dz/2);
C=denss*cs*dv;
CalculateNode(T[i+1][j],T[i+1][j],0,T[i][j-1]);
}else if(j==p3){ /* corner between target and arm */
Rip=dr/((r+dr/2)*dz/2)*(1/ks+1/kt);
Rim=INFINITE;
Rjm=dz/((pi/8)*dr*dr*kt);
Rjp=dz/((pi/8)*dr*dr*ks);
dv=(pi/8)*dr*dr*dz/2;
C=(denss*cs + denst*ct)*dv;
CalculateNode(T[i+1][j],T[i+1][j],T[i][j+1],T[i][j-1]);
}else if(j<p3){ /* interior target nodes */
Rip=dr/((r+dr/2)*pi*dz*kt);
Rim=INFINITE;
Rjm=dz/((pi/8)*dr*dr*kt);
Rjp=dz/((pi/8)*dr*dr*kt);
dv=(pi/8)*dr*dr*dz;
C=denst*ct*dv;
CalculateNode(T[i+1][j],T[i+1][j],T[i][j+1],T[i][j-1]);
}else if(j>p3){ /* interior steel nodes */
Rip=dr/((r+dr/2)*pi*dz/2*ks);
Rim=INFINITE;
Rjm=dz/((pi/8)*dr*dr*ks);
Rjp=dz/((pi/8)*dr*dr*ks);
dv=(pi/8)*dr*dr*dz;
C=denss*cs*dv;
CalculateNode(T[i+1][j],T[i+1][j],T[i][j+1],T[i][j-1]);
}
}else if(j==0){ /* along flat face */
if(i==NUMR-1){ /* corner node */
Rip=1/(pi*r*(dz/2)*h2);
Rim=dr/((r-dr/2)*pi*(dz/2)*kt);
#ifdef SEMI_INFINITE
Rip=INFINITE;

```

```

#endif
Rjm=1/(.5*pi*(r*dr-dr*dr/4)*h1);
Rjp=(dz)/(.5*pi*(r*dr-dr*dr/4)*kt);
dv=.5*pi*(r*dr-dr*dr/4)*(dz/2);
C=denst*ct*dv;
CalculateNode(T2,T[i-1][j],T[i][j+1],T1);
}else{ /* exterior convection nodes */
Rip=dr/((r+dr/2)*pi*(dz/2)*kt);
Rim=dr/((r-dr/2)*pi*(dz/2)*kt);
Rjm=1/(r*dr*pi*h1);
Rjp=(dz)/(r*dr*pi*kt);
dv=r*dr*pi*(dz/2);
C=denst*ct*dv;
CalculateNode(T[i+1][j],T[i-1][j],T[i][j+1],T1);
}
}else if(i==NUMR-1){ /* along curved exposed surface */
if(j==NUMZ-1){ /* insulated corner */
Rip=1/(pi*r*(dz/2)*h2);
Rim=dr/((r-dr/2)*pi*(dz/2)*ks);
#ifdef SEMI_INFINITE
Rip=INFINITE;
#endif
Rjm=dz/(.5*pi*(r*dr-dr*dr/4)*ks);
Rjp=INFINITE;
dv=.5*pi*(r*dr-dr*dr/4)*(dz/2);
C=denss*cs*dv;
CalculateNode(T2,T[i-1][j],0,T[i][j-1]);
}else if(j==p1){ /* boundary between materials */
Rip=1/(pi*r*dz*h2);
Rim=dr/(((r-dr/2)*pi*(dz/2))*(1/ks+1/kt));
#ifdef SEMI_INFINITE
Rip=INFINITE;
#endif
Rjm=dz/(.5*pi*(r*dr-dr*dr/4)*kt);
Rjp=dz/(.5*pi*(r*dr-dr*dr/4)*ks);
dv=.5*pi*(r*dr-dr*dr/4)*dz;
C=.5*denss*cs*dv + .5*denst*ct*dv;
CalculateNode(T2,T[i-1][j],T[i][j+1],T[i][j-1]);
}else if(j<p1){ /* target convection nodes */
Rip=1/(pi*r*dz*h2);
Rim=dr/((r-dr/2)*pi*dz*kt);
#ifdef SEMI_INFINITE
Rip=INFINITE;

```

```

#endif
Rjm=dz/(.5*pi*(r*dr-dr*dr/4)*kt);
Rjp=dz/(.5*pi*(r*dr-dr*dr/4)*kt);
dv=.5*pi*(r*dr-dr*dr/4)*dz;
C=denst*ct*dv;
CalculateNode(T2,T[i-1][j],T[i][j+1],T[i][j-1]);
}else if(j>p1){ /* steel convection nodes */
Rip=1/(pi*r*dz*h2);
Rim=dr/((r-dr/2)*pi*dz*ks);
#ifdef SEMI_INFINITE
Rip=INFINITE;
#endif
Rjm=dz/(.5*pi*(r*dr-dr*dr/4)*ks);
Rjp=dz/(.5*pi*(r*dr-dr*dr/4)*ks);
dv=.5*pi*(r*dr-dr*dr/4)*dz;
C=denss*cs*dv;
CalculateNode(T2,T[i-1][j],T[i][j+1],T[i][j-1]);
}
}else if(i==p2){ /* along longitudinal boundary */
if(j==p1){ /* front corner of stem */
Rip=dr/((r+dr/2)*pi*dz/2)*(1/ks+1/kt);
Rim=dr/((r-dr/2)*pi*dz*kt);
Rjm=dz/(r*dr*pi*kt);
Rjp=dz/((pi/2*(dr*dr/4+r*dr)*ks)+(pi/2*(r*dr-
dr*dr/4)*kt));
C=denst*ct*pi*r*dr*(dz/2) +
denss*cs*pi/2*(r*dr+dr*dr/4)*dz/2 +
denst*ct*pi/2*(r*dr-dr*dr/4)*dz/2;
CalculateNode(T[i+1][j],T[i-1][j],T[i][j+1],T[i][j-1]);
}else if(j==p3){ /* rear corner of stem */
Rip=dr/((r+dr/2)*pi*dz*ks);
Rim=dr/((r-dr/2)*pi*dz/2)*(1/ks+1/kt);
Rjm=dz/((pi/2*(dr*dr/4+r*dr)*ks)+(pi/2*(r*dr-
dr*dr/4)*kt));
Rjp=dz/(r*dr*pi*ks);
C=denss*cs*pi/2*(r*dr+dr*dr/4)*dz +
.5*denss*cs*pi/2*(r*dr-dr*dr/4)*dz +
.5*denst*ct*pi/2*(r*dr-dr*dr/4)*dz;
CalculateNode(T[i+1][j],T[i-1][j],T[i][j+1],T[i][j-1]);
}else if(j<p1){ /* target nodes */
Rip=dr/((r+dr/2)*pi*dz*kt);
Rim=dr/((r-dr/2)*pi*dz*kt);
Rjm=dz/(r*dr*pi*kt);

```

```

Rjp=dz/(r*dr*pi*kt);
dv=r*dr*pi*dz;
C=denst*ct*dv;
CalculateNode(T[i+1][j],T[i-1][j],T[i][j+1],T[i][j-1]);
}else if(j==NUMZ-1){ /* insulated face */
Rip=dr/((r+dr/2)*pi*dz/2*ks);
Rim=dr/((r-dr/2)*pi*dz/2*ks);
Rjm=dz/(r*dr*pi*ks);
Rjp=INFINITE;
dv=r*dr*pi*dz/2;
C=denss*cs*dv;
CalculateNode(T[i+1][j],T[i-1][j],0,T[i][j-1]);
}else if(j>p3){ /* steel nodes */
Rip=dr/((r+dr/2)*pi*dz*ks);
Rim=dr/((r-dr/2)*pi*dz*ks);
Rjm=dz/(r*dr*pi*ks);
Rjp=dz/(r*dr*pi*ks);
dv=r*dr*pi*dz;
C=denss*cs*dv;
CalculateNode(T[i+1][j],T[i-1][j],T[i][j+1],T[i][j-1]);
}else{ /* nodes on boundary */
Rip=dr/((r+dr/2)*pi*dz*ks);
Rim=dr/((r-dr/2)*pi*dz*kt);
Rjm=dz/((pi/2*(dr*dr/4+r*dr)*ks)+(pi/2*(r*dr-
dr*dr/4)*kt));
Rjp=dz/((pi/2*(dr*dr/4+r*dr)*ks)+(pi/2*(r*dr-
dr*dr/4)*ks));
C=denss*cs*pi/2*(r*dr+dr*dr/4)*dz +
denst*ct*pi/2*(r*dr-dr*dr/4)*dz;
CalculateNode(T[i+1][j],T[i-1][j],T[i][j+1],T[i][j-1]);
}
}else if(j==p1){ /* nodes along outer radial boundary */
if(i>p2){ /* nodes along boundary */
Rip=dr/((r+dr/2)*pi*dz/2)*(1/kt+1/ks);
Rim=dr/((r-dr/2)*pi*dz/2)*(1/kt+1/ks);
Rjm=dz/(r*dr*pi*kt);
Rjp=dz/(r*dr*pi*ks);
dv=r*dr*pi*dz;
C=.5*denst*ct*dv + .5*denss*cs*dv;
CalculateNode(T[i+1][j],T[i-1][j],T[i][j+1],T[i][j-1]);
}else{ /* nodes in target */
Rip=dr/((r+dr/2)*pi*dz*kt);
Rim=dr/((r-dr/2)*pi*dz*kt);

```

```

    Rjm=dz/(r*dr*pi*kt);
    Rjp=dz/(r*dr*pi*kt);
    dv=r*dr*pi*dz;
    C=denst*ct*dv;
    CalculateNode(T[i+1][j],T[i-1][j],T[i][j+1],T[i][j-1]);
}
} else if(j==p3){ /* nodes along inner radial boundary */
    if(i<p2){ /* nodes along boundary */
        Rip=dr/((r+dr/2)*pi*dz/2)*(1/kt+1/ks);
        Rim=dr/((r-dr/2)*pi*dz/2)*(1/kt+1/ks);
        Rjm=dz/(r*dr*pi*kt);
        Rjp=dz/(r*dr*pi*ks);
        dv=r*dr*pi*dz;
        C=.5*denst*ct*dv + .5*denss*cs*dv;
        CalculateNode(T[i+1][j],T[i-1][j],T[i][j+1],T[i][j-1]);
    } else { /* nodes in steel */
        Rip=dr/((r+dr/2)*pi*dz*ks);
        Rim=dr/((r-dr/2)*pi*dz*ks);
        Rjm=dz/(r*dr*pi*ks);
        Rjp=dz/(r*dr*pi*ks);
        dv=r*dr*pi*dz;
        C=denss*cs*dv;
        CalculateNode(T[i+1][j],T[i-1][j],T[i][j+1],T[i][j-1]);
    }
} else if(j==NUMZ-1){ /* nodes along insulated boundary */
    Rip=dr/((r+dr/2)*pi*dz/2*ks);
    Rim=dr/((r-dr/2)*pi*dz/2*ks);
    Rjm=dz/(r*dr*pi*ks);
    Rjp=INFINITE;
    dv=r*dr*pi*(dz/2);
    C=denss*cs*dv;
    CalculateNode(T[i+1][j],T[i-1][j],0,T[i][j-1]);
} else if(j<p1){ /* nodes in target front interior */
    Rip=dr/((r+dr/2)*pi*dz*kt);
    Rim=dr/((r-dr/2)*pi*dz*kt);
    Rjm=dz/(r*dr*pi*kt);
    Rjp=dz/(r*dr*pi*kt);
    dv=r*dr*pi*dz;
    C=denst*ct*dv;
    CalculateNode(T[i+1][j],T[i-1][j],T[i][j+1],T[i][j-1]);
} else if(j<p3){ /* nodes in target stem region */
    if(i<p2){ /* target nodes */
        Rip=dr/((r+dr/2)*pi*dz*kt);

```

```

        Rim=dr/((r-dr/2)*pi*dz*kt);
        Rjm=dz/(r*dr*pi*kt);
        Rjp=dz/(r*dr*pi*kt);
        dv=r*dr*pi*dz;
        C=denst*ct*dv;
        CalculateNode(T[i+1][j],T[i-1][j],T[i][j+1],T[i][j-1]);
    }else{
        /* steel nodes */
        Rip=dr/((r+dr/2)*pi*dz*ks);
        Rim=dr/((r-dr/2)*pi*dz*ks);
        Rjm=dz/(r*dr*pi*ks);
        Rjp=dz/(r*dr*pi*ks);
        dv=r*dr*pi*dz;
        C=denss*cs*dv;
        CalculateNode(T[i+1][j],T[i-1][j],T[i][j+1],T[i][j-1]);
    }
}
} else{
    /* remaining steel nodes */
    Rip=dr/((r+dr/2)*pi*dz*ks);
    Rim=dr/((r-dr/2)*pi*dz*ks);
    Rjm=dz/(r*dr*pi*ks);
    Rjp=dz/(r*dr*pi*ks);
    dv=r*dr*pi*dz;
    C=denss*cs*dv;
    CalculateNode(T[i+1][j],T[i-1][j],T[i][j+1],T[i][j-1]);
}
} /* end else */
} /* end i loop */
}while(!converged); /* end inner do loop */

gotoxy(1,5);
printf("current time: %4.1lf ms\n",t*1000);
printf("temp at center of target is %4.0lf %4.0lf %4.0lf %4.0lf %4.0lf\n",
        T[0][0],T[0][1],T[0][2],T[0][3],T[0][4]);
printf("temp at edge of target is %4.0lf %4.0lf %4.0lf %4.0lf %4.0lf\n",
        T[NUMR-1][0],T[NUMR-1][1],T[NUMR-1][2],
        T[NUMR-1][3],T[NUMR-1][4]);
printf("\nfront      stem      insulated\n");

for(l=NUMR-1;l>=0;l--)
    printf("%4.0lf %4.0lf %4.0lf %4.0lf %4.0lf %4.0lf %4.0lf\n",
        T[l][0],T[l][p1/2],T[l][p1],T[l][(p3+p1)/2],T[l][p3],
        T[l][(NUMZ-1 + p3)/2],T[l][NUMZ-1]);

fprintf(Front,"%n%4.1lf ",t*1000);

```

```

    fprintf(Side, "\n%4.1lf ", t*1000);
    fprintf(Center, "\n%4.1lf ", t*1000);
    for(l=0; l<NUMZ; l++){
        fprintf(Side, "%4.0lf ", 1.8*T[NUMR-1][l]);
        fprintf(Center, "%4.0lf ", 1.8*T[0][l]);
    }
    for(l=0; l<NUMR; l++) fprintf(Front, "%4.0lf ", 1.8*T[l][0]);

    for(l=0; l<NUMR; l++){
        CheckForCritical(T[l][0], Tcritt, l, 0);
        if(l<p2) CheckForCritical(T[l][p3], Tcrits, l, p3);
        else CheckForCritical(T[l][p1], Tcrits, l, p1);
    }
    for(l=0; l<=p3; l++){
        if(l<p1) CheckForCritical(T[NUMR-1][l], Tcrits, NUMR-1, l);
        else CheckForCritical(T[p2][l], Tcrits, p2, l);
    }
    CheckForCritical(T[NUMR-1][p1], Tcrits, NUMR-1, p1);
    CheckForCritical(T[p1][p2], Tcrits, p1, p2);

    for(i=0; i<NUMR; i++)
        for(j=0; j<NUMZ; j++) Told[i][j]=T[i][j];

    } while(1);
    _setcursortype(_NORMALCURSOR);
    fclose(Front);
    fclose(Side);
    fclose(Center);
}

void CheckForCritical(double temp, double tcrit, int noder, int nodez){
    if(temp>=tcrit){
        gotoxy(1,20);
        printf("\n\nunsafe residence time is %4.1lf ms", t*1000);
        printf(" at r=%1.2e and z=%1.2e", noder*dr*39.37, nodez*dz*39.37);
        printf("\nT=%4.0lf Tcrit=%4.0lf\n", temp, tcrit);
        exit(0);
    }
}

void CalculateNode(double Tip, double Tim, double Tjp, double Tjm){

```

```
SumR=1/Rip + 1/Rim + 1/Rjp + 1/Rjm;  
SumTR=Tip/Rip + Tim/Rim + Tjp/Rjp + Tjm/Rjm;  
T[i][j]=(SumTR + (C/dt)*Told[i][j])/(SumR + C/dt);  
if(fabs(T[i][j]-To) < EPS){  
    converged*=1;  
}else converged*=0;
```

```
}
```


APPENDIX B

**TABULATED DATA FROM THE THERMAL
RESPONSE PROGRAM**

Table B1. Temperature Profiles (°R) Along Exposed Flat Surface of Aluminum Target (Figure 13)

Time ms	Centerline	0.05 inch	0.1 inch	0.15 inch	0.2 inch	Outer Edge
1	595	595	595	595	596	607
10	805	805	806	808	820	861
20	918	918	921	929	951	997
30	1002	1003	1009	1023	1051	1098
40	1074	1076	1084	1102	1134	1181
51	1144	1148	1158	1179	1213	1260

Table B2. Temperature Profiles (°R) Along the Exposed Flat Surface of Copper Target (Figure 14)

Time ms	Centerline	0.05 inch	0.1 inch	0.15 inch	0.2 inch	Outer Edge
1	576	576	576	576	576	584
50	929	931	939	953	974	1003
100	1114	1118	1127	1143	1165	1194
150	1264	1268	1277	1292	1314	1341
200	1393	1396	1405	1420	1440	1466
250	1507	1510	1519	1533	1552	1577
300	1611	1614	1622	1635	1654	1678
350	1706	1709	1717	1730	1748	1771
384	1768	1770	1778	1791	1809	1831

Table B3. Temperature Profiles (°R) Along Centerline of Aluminum Target and Steel Holder (Figure 15)

Time ms	0 inch	0.1	0.2	0.3	0.4	0.5	0.6	1	2	3 inch
1	595	540	540	540	540	540	540	540	540	540
10	805	550	540	540	540	540	540	540	540	540
20	918	584	543	541	540	540	540	540	540	540
30	1002	628	551	543	542	541	540	540	540	540
40	1074	676	566	549	547	543	540	540	540	540
51	1144	730	589	560	554	547	541	540	540	540

Table B4. Temperature Profiles (°R) Along Centerline of Copper Target and Steel Holder (Figure 16)

Time ms	0 inch	0.1	0.2	0.3	0.4	0.5	0.6	0.7	1	2	3 inch
1	576	540	540	540	540	540	540	540	540	540	540
50	929	676	581	558	553	547	542	540	540	540	540
100	1114	842	694	628	599	576	555	546	542	540	540
150	1264	988	813	716	663	620	584	565	550	541	541
200	1393	1116	927	809	735	676	626	596	565	545	545
250	1507	1232	1034	902	813	740	677	636	589	552	554
300	1611	1338	1135	993	893	809	735	684	619	565	567
350	1706	1437	1231	1082	974	881	797	737	655	582	585
384	1768	1501	1294	1141	1029	931	841	776	682	597	600

Table B5. Temperature Profiles (°R) Along Exposed Curved Surface of Aluminum Target and Steel Holder (Figure 17)

Time ms	0 inch	0.1	0.2	0.3	0.4	0.5	0.6	1	2	3 inch
1	607	552	552	552	552	552	550	550	550	550
10	861	609	599	599	599	634	618	618	618	618
20	997	670	630	628	628	684	669	669	669	669
30	1098	733	658	651	651	717	708	708	708	708
40	1181	794	688	672	671	744	739	739	739	739
51	1260	858	722	694	691	768	768	768	768	768

Table B6. Temperature Profiles (°R) Along Exposed Curved Surface of Copper Target and Steel Holder (Figure 18)

Time ms	0 inch	0.1	0.2	0.3	0.4	0.5	0.6	1	2	3 inch
1	584	548	548	548	548	550	550	550	550	550
50	1003	755	662	640	638	695	765	765	765	765
100	1194	927	783	720	701	760	866	867	867	867
150	1341	1070	900	808	770	821	942	944	944	944
200	1466	1195	1011	900	844	887	1006	1009	1009	1009
250	1577	1308	1116	991	922	956	1064	1065	1066	1066
300	1678	1411	1214	1080	1001	1029	1119	1117	1118	1118
350	1771	1508	1308	1167	1081	1102	1174	1165	1166	1166
384	1831	1569	1369	1225	1135	1152	1210	1195	1197	1197

APPENDIX C

**PARTICLE VELOCITY PROGRAM IN THE
C PROGRAMMING LANGUAGE**

```

/* This program calculates the velocity of particles in the rocket exhaust
   and on impact with the probe. It also calculates gas velocity, Mach number,
   and density in the exhaust flow */

```

```

#include <stdio.h>
#include <math.h>
#include <conio.h>
#include <stdlib.h>

```

```

#define N 1000

```

```

FILE *density,*mach,*gasvel,*AR,*impct,*dragcoeff;
FILE *p10,*p50;
FILE *p100,*p300,*p500;
FILE *p1000,*p3000,*p5000;

```

```

double M,IVp,Vp_iplus1,Vg_i,Vg_iplus1,RHOg_i,RHOg_iplus1;
double Vp10,Vp50;
double Vp100,Vp300,Vp500;
double Vp1000,Vp3000,Vp5000;
double RHOp,Cd,dx,pi;

```

```

void main(){
  double a,b,c;
  double Astar,gamma,Ac,x,xstar,xr,RHOo,To,T,R,as,Ae,Po;
  double Ar,f,dfdm;
  int i,j;

```

```

  void Open_Files(void);
  void Close_Files(void);
  double ParticleVelocity(double,double);
  double ImpactVelocity(double,double);
  double interp(double,double,double,double,double);

```

```

  pi=4.0*atan(1.0);gamma=1.2;
  xr=48.0;xstar=xr/3.0;dx=xr/(N+1);
  Po=473.0*144;R=2093.0;To=6300.0;
  RHOo=Po/(R*To)*32.174;
  Ac=4.0;Ae=6.0;Astar=1.0;
  RHOp=115.4879;

```

```

  clrscr();
  Open_Files();

```

```

T=To/(1.0+(gamma-1.0)/2.0);
as=sqrt(gamma*R*T);

for(x=0.0;x<=xe;x+=dx){
/* calculate Area ratio */
  if(x/xstar<=1){
// Ar = (1.0-Ac/Astar)*x/xstar + Ac/Astar;
  Ar=((Ac-.5*(Ac+Astar))*cos(pi*x/xstar)+.5*(Ac+Astar))/Astar;
  M = 0.0;
} else {
// Ar = (Ae/Astar - 1.0)*(x-xstar)/(xe-xstar) + 1.0;
  Ar=((Ae-.5*(Ae+Astar))*cos(pi*(x-xe)/(xstar-xe))+.5*(Ae+Astar))/Astar;
  M = 1.5;
}

/* calculate M */
  a=pow((gamma+1.0)/2.0,(gamma+1.0)/(2.0*(gamma-1.0)));
  b=(gamma-1.0)/2.0;
  c=-(gamma+1.0)/(2.0*(gamma-1.0));
  do {
f=a*M*pow((1.0+b*M*M),c)-1.0/Ar;
  dfdm = a*M*c*pow((1.0+b*M*M),c-1.0)*2.0*b*M + a*pow((1.0+b*M*M),c);
  M=M-f/dfdm;
} while(fabs(f/dfdm)>.00001);

if(x==0){
  Vg_i = as*sqrt( (gamma+1.0)/2.0 * M*M / (1.0+(gamma-1.0)/2.0*M*M)
);
  RHOG_i = RHOO*pow((1.0+(gamma-1.0)/2.0*M*M),-1.0/(gamma-1.0));
  Vp10=Vp50=0;//Vg_i;
  Vp100=Vp300=Vp500=0;// Vg_i;
  Vp1000=Vp3000=Vp5000=0;//Vg_i;
} else {
  Vg_iplus1 = as*sqrt( (gamma+1.0)/2.0 * M*M / (1.0+(gamma-1.0)/2.0*M*M) );
  RHOG_iplus1 = RHOO*pow((1.0+(gamma-1.0)/2.0*M*M),-1.0/(gamma-1.0));

if(M<0.2)Cd=0.48;
else if(M<=0.4)Cd=interp(0.2,0.48,0.4,0.5,M);
  else if(M<=0.6)Cd=interp(0.4,0.5, 0.6,0.55,M);
else if(M<=0.8)Cd=interp(0.6,0.55,0.8,0.62,M);
else if(M<=1.0)Cd=interp(0.8,0.62,1.0,0.8,M);
else if(M<=1.2)Cd=interp(1.0,0.8, 1.2,0.93,M);
else if(M<=1.4)Cd=interp(1.2,0.93,1.4,1.05,M);

```

```

else if(M<=2.0)Cd=interp(1.4,1.05,2.0,1.04,M);
      else if(M<=3.0)Cd=interp(2.0,1.04,3.0,0.95,M);
else Cd=.95;

Vp_iplus1=ParticleVelocity(0.0000033*10,Vp10);
fprintf(p10,"%5.3lf %5.0lf\n",x/xe,Vp10);
Vp10=Vp_iplus1;

Vp_iplus1=ParticleVelocity(0.0000033*50,Vp50);
fprintf(p50,"%5.3lf %5.0lf\n",x/xe,Vp50);
      Vp50=Vp_iplus1;

Vp_iplus1=ParticleVelocity(0.0000033*100,Vp100);
fprintf(p100,"%5.3lf %5.0lf\n",x/xe,Vp100);
Vp100=Vp_iplus1;

Vp_iplus1=ParticleVelocity(0.0000033*300,Vp300);
      fprintf(p300,"%5.3lf %5.0lf\n",x/xe,Vp300);
      Vp300=Vp_iplus1;

      Vp_iplus1=ParticleVelocity(0.0000033*500,Vp500);
      fprintf(p500,"%5.3lf %5.0lf\n",x/xe,Vp500);
Vp500=Vp_iplus1;

Vp_iplus1=ParticleVelocity(0.0000033*1000,Vp1000);
      fprintf(p1000,"%5.3lf %5.0lf\n",x/xe,Vp1000);
      Vp1000=Vp_iplus1;

Vp_iplus1=ParticleVelocity(0.0000033*3000,Vp3000);
IVp=ImpactVelocity(0.0000033*3000,Vp3000);
fprintf(p3000,"%5.3lf %5.0lf\n",x/xe,Vp3000);
Vp3000=Vp_iplus1;

      Vp_iplus1=ParticleVelocity(0.0000033*5000,Vp5000);
      fprintf(p5000,"%5.3lf %5.0lf\n",x/xe,Vp5000);
Vp5000=Vp_iplus1;

Vg_i=Vg_iplus1;
RHOg_i=RHOg_iplus1;
}

fprintf(density,"%5.3lf %lf\n",x/xe,RHOg_i);
fprintf(AR,"%5.3lf %5.3lf\n",x/xe,Ar);

```

```

    fprintf(mach,"%5.3lf %5.3lf\n",x/xe,M);
    fprintf(gasvel,"%5.3lf %5.0lf\n",x/xe,Vg_i);
        fprintf(dragcoeff,"%5.3lf %5.3lf\n",M,Cd);
    }
    x-=dx;
    IVp=ImpactVelocity(0.0000033*.001,Vg_i);
    fprintf(impct,"%5.3lf %5.0lf %5.0lf\n",.001,Vg_i,IVp);

    IVp=ImpactVelocity(0.0000033*.01,Vg_i);
    fprintf(impct,"%5.3lf %5.0lf %5.0lf\n",.01,Vg_i,IVp);

    IVp=ImpactVelocity(0.0000033*.1,Vg_i);
    fprintf(impct,"%5.3lf %5.0lf %5.0lf\n",.1,Vg_i,IVp);

    IVp=ImpactVelocity(0.0000033*10,Vp10);
    fprintf(impct,"%5.3lf %5.0lf %5.0lf\n",10.0,Vp10,IVp);

    IVp=ImpactVelocity(0.0000033*50,Vp50);
    fprintf(impct,"%5.3lf %5.0lf %5.0lf\n",50.0,Vp50,IVp);

    IVp=ImpactVelocity(0.0000033*100,Vp100);
    fprintf(impct,"%5.3lf %5.0lf %5.0lf\n",100.0,Vp100,IVp);

    IVp=ImpactVelocity(0.0000033*300,Vp300);
    fprintf(impct,"%5.3lf %5.0lf %5.0lf\n",300.0,Vp300,IVp);

    IVp=ImpactVelocity(0.0000033*500,Vp500);
    fprintf(impct,"%5.3lf %5.0lf %5.0lf\n",500.0,Vp500,IVp);

    IVp=ImpactVelocity(0.0000033*1000,Vp1000);
    fprintf(impct,"%5.3lf %5.0lf %5.0lf\n",1000.0,Vp1000,IVp);

    IVp=ImpactVelocity(0.0000033*3000,Vp3000);
    fprintf(impct,"%5.3lf %5.0lf %5.0lf\n",3000.0,Vp3000,IVp);

    IVp=ImpactVelocity(0.0000033*5000,Vp5000);
    fprintf(p5000,"%5.3lf %5.0lf %5.0lf\n",5000.0,Vp5000,IVp);

    Close_Files();
    printf("Calculations completed successfully\n");
}

void Open_Files(){

```



```
if ((density = fopen("c:\\partvel\\density.dat", "wt")) == NULL){
    fprintf(stderr, "Cannot open output file DENSITY.DAT.\n");
    exit(1);
}
if ((mach = fopen("c:\\partvel\\mach.dat", "wt")) == NULL){
    fprintf(stderr, "Cannot open output file MACH.DAT.\n");
    exit(1);
}
if ((gasvel = fopen("c:\\partvel\\gasvel.dat", "wt")) == NULL){
    fprintf(stderr, "Cannot open output file GASVEL.DAT.\n");
    exit(1);
}
if ((AR = fopen("c:\\partvel\\AR.dat", "wt")) == NULL){
    fprintf(stderr, "Cannot open output file AR.DAT.\n");
    exit(1);
}
if ((p10 = fopen("c:\\partvel\\p10e.dat", "wt")) == NULL){
    fprintf(stderr, "Cannot open output file P10.DAT.\n");
    exit(1);
}
if ((p50 = fopen("c:\\partvel\\p50e.dat", "wt")) == NULL){
    fprintf(stderr, "Cannot open output file P50.DAT.\n");
    exit(1);
}
if ((p100 = fopen("c:\\partvel\\p100e.dat", "wt")) == NULL){
    fprintf(stderr, "Cannot open output file P100.DAT.\n");
    exit(1);
}
if ((p300 = fopen("c:\\partvel\\p300e.dat", "wt")) == NULL){
    fprintf(stderr, "Cannot open output file P300.DAT.\n");
    exit(1);
}
if ((p500 = fopen("c:\\partvel\\p500e.dat", "wt")) == NULL){
    fprintf(stderr, "Cannot open output file P500.DAT.\n");
    exit(1);
}
if ((p1000 = fopen("c:\\partvel\\p1000e.dat", "wt")) == NULL){
    fprintf(stderr, "Cannot open output file P1000.DAT.\n");
    exit(1);
}
if ((p3000 = fopen("c:\\partvel\\p3000e.dat", "wt")) == NULL){
    fprintf(stderr, "Cannot open output file P3000.DAT.\n");
    exit(1);
}
```

```

    }
    if ((p5000 = fopen("c:\\partvel\\p5000e.dat", "wt")) == NULL){
        fprintf(stderr, "Cannot open output file P5000.DAT.\n");
        exit(1);
    }
    if ((impct = fopen("c:\\partvel\\impvele.dat", "wt")) == NULL){
        fprintf(stderr, "Cannot open output file P5000.DAT.\n");
        exit(1);
    }
    if ((dragcoeff = fopen("c:\\partvel\\cd.dat", "wt")) == NULL){
        fprintf(stderr, "Cannot open output file cd.DAT.\n");
        exit(1);
    }
}

```

```

void Close_Files(){
    fclose(density);
    fclose(AR);
    fclose(mach);
    fclose(gasvel);
    fclose(p10);
    fclose(p50);
    fclose(p100);
    fclose(p300);
    fclose(p500);
    fclose(p1000);
    fclose(p3000);
    fclose(p5000);
    fclose(impct);
    fclose(dragcoeff);
}

```

```

double ParticleVelocity(double D,double Vpi){
    double a,b,c,d,A,B,C,srt;
    double Vgbar,RHObar;

```

```

    Vgbar=.5*(Vg_iplus1 + Vg_i);
    RHObar=.5*(RHOG_i+RHOG_iplus1);

```

```

    a=2.0*RHOp*D/(Cd*RHObar);
    b=-1.0;
    c=2.0*Vgbar;
    d=-Vgbar*Vgbar;

```

```
A=a/dx + b/2.0;
B=b*Vpi + c;
C=Vpi*Vpi*(b/2.0-a/dx) + c*Vpi + 2.0*d;

srt=sqrt(B*B-4.0*A*C);
if((-B+srt)<0)srt=-srt;

return (-B+srt)/(2.0*A);
}

double ImpactVelocity(double D,double Vp){
double del;
del=.143*exp(3.24/(M*M))*25/12;
return Vp*exp(-Cd*del*RHOg_i/(4.0/3.0*D*RHOp));
}

double interp(double x1, double f1, double x2, double f2, double x){
return f1+(f2-f1)/(x2-x1)*(x-x1);
}
```

APPENDIX D

**TABULATED DATA FROM THE PARTICLE
VELOCITY PROGRAM**

Table D1. Nozzle Flow Properties as a Function of X/X_e

X/X_e	A/A*	Mach Number	Gas Velocity ft/sec	Gas Density lbm/ft ³
Chamber	4	0.15	595	0.1643
0.1	3.383	0.178	707	0.1636
0.2	2.039	0.306	1210	0.1587
0.3	1.075	0.737	2854	0.1037
Throat	1	1	3773	0.1276
0.4	1.121	1.383	5040	0.0693
0.5	1.736	1.922	6534	0.0345
0.6	2.732	2.322	7445	0.0192
0.7	3.895	2.599	7987	0.0126
0.8	4.971	2.781	8307	0.0095
0.9	5.728	2.884	8476	0.0081
Exit	6	2.917	8529	0.0076

Table D2. Velocity (ft/sec) of a 10 μm Particle in the Exhaust Flow of Various Size Rockets as a Function of X/X_e

X/X_e	$X_e=1$ inch	$X_e=6$ inch	$X_e=12$ inch	$X_e=24$ inch	$X_e=48$ inch
Chamber	0	0	0	0	0
0.1	439	579	612	636	654
0.2	684	907	974	1029	1073
0.3	1460	2039	2220	3172	2488
Throat	1961	2740	2979	2369	3324
0.4	2977	3975	4245	4453	4609
0.5	3998	5210	5538	5795	5990
0.6	4587	5949	6321	6613	6835
0.7	4956	6413	6811	7122	7359
0.8	5214	6730	7141	7459	7699
0.9	5410	6961	7376	7692	7927
Exit	5573	7138	7548	7855	8076

Table D3. Velocity (ft/sec) of a 50 μm Particle in the Exhaust Flow of Various Size Rockets as a Function of X/X_e

X/X_e	$X_e=1$ inch	$X_e=6$ inch	$X_e=12$ inch	$X_e=24$ inch	$X_e=48$ inch
Chamber	0	0	0	0	0
0.1	279	456	517	566	603
0.2	451	710	801	883	954
0.3	926	1523	1758	1975	2165
Throat	1235	2046	2363	2654	2907
0.4	1925	3094	3513	3873	4165
0.5	2653	4143	4654	5088	5441
0.6	3068	4749	5322	5811	6210
0.7	3328	5130	5743	6265	6693
0.8	3510	5395	6033	6577	7019
0.9	3652	5597	6251	6806	7253
Exit	3774	5762	6426	6983	7428

Table D4. Velocity (ft/sec) of a 100 μm Particle in the Exhaust Flow of Various Size Rockets as a Function of X/X_e

X/X_e	$X_e=1$ inch	$X_e=6$ inch	$X_e=12$ inch	$X_e=24$ inch	$X_e=48$ inch
Chamber	0	0	0	0	0
0.1	218	388	456	517	566
0.2	359	611	710	801	883
0.3	728	1284	1523	1758	1975
Throat	968	1722	2046	2363	2654
0.4	1520	2641	3094	3513	3873
0.5	2112	3577	4143	4654	5088
0.6	2451	4113	4749	5322	5811
0.7	2662	4450	5130	5743	6265
0.8	2812	4685	5395	6033	6577
0.9	2928	4865	5597	6251	6806
Exit	3029	5017	5762	6426	6983

Table D5. Velocity (ft/sec) of a 300 μ m Particle in the Exhaust Flow of Various Size Rockets as a Function of X/X_e

X/X_e	$X_e=1$ inch	$X_e=6$ inch	$X_e=12$ inch	$X_e=24$ inch	$X_e=48$ inch
Chamber	0	0	0	0	0
0.1	140	279	347	417	482
0.2	236	451	551	652	749
0.3	475	926	1147	1383	1622
Throat	630	1235	1535	1856	2180
0.4	994	1925	2371	2831	3274
0.5	1397	2653	3233	3817	4363
0.6	1627	3068	3726	4383	4996
0.7	1772	3328	4035	4738	5394
0.8	1874	3510	4251	4986	5670
0.9	1954	3652	4418	5176	5879
Exit	2024	3774	4559	5334	6049

Table D6. Velocity (ft/sec) of a 500 μ m Particle in the Exhaust Flow of Various Size Rockets as a Function of X/X_e

X/X_e	$X_e=1$ inch	$X_e=6$ inch	$X_e=12$ inch	$X_e=24$ inch	$X_e=48$ inch
Chamber	0	0	0	0	0
0.1	112	233	296	365	435
0.2	191	382	477	578	678
0.3	383	777	982	1208	1446
Throat	507	1035	1311	1618	1942
0.4	803	1621	2040	2492	2951
0.5	1132	2249	2803	3388	3965
0.6	1321	2607	3239	3901	4550
0.7	1439	2831	3511	4222	4917
0.8	1523	2989	3703	4447	5173
0.9	1589	3112	3851	4620	5368
Exit	1646	3218	3978	4766	5530

Table D7. Velocity (ft/sec) of a 1000 μm Particle in the Exhaust Flow of Various Size Rockets as a Function of X/X_e

X/X_e	$X_e=1$ inch	$X_e=6$ inch	$X_e=12$ inch	$X_e=24$ inch	$X_e=48$ inch
Chamber	0	0	0	0	0
0.1	82	179	233	296	365
0.2	141	297	382	477	578
0.3	283	601	777	982	1208
Throat	374	798	1035	1311	1618
0.4	593	1256	1621	2040	2492
0.5	839	1755	2249	2803	3388
0.6	981	2041	2607	3239	3901
0.7	1070	2219	2831	3511	4222
0.8	1133	2346	2989	3703	4447
0.9	1182	2445	3112	3851	4620
Exit	1226	2530	3218	3978	4766

Table D8. Velocity (ft/sec) of a 3000 μm Particle in the Exhaust Flow of Various Size Rockets as a Function of X/X_e

X/X_e	$X_e=1$ inch	$X_e=6$ inch	$X_e=12$ inch	$X_e=24$ inch	$X_e=48$ inch
Chamber	0	0	0	0	0
0.1	49	112	151	200	258
0.2	86	191	254	331	421
0.3	171	383	512	670	859
Throat	226	507	678	891	1145
0.4	359	803	1071	1400	1789
0.5	510	1132	1502	1951	2473
0.6	597	1321	1748	2266	2863
0.7	651	1439	1903	2463	3107
0.8	690	1523	2012	2602	3279
0.9	721	1589	2098	2711	3413
Exit	748	1646	2173	2805	3527

Table D9. Velocity (ft/sec) of a 5000 μm Particle in the Exhaust Flow of Various Size Rockets as a Function of X/X_e

X/X_e	$X_e=1$ inch	$X_e=6$ inch	$X_e=12$ inch	$X_e=24$ inch	$X_e=48$ inch
Chamber	0	0	0	0	0
0.1	39	90	122	163	214
0.2	67	153	206	273	354
0.3	135	307	414	550	717
Throat	177	406	549	730	954
0.4	282	643	868	1151	1497
0.5	401	909	1221	1612	2082
0.6	470	1062	1424	1876	2416
0.7	513	1158	1552	2041	2625
0.8	544	1226	1642	2158	2773
0.9	568	1280	1713	2250	2888
Exit	589	1327	1774	2329	2987

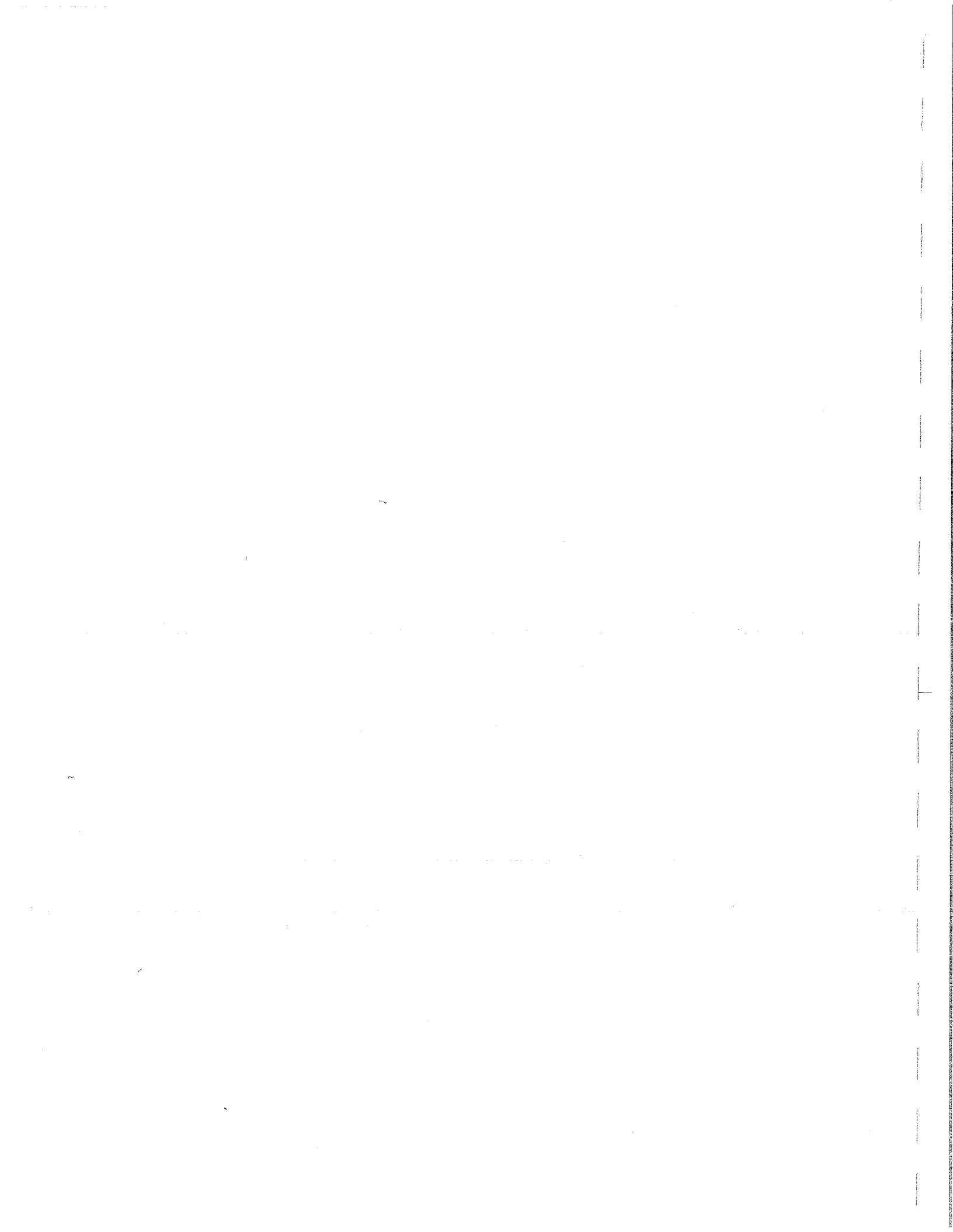
Table D10. Particle Velocity at the Nozzle Exit Plane, V_{pe} (ft/sec), and Particle Impact Velocity, V_p (ft/sec)

D_p μm	$X_e=1$ inch		$X_e=6$ inch		$X_e=12$ inch		$X_e=24$ inch		$X_e=48$ inch	
	V_{pe}	V_p	V_{pe}	V_p	V_{pe}	V_p	V_{pe}	V_p	V_{pe}	V_p
0.001	8529	0	8529	0	8529	0	8529	0	8529	0
0.01	8529	16	8529	16	8529	16	8529	16	8529	16
0.1	8529	4551	8529	4551	8529	4551	8529	4551	8529	4551
10	5574	5539	7140	7095	7549	7502	7856	7807	8078	8027
50	3775	3770	5764	5757	6427	6419	6985	6976	7429	7420
100	3030	3028	5018	5015	5764	5760	6427	6423	6985	6980
300	2024	2024	3775	3774	4560	4559	5335	5334	6051	6050
500	1647	1647	3219	3219	3979	3979	4767	4767	5531	5530
1000	1226	1226	2531	2531	3219	3219	3979	3979	4767	4767
3000	748	748	1647	1647	2173	2173	2806	2806	3528	3528

LIST OF WORKS CITED

- Anderson, John D., Jr., *Hypersonic and High Temperature Gas Dynamics*, McGraw-Hill, New York, 1989.
- Bailey, A. B., and Koch, K. E., "Data for Use with Hypervelocity Ballistics Ranges," ARO, Inc., AEDC-TM-65-16, June, 1965.
- Beer, Ferdinand P., and Johnston, E. Russell, Jr., *Mechanics of Materials*, Second Edition, McGraw-Hill, New York, 1992.
- Bennet, J. C., "Use of Five-Hole Pneumatic probe in Unsteady Flows," *Experimental Diagnostics in Gas Phase Combustion Systems*, American Institute of Astronautics and Aeronautics, *Progress in Astronautics and Aeronautics*, Vol. 53, 1977.
- Bilger, R.W., "Probe Measurements in Turbulent Combustion," *Experimental Diagnostics in Gas Phase Combustion Systems*, American Institute of Astronautics and Aeronautics, *Progress in Astronautics and Aeronautics*, Vol. 53, 1977.
- Bowman, Craig T., "Probe Measurements in Flames," *Experimental Diagnostics in Gas Phase Combustion*, American Institute of Astronautics and Aeronautics, *Progress in Astronautics and Aeronautics*, Vol. 53, New York, 1977.
- Callens, E. Eugene, "Feasibility of an Impact Probe for Particle Characterization in Rocket Exhaust Plumes", Louisiana Tech University, Ruston, LA, 1994.
- Chernansky, N. P., "Sampling and Measuring of NO and NO₂ in Combustion Systems," *Experimental Diagnostics in Gas Phase Combustion*, American Institute of Astronautics and Aeronautics, *Progress in Astronautics and Aeronautics*, Vol. 53, New York, 1977.
- Cofer, Wesley R III., Lala, G. Garland., and Wightman, James P., "Analysis of Mid-Tropospheric Space Shuttle Exhaust Aluminum Oxide Particles," *Atmospheric Environment*, Vol. 21, No.5, 1987.

- Dill, K. M., Reed, R. A., Calia, V. S., and Schulz, R. J., "Analysis of Crystalline Phase Aluminum Oxide Particles from Solid Propellant Exhausts," *Journal of Propulsion*, Tech Notes, Vol. 6, No. 5, 1990.
- Holman, J. P., *Heat Transfer*, Seventh Edition, McGraw-Hill, New York, 1990.
- Juvinall, Robert C. and Marshek, Kurt M., *Fundamentals of Machine Component Design*, Second Edition, John Wiley & Sons, New York, 1991.
- John, James E. A., *Gas Dynamics*, Prentice-Hall, Englewood Cliffs, NJ, 1984.
- Konopka, W. L., Reed, R. A., and Calia, V. S., "Measurements of Infrared Optical Properties of Al_2O_3 Rocket Particles," AIAA 18th Thermophysics Conference, Montreal, Canada, 1983.
- Kraeutle, Karl J., "Particle Size Analysis in Solid Propellant Combustion Research," Experimental Diagnostics in Combustion of Solids, American Institute of Astronautics and Aeronautics, *Progress in Astronautics and Aeronautics*, Vol. 63, 1979.
- Laredo, D., McCrorie, J. D. II, Vaughn, J. K., and D.W., Netzer., "Motor and Plume Particle Size Measurements in Solid Propellant Micromotors," *Journal of Propulsion and Power*, Vol. 10, No. 3, May-June 1994.
- McMurtry, J. Scott., "An Investigation of the Effects of Nosetip Shape in Terminal Ballistics Using a Wave Mechanics Model," Doctoral Dissertation, College of Engineering and Science, Louisiana Tech University, August 1997.
- Olive, Dan., "X-Ray Spectroscopy of the SSME Plume," NASA CR-185308, Sverdurp Technology, 1988.
- Sambamurthi, Jay K., " Al_2O_3 Collection and Sizing from Solid Rocket Motor Plumes," *Journal of Propulsion and Power*, Vol. 12, No. 3, 1996.
- Strand, Leon D., Bowyer, James M., Varsi, Guilio., Laue, Eric G., and Gauldin, Robert, "Characterization of Particulates in the Exhaust Plume of Large Solid-Propellant Rockets," *Journal of Spacecraft and Rockets*, Vol. 18, No. 4, July-August, 1981.
- White, Frank M., *Fluid Dynamics*, Third Edition, McGraw Hill, New York, 1994.



REPORT DOCUMENTATION PAGE			Form Approved OMB No. 0704-0188	
Public reporting burden for this collection of information is estimated to average 1 hour per response, including the time for reviewing instructions, searching existing data sources, gathering and maintaining the data needed, and completing and reviewing the collection of information. Send comments regarding this burden estimate or any other aspect of this collection of information, including suggestions for reducing this burden, to Washington Headquarters Services, Directorate for Information Operations and Reports, 1215 Jefferson Davis Highway, Suite 1204, Arlington, VA 22202-4302, and to the Office of Management and Budget, Paperwork Reduction Project (0704-0188), Washington, DC 20503.				
1. AGENCY USE ONLY (Leave blank)	2. REPORT DATE July 1997	3. REPORT TYPE AND DATES COVERED Final Contractor Report		
4. TITLE AND SUBTITLE Particle Characterization in Rocket Exhaust Plumes			5. FUNDING NUMBERS Contract No. 31-4136-59060 and NAS13-580	
6. AUTHOR(S) E. Eugene Callens, Jr J. Scott Fisher				
7. PERFORMING ORGANIZATION NAME(S) AND ADDRESS(ES) Department of Mechanical and Industrial Engineering Louisiana Tech University P.O. Box 10348 Ruston, LA 71272-0046			8. PERFORMING ORGANIZATION REPORT NUMBER	
9. SPONSORING/MONITORING AGENCY NAME(S) AND ADDRESS(ES) National Aeronautics and Space Administration Washington, DC 20546-0001			10. SPONSORING/MONITORING AGENCY REPORT NUMBER SE-1998-01-0002-SSC	
11. SUPPLEMENTARY NOTES				
12a. DISTRIBUTION/AVAILABILITY STATEMENT Subject Category: Availability: NASA CASI (301) 621-0390			12b. DISTRIBUTION CODE Distribution:	
13. ABSTRACT (Maximum 200 words) A method to characterize particles in rocket exhaust plumes is developed. The particle velocity, size, and material composition are determined from crater characteristics resulting from impacts into aluminum and copper targets passed through the plume. The targets are mounted on a steel arm approximately 21 inches (53 cm) long which is rotated through the plume at sufficient velocity to prevent material failure resulting from thermal effects. A Scanning Electron Microscope (SEM) with secondary x-ray detectors is used to determine the particle material, and a standard optical measurement microscope is used to determine the crater diameter and depth. The crater diameter and depth are used, in turn, as inputs to a ballistics computer code to estimate the velocity and size of the particle. The target has a safe residence time in the plume of approximately 50 ms before reaching an unacceptably high temperature. The arm must reach a velocity of 104 ft/s (32 m/s) before entering the plume to produce the design residence time of 20 ms. The arm is actuated by a torsion spring with a 5-inch (13 cm) outer diameter, 0.625-inch (16 mm) wire diameter, and 11 coils. A prototype of the entire rocket exhaust particle impact characterization system (PICS) was constructed and statically tested.				
14. SUBJECT TERMS Rocket Exhaust, Plumes			15. NUMBER OF PAGES 142	
			16. PRICE CODE	
17. SECURITY CLASSIFICATION OF REPORT UNCLASSIFIED	18. SECURITY CLASSIFICATION OF THIS PAGE UNCLASSIFIED	19. SECURITY CLASSIFICATION OF ABSTRACT UNCLASSIFIED	20. LIMITATION OF ABSTRACT UL	

